FLNA Variants Associated with Single Suture Craniosynostosis

Deema Abdullah Alroweilly

A dissertation

submitted in partial fulfillment of the

requirements for the degree of

Doctor of Philosophy

University of Washington

2022

Reading Committee:

Michael Cunningham, Chair

Susan Herring

Carol Ware

Nathan Sniadecki

Dolphine Oda

Program Authorized to Offer Degree:

Department of Oral Health Sciences

University of Washington

Abstract

FLNA Variants Associated with Single Suture Craniosynostosis

Deema Abdullah Alroweilly

Chair of the Supervisory Committee:

Michael Cunningham

Department of Pediatrics

Craniosynostosis (CS) is a common birth defect affecting the skull vault. It is characterized by premature ossification of one or more of the cranial sutures. Single suture craniosynostosis (SSC) accounts for approximately 85% of all CS cases and affects approximately 1 in 2000-2500 live births worldwide, with a higher rate in males than females. It is a significant craniofacial disorder associated with increased intracranial pressure, distortion of the skull shape, facial deformities, misalignment of the teeth, and mortality. Patients with CS may undergo invasive surgical procedures and experience neuropsychological trauma associated with self-image. Although several genetic mutations have been attributed to the pathogenesis of syndromic craniosynostosis, the etiology and molecular mechanisms of SSC remain largely unknown. Thus, identification of candidate genes or signaling pathways involved in intramembranous ossification and suture development is critical in understanding the underlying biology of SSC. Through generation of primary cell lines from individuals with SSC and the use of Next Generation RNA sequencing (RNA-Seq), our lab has identified a set of rare genetic variants we propose are associated with craniosynostosis. Among these are nine variants in

Filamin A (*FLNA*), a gene which codes for a mechanosensitive, actin-binding extracellular matrix protein. *FLNA* is one of the most abundant proteins in the cytoskeleton and regulates cell polarization, cell shape, cell adhesion, cell contraction and cell migration and protects the cell from mechanical shear stress. *FLNA* also modulates the functional activities of several other matrix proteins. It binds and crosslinks actin filaments and remodels the cytoskeleton by interacting with the adhesive transmembrane receptor Integrin β1, vimentin, and the Rho family GTPases (Rac1, Cdc42, RaIA and RhoA). In doing so, *FLNA* coordinates a variety of cellular processes and cell signaling. In the context of osteogenesis, *FLNA* plays an important role in the regulation of calvarial mesenchymal stem cells and osteoblasts as it acts on pivotal signaling pathways. FLNA influences osteogenic gene expression by binding transcription factor FOXC1 and mediating BMP signaling. It also binds SMAD2 and SMAD5 regulating both TGFβ and BMP signaling, respectively. Missense mutations in *FLNA* have been described in otopalatodigital spectrum disorders which are associated with bone dysplasia and craniosynostosis.

In this dissertation, I isolated and characterized primary human calvarial MSCs (cMSCs) from primary calvarial osteoblasts (cOBs). Then, I tested the hypothesis that the *FLNA* variants we identified in patients with SSC contribute to craniosynostosis through dysregulating cellular proliferation and differentiation, and attenuating cell mechanics. I assessed the contribution of *FLNA* mutations in the pathogenesis of craniosynostosis through characterizing the impact of nine rare variants on the development and cellular mechanics of cMSCs and cOBs. This work has revealed that cMSCs have a distinct gene expression profile from bone morrow mesenchymal stem cells (BMMSCs). We have also found that the identified rare *FLNA* variants affected biological properties, attenuated cellular mechanics, and altered osteogenic gene expression pattern in SSC patients

Table of Contents

List of Figures

List of Tables

Acknowledgment

This degree would not have been possible without the help and support from many individuals. First and foremost, I would like to express my gratitude to my advisor Prof. Michael Cunningham for his invaluable guidance and teaching throughout my PhD training. Michael's office door was always open whenever I encountered trouble or had a question. He has always had time to discuss my research project and steer me in the right direction. Michael has always been open to the new ideas and experiments I proposed. He has invested an incredible amount of time and funding toward my training to become a fine scientist. Without his exceptional mentorship, none of this would have been possible - thank you Michael! I am very grateful for the opportunity to join such a distinguished institute such Seattle Children Research Institute.

I am also grateful for Prof. Oda who introduced me to the world of research during my master's study and has always motivated me to move forward during my journey. Special thanks for Prof. Carol Ware who motivated me to move forward at the beginning of my PhD journey.

I am also indebted to Prof. Susan Herring for her constant guidance throughout my PhD and to her valuable suggestions to improve my work and further my critical reasoning. I would also like to acknowledge Prof. Nate Sniadecki for sharing his expertise and for facilitating my cell mechanic's studies.

Thanks to my lab mate Jonas (Gus) Gustafson who trained and taught me how to conduct most of the lab tasks and techniques. Gus helped troubleshoot experiments and brainstorm ideas for my research project on a daily basis. He has also been a great friend who overwhelmed me with his kindness and our frequent conversations and laughter helped me endure frustration and hard times.

I would like to express my propound gratitude to my family and friends. I wouldn't be where I am today without their constant prayers, love, and support. My parents, Abdullah and Jozah, believed in me and provided me with the opportunity to seek my dreams and reach for the stars. I am forever grateful for their unconditional care and selfless encouragement. I am also indebted to my loving husband Homood. It wouldn't have been possible to accomplish this PhD without his tremendous understanding, patience, and the sacrifices he made over the past five years. Along with my husband, I would like to wholeheartedly thank my daughter, Noufi for the happy distraction from work and for being a great resource of love and relief.

Lastly, I would like to acknowledge my deceased grandmothers, Nouf and Telhowah who passed away during my journey. Their pride in me, prayers, love, and frequent calls to check on me had always sustained me in hard times.

DEDICATION

To my grandmothers, my parents, my five brothers and my sister Dana, my husband and my daughter Noufi.

For your unconditional love and support.

1. Introduction

The skull is a complex bony structure surrounding the brain and making up the head and the face (1). It is comprised of bones joined by fibrous structures called sutures (2). These sutures allow continues expansion of the skull to accommodate the brain growth. Craniosynostosis is a birth defect, which may either be isolated or as part of a syndrome. It is characterized by the premature fusion of one or more of the cranial sutures (2, 3). Although mutations in genes have been attributed to the pathogenesis of craniosynostosis, few biologic mechanisms have been elucidated. The identified genes in craniosynostosis mostly explain the etiology of the syndromic forms. Otherwise, little is known about the causes of non-syndromic single suture craniosynostosis (SSC). Thus, to understand the molecular mechanisms that lead to craniosynostosis, identification of genes or signaling pathways affecting intramembranous ossification and suture development is critical. Using RNA sequencing (RNA-Seq), we have identified nine rare variants in the strain-responsive gene Filamin A (*FLNA*) associated with single suture craniosynostosis.

In my PhD thesis, I thoroughly describe a homogenous MSC population isolated from calvarial osteoblasts. Then, I assess the contribution of FLNA in the pathogenesis of craniosynostosis through characterizing the impact of nine rare FLNA variants on the development and cellular mechanics of primary calvarial osteoblasts (cOBs) and primary calvarial mesenchymal stem cells (cMSCs). Lastly, I investigate the phenotype of cMSCs lacking *FLNA*.

1.1. Morphogenesis of the Cranial Bones and Sutures

In humans, the skull is composed of the neurocranium which surrounds and protects the brain and the sensory organs, and the viscerocranium, which forms the facial, palatal, pharyngeal, and temporal bones. The neurocranium is split into two parts; the chondrocranium which is the cartilaginous area that forms the skull base and the membranous part that forms

the cranial vault (1, 4). The cranial vault is composed of flat bones (calvaria) that develop in tight coordination: the paired frontal, paired parietal, and a single occipital bone; the greater wing of the sphenoid bone and the squamous part of the temporal bone also contribute to the vault sides (2, 5).

The skull morphogenesis begins during early embryogenesis and continues throughout adulthood. Two distinct origins contribute to formation of the skull: neural crest and mesoderm derived cells. The paired frontal bones and the suture that separates them (metopic), as well as the sagittal suture, are derived from neural crest cells, while the parietal bones are derived from mesoderm. The coronal suture which is located along the interface of the frontal and parietal bones is also of a mesodermal origin. The occipital bone has a mixed origin of both neural crest and mesoderm (2, 6, 7).

During the first four weeks of gestation, pre-condensation of mesenchymal stem cells (MSCs) initiates cranial bone formation. It starts with the epithelial-mesenchymal transition (EMT), a process during which epithelial cells differentiate into a more migratory, multipotent mesenchymal state (1, 8, 9). Afterwards, mesenchymal tissue accumulates as membrane around the developing brain as bone plates to form the calvaria in the fifth week of gestation. The plates are the expanding center of ossification, and they extend to the base of the skull and the sides to join each other separated by a suture (1, 10, 11).

In the seventh and eighth week of gestation, the ossification of the cranial vault is initiated by generating ossification centers (primordia). The area of primordia corresponds to the future eminences. After that, the calcification begins through the production of osteoid by osteoblasts. Then, bone spicules form and extend from the ossification centers toward the periphery (1). Mainly, the growth is defined by cell proliferation and migration rather than recruiting mesenchymal stem cells (7, 12). The produced osteoid calcifies forming the trabecular

bone, an immature woven bone with a random arrangement of collagen fibers. At the time of birth, mature lamellar bone gradually replaces the woven bone (1).

In the eighth week, in the frontal eminence, two frontal bones form from the primary ossification center and extend to the periphery. During the same time at the parietal eminence, two primary ossification centers appear to form the two parietal bones and the ossification extends from the centers to the periphery. At week 14, the ossification becomes more extensive in the parietal bones. Lastly, the ossification of the occipital bone occurs through two different ways, intramembranously from two centers and the rest calcified by endochonral ossification (1, 13, 14).

The Calvaria develop in tight coordination and are connected by complexes of fibrous tissues and cells (cranial sutures) that play an essential role during the skull growth. The metopic suture is located between the two frontal bones and the sagittal suture separates the two paired parietal bones. The coronal suture exists between the frontal and parietal bones; the paired frontal and parietal bones compose most of the skull vault. The lambdoid suture is between the occipital and parietal bones (2, 5). Lastly, the squamosal suture separates the parietal and squamous temporal bones(15).

Significant roles of these sutures include absorbing mechanical stress, maintaining skull integrity while allowing for changes and movement during childbirth, expansion during brain growth, and as regulatory centers for osteoprogenitors (16, 17). The skull growth continues at the bone margins and relies on the sutures; thus, they must stay patent to function—and any premature fusion (synostosis) will inhibit further bone growth.

Sutures are the major sites of bone growth for the cranial vault. Preosteoblasts and osteoprogenitor cells are located within the osteogenic area that form and advance bone growth. Each cranial suture is comprised of five components: the underlying dura mater, the overlying pericranium, the two osteogenic bones on either side, and between the osteogenic

fronts of the adjacent calvaria (17, 18). It is important that the mesenchymal sutures remain in a patent state to function properly at the bone edges (19). These sutures receive external signals from the expanding brain and the dura mater. The presence of the dura is essential because it secretes osteoinhibitory molecules which signal to maintain suture patency. These include heparin binding factors such as some members of the FGF and TGFß families. These factors prevent differentiation into mature osteoblasts through stimulating proliferation and matrix production. Dural reflections, a double folding of the meningeal dura, are attached firmly at the underside of the suture (junction of two calvaria). These reflections act as dividers and define the cranial cavity under the skull bones (1, 16, 20). After receiving a stimulus from the growing brain, preosteogenic cells within the suture migrate to the osteogenic front of the adjacent bone and start adding bone to the edges, to increase the cranial vault size and accommodate the expanding brain.

Once the brain growth is complete, the mesenchyme of the suture is replaced by fibrous connective tissue (21). Sutures fuse at different times throughout life. The metopic suture usually is fused by the ninth month (postnatal), although it can take up to 2–5 years to fuse, and it becomes fused by 7 years of age (16). The sagittal suture closes at approximately 22 years, the coronal suture after 24 years, and the lambdoid after 26 years (22).

1.2. Non-syndromic Craniosynostosis

Craniosynostosis is one of the common congenital birth defects that affects the skull vault. It is characterized by premature ossification of one or more of the cranial sutures. Worldwide, craniosynostosis affects 1 in 2,000–2,500 live births (2-4, 23), and males are more affected than females (24-27). It can be classified as: primary (caused by developmental defects during embryogenesis) or secondary (as a result of environmental factors such as maternal hyperthyroidism, intrauterine compression, and others), simple (involving only one suture),

complex (involving more than one suture), isolated (occurring without other defects), or syndromic (associated with other anomalies) (28). Children with prematurely fused sutures often experience several medical problems including increased cranial pressure, frontal bossing, strabismus, amblyopia, hyper- or hypotelorism, exorbitism, midface hypoplasia, dental anomalies, and cognitive and neuropsychological issues (29-34).

In general, the suture most frequently involved in craniosynostosis is the sagittal (40–55%), followed by coronal (20–25%), metopic (5–15%), and lambdoid (0–5%). Multiple suture synostosis accounts for only 5–15% of cases (3, 35). About 85% of the cases are known to be non-syndromic SSC with only one fused suture (36). Craniosynostosis has been associated with more than 180 syndromes, the most common of which include: Crouzon, Apert, Saethre-Chotzen, Muenke, and Pfeiffer syndromes (more information about syndromic craniosynostosis can be found in the Appendix). A variety of cellular mechanisms mediated by genes and signaling pathways have been described in those syndromes (*TWIST1*, *EFNB1*, *EFNA4*, *MSX2* (3, 4), *FGFR1*, *TGFR2*, and *TGFR3* (37)).

Despite the common genes, mutations in other genes and regulatory pathways have been shown to contribute to the pathogenesis of craniosynostosis in both syndromic and isolated cases. These genes include: *TGFBR1*, TGFBR2 (38) *FBN1* (39), *RAB23* (40), the Notch ligand, *JAGGED1* (41), *RECQL4* (42), *MASP1* (43), *SH3PXD2B* (44), *FREM1* (45), ALX4 (46), *SKI* (47), and *TCF12 (48)*. Even though several disease-causing mutations have been identified and associated with syndromic CS, the molecular causes of most SSC cases have yet to be elucidated. Thus, to better understand the mechanisms that lead to SSC, identification of genes or signaling pathways affecting intramembranous ossification and suture development is critical.

2. Isolation and Characterization of Human Calvarial Mesenchymal Stem Cells

2.1. Abstract

Although mesenchymal stem cells (MSCs) are routinely isolated from many different tissues, little is known about pluripotent properties and gene expression profile of those derived from human calvaria (cMSCs). We compared the immunophenotype and differentiation potential of FACS-isolated primary cMSCs from a heterogenous population of human calvarial tissue-derived osteoblasts. We then expanded the homogenous primary cMSC population and demonstrated that it shares common biological MSC characteristics (trilineage differentiation capacity and cell surface markers) with a well-characterized, commercial bone marrow mesenchymal stem cell (BMMSC) line. We performed expression profiling of genes known to be involved in bone development on each line in vitro. We compared different cMSC lines with BMMSCs and found that our primary cMSCs a) express MSC antigens CD73, CD90, CD105, CD29 and CD44 and lacked non-MSC hematopoietic markers CD31, CD45 and CD34, b) present a distinct gene expression profile, specifically related to proliferation and regeneration potency, c) exhibit distinct gene expression manifested by upregulation of genes involved in early stages of calvarial development and MSC maturation, suggesting a unique stem cell niche and d) have vital stem cell properties and can expand and differentiate to osteoblasts, chondrocytes and adipocytes. These findings provide insights into cMSCs' role in supporting calvarial tissue turnover and homeostasis. Further investigation into their biologic properties and therapeutic efficiency could make cMSCs a favorable candidate for regenerative medicine.

2.2. Introduction

The cranial vault is composed of five calvarial bones connected by fibrous tissue referred to as cranial sutures (2, 5), which are major growth sites and a niche for MSCs. Cranial bone formation is achieved through intramembranous ossification and sutures serve as major intramembranous bone growth sites (16). MSC differentiation into osteoprogenitors and osteoblasts occurs at the edges of the adjacent calvarial bones (osteogenic fronts) where MSCs are recruited from the surrounding mesenchyme (18, 49).

Cranial bone development starts with MSC condensation, where the cells arrange to form a membrane to initiate the intramembranous bone formation. Condensation involves a variety of genes, signaling pathways and cell surface and extracellular matrix (ECM) molecules. TGF*β* signaling is critical during the condensation process. The TGFβ family members involve *TGFβ1, TGFβ2, TGFβ3, SMAD2, SMAD3, SMAD4, TGFβR1*, and *TGFβR2.* *TGFβ1, TGFβ2,* and *TGFβ3* are known as main factors that regulate proliferation and early differentiation of osteoprogenitors during bone formation (50-52). *TGFβR2* has a critical role in intramembranous bone formation via regulating MSC proliferation and the expression of osteoblast marker genes: *DLX5, MSX2, RUNX2, and SP7* (53). Moreover, BMPs and their antagonist Noggin are thought to be important in cell aggregation and the initial stage of condensation (54).

Once the cell condensation process is complete, osteogenesis is activated by upregulating osteogenic genes and downregulating condensation genes (1). During this phase, elevated levels of *RUNX2, SP7* and *ALP* result in osteoprogenitor cells (55, 56). *RUNX2* activates osteogenic genes during differentiation (e.g., *COL1A1, BGLAP, IBSP*) (57).

FGF signaling is key during suture formation: *FGFR1, 2* and *3* are expressed in the suture area and *FGF2* expression is associated with normal and induced suture fusion (52). Accordingly, localized decrease in cell proliferation occurs as osteoblasts in the bone fronts

change their *FGFR2* expression to *FGFR1*. Moreover, FGF signaling has been associated with activating the transcription factor *TWIST1* that regulates osteoblast differentiation (3, 58, 59) and also has been shown to interact with the BMP pathway during osteogenesis (60).

MSCs residing in the calvaria mark the beginning of cranial bone development and growth. MSCs are a population of heterogenous cells that have the potency for self-renewal and trilineage differentiation (61, 62). They can be derived from various tissues in the human body and their biological characteristics differ according to the specific source (63). MSCs have been intensively studied due to their therapeutic potential (64-66). Bone marrow generally has been the most common source for isolation and characterization of MSCs and has been studied thoroughly in many species (67-71). MSCs from periosteum of long bones have been cultured to study bone development (72); these cells are used for bone and cartilage regeneration because they have been reported to possess higher pluripotency than BMMSCs (73-76) and distinct biological functions during regeneration and bone healing (77-79). Although numerous studies report on MSC isolation and properties, there are limited reports of isolating MSCs from human calvaria (cMSCs) (80): little is known about the characteristics, genetic profile and biological function of cMSCs.

In the present study, we isolated and enriched a homogenous population of primary MSCs derived from a mixed population of human calvarial osteoblasts (cOBs) from surgical explants. The existence of cMSCs in these explants suggests that calvarial bones retain discrete pools of progenitor cells, which could provide insights into the cellular mechanisms specific for intramembranous ossification in the human calvaria. We demonstrate that primary cMSCs meet the agreed-on criteria for stem cells by the International Society for Cellular Therapy (ISCT) and share common biological characteristics with highly studied commercial BMMSCs (81). Our isolated primary cMSCs possess the capability to differentiate to osteoblasts, chondrocytes, and adipocytes, in addition to maintaining the ISCT MSC markers throughout 3 passages. To further

investigate their gene expression profile, we used quantitative PCR (qPCR) to look for features unique to this MSC population in comparison to BMMSCs. The genetic profile of the homogenous primary cMSCs provides compelling evidence for stemness and confirms proliferative behavior of the isolated cMSCs. Our study represents a first step in the elucidation of a distinct population of cMSCs.

2.3. Materials and Methods

2.3.1. Calvarial osteoblast culture

Calvarial bone samples were collected, within 24 hours, from autopsy specimens or discarded surgical tissues of patients ages 2–12 months with no known skeletal disorders who had undergone craniotomy for reasons such as brain tumor, hydrocephalus, trauma, or autopsies. A waiver was obtained for the use of anonymous control samples (Seattle Children's Hospital IRB #12394). Bone fragments were transported in Waymouth media (WM) (Sigma-Aldrich) supplemented with 2% antibiotic/antimycotic solution (Corning) and 10% fetal bovine serum (FBS) (Invitrogen). A sterile scalpel was used to cut calvaria into 1–2 mm pieces; 2 pieces per well were cultured in 12-well plates at 37°C, 5% CO_2 and 99% humidity. On reaching confluence, cells were washed with PBS, trypsinized with 0.05% trypsin-EDTA (Invitrogen) and passaged into T75 flasks. Upon confluency, cells were stored in freezing media containing 90% FBS and 10% dimethyl sulfoxide in a liquid nitrogen freezer then thawed, plated, and expanded as needed in T75 flasks. Five cell lines from five different individuals were utilized (Table 2.1).

Table 2.1. Cell lines used in the study

cMSC line	Sex	Age (months)	Primary tissue
1	M	12	Calvarial bone
2	F	2	Calvarial bone
3	M	9	Calvarial bone
4	M	7	Calvarial bone
5	M	4	Calvarial bone

2.3.2. Calvarial MSC culture

cOB from cell lines were passaged 6 times in culture. Cells were then sorted using FACS Aria II, gated for size and singlets for CD73, CD90, CD105, CD29 positivity and CD34 negativity (Fig. 2.1). Next, the cells were expanded and grown in 5 µg/ml fibronectin-coated culture flasks in StemXVivo serum-free (SF) media (R&D Systems). Cells were incubated at 37°C with 5% CO_2. At 90–100% confluence, cells were dissociated using TrypLE Express (Gibco), split 1:2, and replated.

2.3.3. BMMSCs culture

Adult human bone marrow-derived mesenchymal stem cell line (hMSCs, ATCC number: PCS-500-012) was cultured in 5 µg/ml fibronectin-coated culture flasks in StemXVivo serum-free (SF) media (R&D Systems). Cells were grown and incubated at 37°C with 5% CO_2 and TrypLE Express (Gibco) was used for cell detachment.

2.3.4. Immunophenotypic analysis

FACS staining was performed using standard methods (82-84). Surface antigens on three different cMSCs and BMMSCs were analyzed after 3 passages in SF medium. Cells were dissociated using TrypLE Express (Gibco); cell suspensions were centrifuged at 300 g for 5 min and washed 2x with staining buffer of 5% FBS in PBS. Then cells were stained with fluorescent-conjugated antibodies against CD73, CD90, CD105, CD29, CD44, CD34, CD31 and CD45 (BD Biosciences). Cells were incubated in 100 µL of staining buffer containing antibodies for 30 min at 4°C in the dark, washed 2x and resuspended in 500 µL of staining buffer. Data were collected using an LSR II flow cytometer (BD Biosciences) and analyzed with flow cytometry software (FlowJo, Ashland, USA).

2.3.5. Multilineage differentiation in vitro

Three different cMSC lines and BMMSCs were differentiated into osteoblast, chondrocyte and adipocyte lineages using StemPro differentiation kits (Life Technologies Carlsbad, CA) according to manufacturer protocols (details below).

Adipogenic differentiation

Cells were seeded at 4×10^4 cells/cm^2 in triplicate and grown for 1 day before a change to differentiation medium for 14 days with medium exchange every 3 days. At the end, medium was removed, and the cells were washed 2x with PBS. Cells were then fixed with 10% formalin, incubated for 30 min at room temperature (RT) and rinsed with distilled H_2O (DH_2O). Next, 60% isopropanol was added for 5 min to cover the bottom of each well. The isopropanol was discarded, and the cells were stained for 5 min with Oil Red O working solution (3:2 dilution with DH_2O). Cells were washed with DH_2O until it ran clear, and hematoxylin counterstain was added

for 1 min. Cells were then rinsed with warm DH_2O, coverslipped and observed under the microscope for intracellular lipid droplets appearing red.

Chondrogenic differentiation

Cells were grown as high-density pellets (1×10^5 cells per well) in U-bottom 96-well plates for aggregate (micromass) formation. cMSC lines and BMMSCs were plated in triplicate and grown for 2 days, then switched to differentiation media that was changed every 3 days for 21 days. Cells were then rinsed with PBS, fixed with 4% formaldehyde solution for 30 min., rinsed again with PBS and stained with 1% Alcian blue solution in acetic acid (EMD Millipore) for 30 min. Cells were rinsed 3x with 3% acetic acid. Next, DH_2O was added to neutralize acidity and aggregates were visualized under a microscope for blue staining that indicates the synthesis of proteoglycans by chondrocytes.

Osteogenic differentiation

1×10^4 cells/cm^2 were seeded in triplicate. The cells were left to grow for 1 day before differentiation medium was added, with medium changes every 3 days. On day 28, cells were washed with PBS, fixed with 10% formaldehyde and incubated at RT for 15 min. Cells were then washed with DH_2O, stained with Alizarin red (Sigma-Aldrich) for 20 min at RT and washed 4x with DH_2O with gentle rocking for 5 min each wash. At the end, DH_2O was added to prevent cells from drying and for microscopic visualization and imaging. Differentiated cells containing calcium phosphate deposits stained bright red.

2.3.6. Osteogenic gene array analysis by qPCR

To examine the difference between cMSCs and BMMSC gene expression profiles by qPCR, RNA was isolated from five cMSC (additional two cell lines were considered) and BMMSC lines using an mRNA isolation kit (85). Then 1 µg of total RNA from each sample was reversed transcribed into cDNA using an RT^2 First Strand Kit (QIAGEN, Germantown, MD). Next, cDNA was combined with RT SYBR Green qPCR Mastermix (QIAGEN) into the Human Osteogenesis RT^2 Profiler PCR Array system (QIAGEN). qPCR was performed using the CFX96 Touch real-time PCR detection system (BioRad). The relative amount of each mRNA transcript normalized to the housekeeping gene beta-2 microglobulin (B2M) was calculated using the $2^{-\Delta\Delta C}{}_T$ method. Out of 84 tested genes, we only considered genes that were concurrently upregulated or downregulated in all 5 cMSC cell lines. Genes were further filtered, as we only classified genes that demonstrated a log2 (fold change) of ≥2 in at least 3 of the 5 cell lines.

2.3.7. Statistical analysis

Values were expressed as mean ± standard error of the mean and analyzed with a one-sample *t*-test using SPSS Statistics (IBM). Differences with p-values <0.05 were considered statistically significant.

2.4. Results

2.4.1. Isolation, Characterization and Differentiation potential of primary cMSCs and BMMSCs

We successfully isolated primary human calvarial cMSCs from a heterogeneous population of human osteoblasts using FACS (Figure. 2.1). Analysis of immunophenotypes indicated uniform expression of the classic positive and negative MSC markers: >97% of the cells

expressed CD73, CD90, CD105, CD29 and CD44 and <5% had minimal expression of the MSC-negative hematopoietic markers CD31, CD45 and CD34 (Fig. 2.2). These immunophenotypic characteristics are consistent with established ISCT parameters and similar to reported surface antigen expression in various types of MSCs including BMMSCs and periosteal MSCs (65, 73, 77, 81).

Osteogenic induction led to bone formation as indicated by Alizarin red staining (Fig. 2.3, A–D). Chondrogenic differentiation conducted on MSC micro-masses led to cartilage formation indicated by Alcian blue staining (Fig. 2.3, E–H). Successful adipogenic induction was demonstrated in the formation and accumulation of lipid droplets revealed by Oil Red O staining (Fig. 2.3, I–L). The differentiation results suggest that our cMSCs have similar differentiation potential to BMMSCs. In summary, isolated cMSCs demonstrated the criteria for MSC progenitor cells by adhering to plastic in culture, expressing the requisite surface markers and having multilineage differentiation potential.

2.4.2. Osteogenic array gene profiling

Quantitative PCR revealed significant differences in the expression of 47 genes: 30 genes were upregulated and 17 were downregulated consistently in the cMSC lines. Notably, the data showed that most of the genes involved in MSC maintenance and proliferation were expressed at higher levels in cMSCs compared with BMMSCs. In contrast, genes that mediate commitment to osteogenic lineages and differentiation had lower expression in cMSCs. To further elucidate the gene expression pattern of cMSCs, we organized the genes by biological function and signal transduction pathways. The 47 identified genes were ECM molecules, growth factors, mediators of TGFβ and BMP signaling pathways, as well as bone developmental genes involved in MSC proliferation, and osteoblast differentiation (86, 87). ECM molecules that

are known to be highly expressed in MSCs and the suture mesenchyme were upregulated in cMSCs relative to BMMSCs (Fig. 2.4, A; Table 2.2) (88-93). ECM genes associated with osteoblast differentiation (*CD36* and *PHEX*), however, were downregulated in cMSCs compared with BMMSCs (94, 95).

Two growth factors, *VEGFA* and *PDGFA*, that enhance bone growth (96-99) were also downregulated in cMSCs compared with BMMSCs (Fig. 2.4, B; Table 2.3). Our analysis further demonstrated that TGFβ members specific for proliferation and regeneration (86, 100) were upregulated in cMSCs, while those controlling osteogenic differentiation (e.g., *TGFβ3*, *SMAD3*) (86, 87) were downregulated relative to BMMSCs (Fig. 2.4, C; Table 2.4).

BMPs involved in bone development were differentially expressed between cMSCs and BMMSCs (Fig. 2.4, D; Table 2.5). Notably, genes that maintain MSCs and suppress osteogenesis (e.g., *BMPR2, BMPR1B*) had high expression in cMSCs compared with BMMSCs (101-104). In contrast, genes that influence late stages of osteoblastic development had lower expression in cMSCs compared with BMMSCs (e.g., *BMP6, BMPR1*) (102, 105, 106). Moreover, the expression of genes that promote proliferation and maintain MSC multipotency had a higher expression in cMSCs compared with BMMSCs: *NFKB1, EGF, ANXA5, MMP2, CDH11,* and *CSF1* (Fig. 2.4, E; Table 2.6). In contrast, genes known for their involvement in osteoblast differentiation and mineralization (*SP7, IGF1R, BGLAP,* and *RANKL*) had a lower expression in cMSCs compared with BMMSCs (Fig. 4, F; Table 2.7).

Noteworthy genes that are essential to bone maturation were differentially expressed in cMSCs compared with BMMSCs (Fig. 2.4, G; Table 2.8). We found an upregulation in the expression of osteoblast gene markers (*FGF2, RUNX2,* and *COL1A1*) associated with initial osteoprogenitor proliferation and differentiation in cMSCs compared to BMMSCs. In contrast, two genes that maintain MSC progenitors and bone homeostasis were downregulated in cMSCs compared to BMMSCs (*GLI1* and *TWIST1*).

2.5. Discussion

In this study, we demonstrated an effective, reproducible method to isolate primary calvarial MSCs from heterogeneous cell populations derived from human calvarial explants. Our goal was to isolate and expand human cMSCs in an efficient, consistent, and reproducible way. Therefore, we utilized SF medium for cMSC cultivation. As far as we know, our study provides the first description of FACS-isolated human cMSCs grown in SF medium. cMSCs grown in SF medium demonstrated higher proliferation rate and higher expression of embryonic stem cell markers compared to MSCs grown in serum-containing media (107). Although Media containing FBS supports MSCs' expansion and proliferation, it promotes heterogeneity and variability in cell growth and differentiation of MSCs (108, 109).

Calvarial bone formation is a multiplex process involving MSC proliferation and differentiation to osteoblasts via intramembranous ossification (7, 12, 110). We chose BMMSCs for the comparison with cMSCs because bone marrow is the main source of MSCs available for research (111). Also, their multipotency, self-renewal and regenerative potential have been described and studied in bone repair and tissue engineering (112-115). Our gene expression data suggest that cMSCs have enhanced capacity for proliferation and regeneration as well as a unique expression profile when compared with BMMSCs. These findings could provide a foundation for understanding cMSCs and intramembranous ossification in the calvaria.

We further investigated the function of the expressed genes in cMSCs relative to BMMSCs. We reviewed these genes in terms of their role in MSC maintenance and bone development. cMSCs maintained higher expression of ECM molecules that drive important biological functions in MSCs and are key regulators in cytoskeletal organization: (*ITGA2, ITGA3, ICAM1, COL1A2, COL10A1, COL3A1, COL15A1, BGN, FN1, FLT1*). *ITGA2, ITGA3* and *ICAM1* were shown to upregulate the expression of MSC markers and increase cellular proliferation (89, 90, 92, 93). Moreover, *COL1A2, COL3A1, COL15A1, BGN* and *FN1* are abundant in

cMSCs and osteoprogenitors (116-122). MSCs are also known to induce angiogenesis through secretion of cytokines including *FLT1* (*VEGFR1*) (123). VEGF signaling governs bone regeneration through inhibiting bone formation and *FLT1* expression (124).

Taken together, a high level of expression was observed in ECM molecules that support proliferation and MSC maintenance. These findings confirm previous reports of MSC properties and strongly suggest the stemness and undifferentiated features of cMSCs.

Moreover, TGFβ members specific for proliferation and regeneration were upregulated in cMSCs compared to BMMSCs. *TGFβ1, TGFβR2, BMPR1B*, and *BMPR2* are expressed in MSCs and play a critical role in MSC maintenance, proliferation, and regeneration (50, 51, 125-127). *TGFβR2* has been reported to specifically regulate and maintain MSCs (127-129). Previous studies are consistent with our observation as high expression of BMPR2 and *BMPR1B* was found in stem cells (101). These data and our present study strongly indicate the enhanced proliferation and suppressed differentiation behavior of the cMSC population.

An additional set of genes that regulate bone homeostasis were highly expressed in cMSCs compared with BMMSCs (*NFKB1, EGF, ANXA5, MMP2, CDH11* and *CSF1*). These genes are associated with proliferation, migration, and suppression of MSC differentiation to osteoblasts. *NFKB1* has been shown to repress the differentiation of osteoblasts. It also regulates the proliferation capability of osteoprogenitors and is downregulated in differentiated cells (130, 131). The upregulation of *EGF* expression induces *EGFR* signaling which results in inhibiting ALP activity and osteogenesis (126, 132). *ANXA5* is used to define multipotent homogenous human MSCs (51, 133, 134). *MMP2* is a key regulator in calvarial bone development and expressed in osteoprogenitors (135, 136). *CDH11* “osteoblast cadherin” is expressed in highly proliferative MSC and required for their migratory activity (116, 137). CSF1 is another gene involved in skeletal remodeling via osteoclastogenesis (138), and was upregulated in cMSCs compared to BMMSCs. *CSF1* manifests a role in regulating cell survival

and proliferation and has been expressed in multipotent and progenitor cells besides osteoclasts (139, 140).

Together, key genes playing essential roles in proliferation and maintaining suture mesenchyme were upregulated in cMSCs relative to BMMSCs. This suggests that cMSCs possess a discrete gene profile, reflecting their proliferative and regenerative potential. High proliferation in MSCs can contribute and stimulate repair in tissues (141, 142). Therefore, cMSCs could be used in therapy and tissue regeneration studies.

In support of this observation, genes known to promote osteogenic differentiation (*CD36, PHEX, VEGFA, PDGFA, TGFβ3, SMAD3, BMPR1A, BMP6, SP7, IGF1R,* and *BGLAP*) were downregulated in cMSCs compared to BMMSCs. *CD36* and *PHEX* enhance osteogenesis by inducing the expression of *SP7, BGLAP* and *BSP* (85, 94, 95, 143-145). Furthermore, Growth factors (e.g., *VEGFA, PDGFA*) function robustly during bone formation and are known to enhance osteoblast proliferation and differentiation (96-99).

TGFβ members controlling osteogenic differentiation (e.g., *TGFβ3, SMAD3*) were downregulated in cMSCs in comparison to BMMSCs. *TGFβ3* promotes osteogenesis via positively regulating *PDGFRA* expression. Consistent with our findings, *TGFβ3* downregulation in MSCs was confirmed in previous studies (86, 100) . It has been shown that *SMAD3* induces differentiation via enhancing *ALP, RUNX2* and *BGLAP* expression in mouse osteoblastic MC3T3-E1 cells (87).

BMP signaling molecules have been shown to be critical in osteogenic potential (126, 127). Both *BMPR1A* and *BMP6* were underexpressed in cMSCs compared with BMMSCs. *BMPR1A* influences late-stage bone development and osteoblastic activity (102, 126). It has been shown that *BMPR1A* induces *Sclersostin (SOST1)* to regulate bone mass through WNT signaling (146). Also, *BMP6* is known to promote bone formation via enhancing differentiation (105) and a

positive correlation has been reported between *BMP6* and *SP7* (147). Both *BMP6* and *SP7* are downregulated in cMSCs compared with BMMSCs.

Well-established genes of initial and late osteogenic differentiation (*IGF1R, SP7,* and *BGLAP*) were downregulated in cMSCs compared with BMMSCs. IGF1R activation promotes osteogenesis and is critical for bone formation (148). *SP7* is a well-established osteogenic gene and is essential for bone development; it demonstrates a role in specifying MSCs commitment toward osteoblastic lineage (19, 149). Moreover, it regulates the expression of osteoblast differentiation and matrix mineralization genes such as *COL1A1*, *BGLAP*, *SPP1*, *SPARC*, and *RUNX2* (150-152). *BGLAP* is a late osteogenic marker expressed by mature osteoblasts during mineralization and it makes up 20% of the total proteins in the bone (153-155).

Simultaneous to *IGF1R, SP7,* and *BGLAP* downregulation, we found upregulation of early osteogenic markers (*RUNX2, FGF2* and *COL1A1*) that are expressed in osteoprogenitors and preosteoblasts. *RUNX2* regulates the proliferation of MSCs and osteoprogenitors in the sutures and is vital for osteoblast differentiation and calvarial bone development (156-158). *RUNX2* is also coexpressed with *FGF2* and positively regulates *COL1A1* (100, 159). Yet, the expression of *COL1A1* is not unique to mature osteoblasts or differentiated cells. A similar result to our study showed that *COL1A1* expression is induced in undifferentiated cMSCs (160) and high expression of *COL1A1* has been reported in undifferentiated cranial suture-associated dural cells (161).

Since most of the genes involved in MSC maintenance and proliferation were upregulated in cMSCs compared to BMMSCs, we expected to see an upregulation in the expression of *TWIST1* and *GLI.* In contrast, we found a downregulation in the expression of *TWIST1* and *GLI1* in comparison to BMMSCs. Both *TWIST1* and *GLI1* play an essential role during calvarial development. They maintain the cranial suture mesenchyme and inhibit osteogenesis in the suture (162, 163). The results suggest that the expression of these two genes might be different

in our cMSC population although we cannot explain their downregulation. Conceivably, *GLI1* could promote osteogenesis by driving the commitment of osteoprogenitors toward bone (164-166). In addition to that, a recent study has shown that *TWIST1* postnatal expression is not required in MSCs to maintain the cranial suture and prevent suture fusion (163).

Taken together, our results exhibit a unique model of human cranial MSCs that can advance study of calvarial development in vitro. We demonstrated that a homogenous population of cMSCs can be efficiently isolated from infant calvarial explant culture. To our knowledge, no previous studies have reported the FACs isolation of human cMSCs, nor conducted a comparison of primary cMSCs and BMMSCs. This work presents a thorough characterization of the genetic expression profile, phenotype, and differentiation capacity of human cMSCs. These cells exhibit a higher proliferative and stemness potential than BMMSCs suggested by the expression of genes essential for regeneration, MSC matrix production and maintenance, which suggest a capability to support tissue regeneration and calvarial tissue homeostasis. Thus, cMSCs can serve as a powerful tool and highly relevant model for studying and understanding cranial suture formation, cranial bone development and craniofacial bone-related diseases.

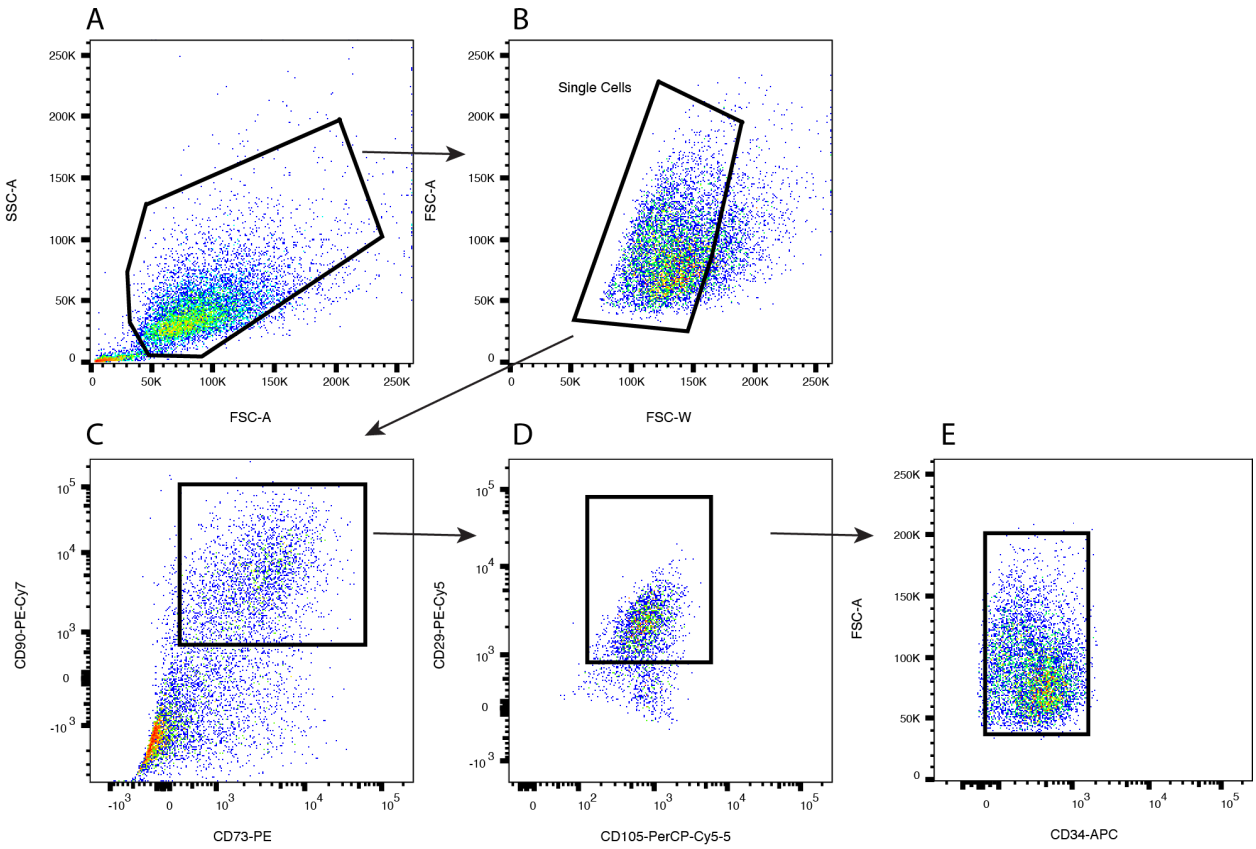

Figure 2.1. Marker expression and isolation by FACS
Gating strategy applied to isolate human cMSCs. Total cells were first gated on a forward scatter (FSC)/side scatter (SSC) (A), then gated on single cells (B). These were then further gated for the markers CD73+, CD90+ (C), CD105+, CD29+ (D) and CD34- cells (E).

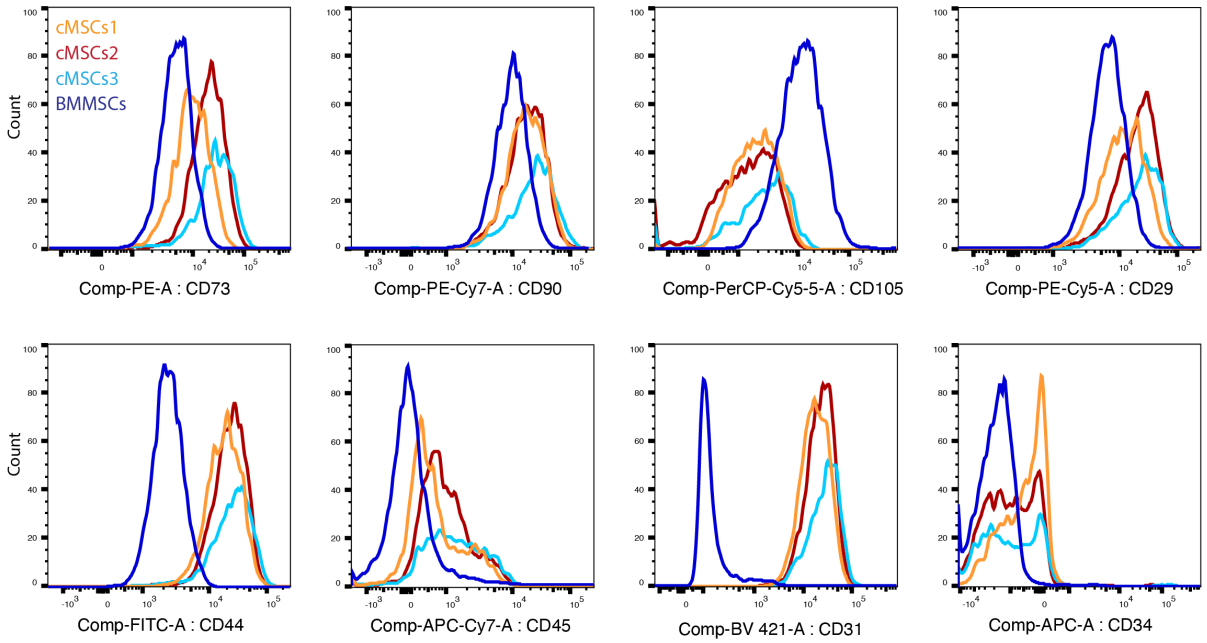

Figure 2.2. Characterization of cell surface markers of three different human cMSCs (cMSCs1: orange, cMSCs2:red, cMSCs3:cyan) and bone-marrow derived human mesenchymal stem cells (BMMSCs-blue) using flow cytometry (at passage 3). The following markers were used to define cMSCs and BMMSCs: CD73, CD90, CD105, CD29, CD44, CD34, CD31, and CD45.

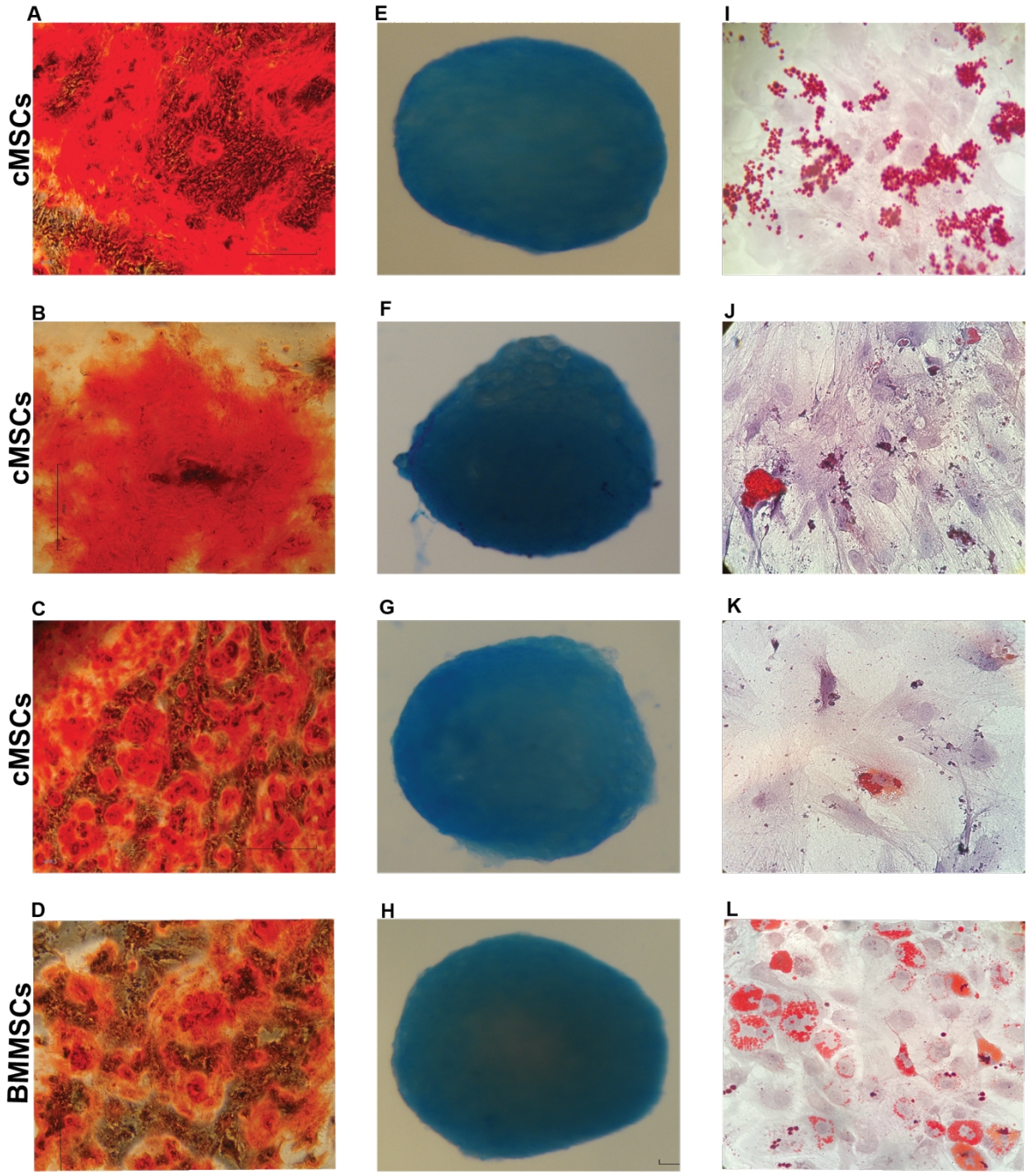

Figure 2.3. Trilineage differentiation potential of three human cMSCs and BMMSCs after passage 3. A, B, C, D: Osteogenic differentiation of cMSCs and BMMSCs, respectively, showed extensive production of calcium deposits after 28 days. Mineralized nodules stained with Alizarin red (10x). E, F, G, H: Chondrogenic-induced cMSCs for 21 days, respectively, stained with Alcian blue (20x). I, J, K, L: Adipogenic differentiation of cMSCs and BMMSCs was confirmed by the formation of lipid droplets after 2 weeks of induction, detected by Oil Red O staining (40x). Phase contrast microscopy was utilized for imaging (A-L).

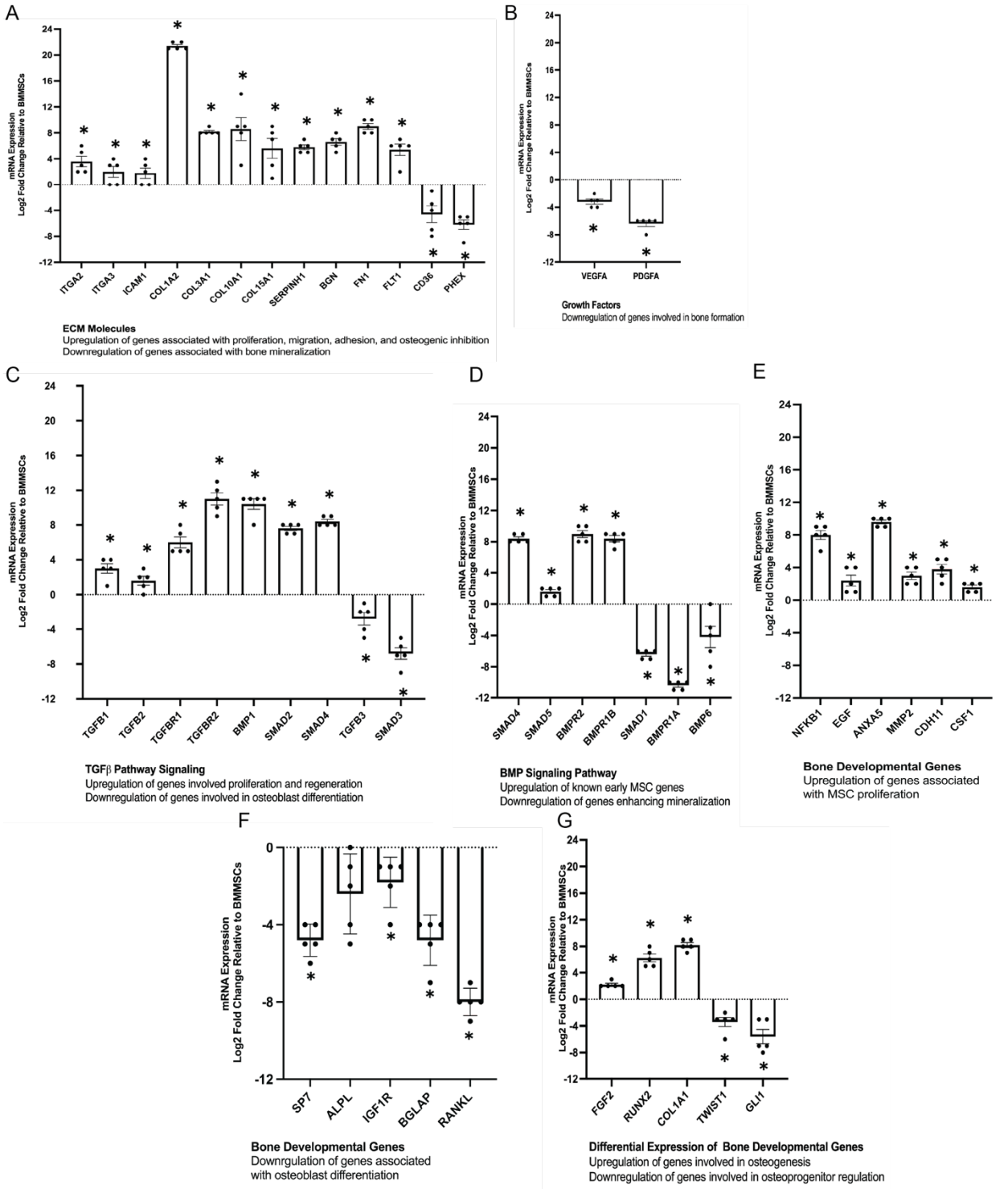

Figure 2.4. Gene expression profiles of cMSCs in comparison with BMMSCs. cMSCs and BMMSCs were cultivated with serum free (SF) media and analyzed by qPCR array for the expression of 47 genes involved in bone development and grouped into: (A) ECM molecules, (B) growth factors, (C) TGFβ signaling pathway, (D) BMP signaling pathway, (E) genes associated with MSC proliferation, (F) Genes associated with osteoblast differentiation, and (G) differential expression of bone developmental genes. B2M was used as the reference gene, and the corresponding BMMSCs were used as control groups n = 5, *p<0.05. Each data point represents an individual cMSC line.

Table 2.2. Expression of ECM Molecules

Gene Symbol	Gene Name	Log2 Fold Change					
		cMSC 1	**cMSC 2**	**cMSC 3**	**cMSC 4**	**cMSC 5**	**P-Value**
ITGA2	Integrin Subunit Alpha 2	6	2	2	5	3	0.009*
ITGA3	Integrin Subunit Alpha 3	4	0	3	3	0	0.06
ICAM1	Intercellular Adhesion Molecule 1	3	2	0	4	0	0.04*
COL1A2	Collagen Type I Alpha 2	22	21	21	22	21	1.9 E-7*
COL3A1	Collagen Type III Alpha 1	8	9	8	8	8	0.000006*
COL10A1	Collagen Type X Alpha 1	8	9	3	14	9	0.006*
COL15A1	Collagen Type XV Alpha 1	8	1	3	9	7	0.02*
SERPINH1	Serpin Family H Member 1	6	7	5	6	5	0.0001*
BGN	Biglycan	7	5	6	7	8	0.0001*
FN1	Fibronectin 1	10	8	9	10	8	0.00002*
FLT1	Fms Related Receptor Tyrosine Kinase 1	6	6	6	7	2	0.004*
CD36	CD36 molecule	-3	-7	-4	-1	-8	0.02*
PHEX	Phosphate Regulating Endopeptidase Homolog X-Linked	-5	-6	-5	-6	-9	0.001*

Significant alterations in several genes consistently observed by five different MSCs derived from human calvaria (cMSCs) relative to Bone marrow-derived human mesenchymal stem cells (BMMSCs). Upregulation and downregulation of two log2 folds in 3 cMSCs lines at least was observed in ECM molecules.
*$p < 0.05$ vs. BMMSCs.

Table 2.3. Expression of Growth Factors

Gene Symbol	Gene Name	Log2 Fold Change					
		cMSC 1	**cMSC 2**	**cMSC 3**	**cMSC 4**	**cMSC 5**	**P-Value**
VEGFA	Vascular Endothelial Growth Factor A	- 3	-2	- 3	- 4	- 4	0.0003*
PDGFA	Platelet Derived Growth Factor Subunit A	-6	- 8	-6	- 6	- 6	0.00007*

Significant alterations in several genes consistently observed by five different MSCs derived from human calvaria (cMSCs) relative to Bone marrow-derived human mesenchymal stem cells (BMMSCs). Upregulation and downregulation of two log2 folds in 3 cMSCs lines at least was observed in ECM molecules.
*$p < 0.05$ vs. BMMSCs.

Table 2.4. Expression of genes mediating TGF*β* pathway

Gene Symbol	Gene Name	Log2 Fold Change					
		cMSC 1	**cMSC 2**	**cMSC 3**	**cMSC 4**	**cMSC 5**	**P- value**
TGFβ1	Transforming Growth Factor Beta 1	4	1	3	4	3	0.009*
TGFβ2	Transforming Growth Factor Beta 2	3	2	1	2	0	0.02*
TGFβR1	Transforming Growth Factor Beta Receptor 1	7	5	5	8	5	0.0004*
TGFβR2	Transforming Growth Factor Beta Receptor 2	12	9	13	11	10	0.00004*
BMP1	Bone Morphogenetic Protein 1	11	8	11	11	11	0.0004*
SMAD2	Smad Family Member 2	8	7	8	8	7	0.000004*
SMAD4	Smad Family Member 4	9	8	8	9	8	0.000008*
TGFβ3	Transforming Growth Factor Beta 3	-2	-5	-2	-1	-4	0.01*
SMAD3	SMAD Family Member 3	-6	-9	-5	-7	-7	0.0005*

Significant alterations in several genes consistently observed by five different MSCs derived from human calvaria (cMSCs) relative to Bone marrow-derived human mesenchymal stem cells (BMMSCs). Upregulation and downregulation of two log2 folds in 3 cMSCs lines at least was observed in bone developmental genes.
*$p < 0.05$ vs. BMMSCs.

Table 2.5. Expression of genes mediating BMP pathway

Gene Symbol	Gene Name	Log2 Fold Change					
		cMSC 1	**cMSC 2**	**cMSC 3**	**cMSC 4**	**cMSC 5**	**P- value**
SMAD4	Smad Family Member 4	9	8	8	9	8	0.000008*
SMAD5	Smad Family Member 5	2	1	2	2	1	0.001*
BMPR2	Bone Morphogenic Protein Receptor Type 2	10	8	9	10	8	0.0003*
BMPR1B	Bone Morphogenic Protein Receptor Type 1 B	9	9	7	9	8	0.00003*
SMAD1	SMAD Family Member 1	-6	-7	-6	-6	-7	0.000025*
BMPR1A	Bone Morphogenetic Protein Receptor Type 1A	-10	-11	-10	-10	-11	0.0002*
BMP6	Bone Morphogenetic Protein 6	-3	-8	-6	-4	0	0.03*

Significant alterations in several genes consistently observed by five different MSCs derived from human calvaria (cMSCs) relative to Bone marrow-derived human mesenchymal stem cells (BMMSCs). Upregulation and downregulation of two log2 folds in 3 cMSC lines at least was observed in bone developmental genes.
*$p < 0.05$ vs. BMMSCs.

Table 2.6. Expression of Bone Developmental Genes Correlated with MSC Proliferation

Gene Symbol	Gene Name	Log2 Fold Change					
		cMSC 1	**cMSC 2**	**cMSC 3**	**cMSC 4**	**cMSC 5**	**P- value**
NFKB1	Nuclear Factor Kappa B Subunit 1	9	6	8	9	8	0.0001*
EGF	Epidermal Growth Factor	4	2	1	4	1	0.03*
ANXA5	Annexin A5	10	10	9	10	9	0.000009*
MMP2	Matrix Metallopeptidase 2	4	2	2	4	3	0.002*
CDH11	Cadherin 11	5	2	3	5	4	0.004*
CSF1	Colony Stimulating Factor 1	2	1	2	2	1	0.001*

Significant alterations in several genes consistently observed by five different MSCs derived from human calvaria (cMSCs) relative to Bone marrow-derived human mesenchymal stem cells (BMMSCs). Upregulation and downregulation of two log2 folds in 3 cMSC lines at least was observed in bone developmental genes.
*$p < 0.05$ vs. BMMSCs.

Table 2.7. Expression of Bone Developmental Genes Correlated with Differentiation and Mineralization

Gene Symbol	Gene Name	Log2 Fold Change					
		cMSC 1	**cMSC 2**	**cMSC 3**	**cMSC 4**	**cMSC 5**	**P- value**
SP7	Osterix	-5	-4	-6	-4	-5	0.0007*
IGF1R	Insulin Like Growth Factor 1 Receptor	-1	-4	-2	-1	-1	0.02*
BGLAP	Osteoclacin	-4	-7	-4	-4	-5	0.0009*
TNFSF11/ RANKL	TNF Superfamily Member 11	-8	-8	-9	-7	-8	0.00001*

Significant alterations in several genes consistently observed by five different MSCs derived from human calvaria (cMSCs) relative to Bone marrow-derived human mesenchymal stem cells (BMMSCs). Upregulation and downregulation of two log2 folds in 3 cMSC lines at least was observed in bone developmental genes.
*$p < 0.05$ vs. BMMSCs.

Table 2.8. Expression of Bone Developmental Genes Mediating Osteoblast Differentiation

Gene Symbol	Gene Name	Log2 Fold Change					
		cMSC 1	**cMSC 2**	**cMSC 3**	**cMSC 4**	**cMSC 5**	**P- value**
FGF2	Fibroblast Growth Factor 2	3	2	2	2	2	0.001*
RUNX2	Runt Related Transcription Factor 2	7	5	5	8	6	0.002*
COL1A1	Collagen Type I Alpha 1	9	7	8	9	8	0.00003*
TWIST1	Twist Family BHLH Transcription Factor 1	-3	-6	-2	-3	-3	0.007*
GLI1	GLI Family Zinc Finger 1	-3	-8	-7	-3	-7	0.004*

Significant alterations in several genes consistently observed by five different MSCs derived from human calvaria (cMSCs) relative to Bone marrow-derived human mesenchymal stem cells (BMMSCs). Upregulation and downregulation of two log2 folds in 3 cMSC lines at least was observed in bone developmental genes.
*$p < 0.05$ vs. BMMSCs.

3. Rare FLNA Variant' Effects on Proliferation and Osteogenesis and Cell Mechanics, and FLNA Knockout effect on Osteogenesis

3.1. FLNA Background

3.1.1. FLNA Structure and biological function

The cytoskeleton is a dynamic, active network in the cytoplasm of both prokaryotic and eukaryotic cells. It influences the mechanical properties, strength, shape, cellular transport, organization of organelles, as well as movement of the cell and other biochemical properties within the cell. The cytoskeleton is composed of three main elements: microtubules, intermediate filaments, and actin filaments (167). Actin filaments (F-actins) are the thinnest cytoskeletal structure and are made of globular actin (G-actin) monomers, which are 42 kD proteins that polymerize to form the actin filaments in a helical structure (168, 169). The actin filaments are held together, crosslinked, and depolymerized by crosslinking (actin-binding) proteins that include spectrin, fimbrin, alpha-actinin, and filamins A, B, and C. All these proteins harbor an actin binding domain (ABD), extended with rod-like segments. Spectrin, fimbrin, and alpha-actinin arrange actin filaments into parallel bundles, whereas filamins cross-link actin filaments to form loose three-dimensional orthogonal networks in a V-shaped organization (168, 170, 171).

Filamin protein was first discovered in 1975 by Wang et al. in an attempt to isolate myosin from chicken smooth muscle (172). The human filamin family is composed of 3 isoforms (filamin A, filamin B, and filamin C) which share 60–80% homology of their amino acid sequences (differing in the two hinge regions between repeats 15–16 and 23–24) and are each widely expressed during human embryonic development (168, 173). Filamin A (FLNA) was the first actin filament cross-linking protein discovered in non-muscle cells; it shows high expression throughout all tissues of the human body, and across species, and is the most abundant of the

filamin family (174-176).

Structurally, human FLNA is a 280 kDA elongated homodimeric protein (Figure. 3.1). The N-terminus consists of an F-actin binding domain that comprises two tandem calponin homology domains (CHD1 and CHD2). The two actin binding domains are not functionally interchangeable and CHD2 is required for the interaction with F-actin (177, 178). In addition, the FLNA structure consists of 24 homologous immunoglobulin like (Ig) repeats and two hinge regions. The two hinges are long and contain calpain cleavage sites, which provide flexibility. They allow the repeats to move and assist in conformational changes of the structure. Dimerization takes place in the C-terminal repeat. Each repeat has approximately 96 amino acid residues (168, 179-181). It has been shown that the first hinge region is fundamental in the viscoelasticity of actin filament networks; its loss leads to breakage and stiffening of the networks even under low stress. The hinge region before Ig repeat 24 has 35 residues and plays a role in dimerization; it is thought to be essential for other regulatory and mechanical functions in the cell cytoskeleton (168, 182, 183).

FLNA is considered a robust gelation factor because it creates a flexible elastic environment by cross-linking actin filaments. It regulates and affects cytoskeleton stability, cell polarization, cell shape, cell adhesion, and cell migration (184). A single FLNA dimer per G-actin molecule is adequate for cytoskeletal polymerization. (168, 170, 171). The organization of actin filaments relies on the molar ratio of filamin to actin, and increasing the ratio leads to a tighter actin filament network. Parallel bundles of actin filament networks are achieved by high filamin to actin ratios (1:10 to 1:50) leading to stable bundles in adherent cells, which are necessary for contractility. Orthogonal cytoskeletal networks are created by ratios of 1:150 to 1:740 resulting in stiffness of the cytoskeleton (185-187). Overall, it has been reported that FLNA can rearrange the cytoskeleton using various means of interacting with more than 90 diverse proteins that are essential in cell signaling. These interactions can be carried out via different mechanisms involving phosphorylation, competition among partners, mechanical forces, and others (168,

173, 181, 188-192). FLNA facilitates the interaction of cells with the extracellular matrix (168). Additionally, FLNA binds integrin and regulates its signaling and interactions (193-195). Moreover, FLNA regulates transcriptional activities positively and negatively. It can prevent some transcription factors from entering the nucleus and being activated, such as regulating the transcriptional activity of *FOXC1*. This interaction can also cause *FLNA* to bind other transcription factors in the nucleus (196, 197).

Cell motility and migration are key features of the cellular mechanics influenced by the interactions between the cytoskeleton and other components of the cytoplasm. The existence and abundance of FLNA in the cytoplasm and cytoskeleton can initiate or restrict processes by interacting with partner proteins and regulating actin filaments (191). These processes involve cytoskeletal remodeling, motility, protrusion, retraction, spreading, and integrin signaling (191). FLNA also functions as a mechanical protector in the cell from shear stress via mediating the distribution of stress across the actin filament networks (198). When external force is applied, the stiffness of the FLNA-F-actin network increases to prevent cell death (199).

Most eukaryotic cells move and migrate in an integrin-dependent way (200-202). FLNA Ig repeats are uniquely positioned to bind beta chains of both integrins and F-actin; exposing integrins to mechanical force leads to FLNA and F-actin recruitment to form focal adhesions (184, 191, 203, 204). Integrins are the major transmembrane adhesion receptors, and they interact with FLNA via multiple cytoplasmic tails of β-integrins. Integrin β1 binds to FLNA repeat 21–24 to regulate cellular motility (205, 206). Integrin β2 binds to FLNA repeat 21 to promote leukocyte extravasation (207), whereas integrin β7 binds FLNA on Ig repeats 19–21 to regulate the migration and homing of lymphocytes (208). FLNA binding to integrins must be balanced, as this process is simultaneously modulating cell signaling, polarization, protrusion, motility, and migration—bonds that are too strong might impair cell migration, for example. It has been reported that by blocking β1-integrins, cell spreading and FLNA localization in cell extensions are reduced. Similarly, low levels of FLNA decrease the expression of endogenous β1-integrins

in the cell; decreased FLNA expression also diminishes the binding of collagen to β1-integrins (184, 191, 206, 209, 210).

FLNA–integrin interactions also facilitate integrin binding with other ligands from the extracellular matrix. Proteins such as migfilin and talin compete for FLNA and integrin binding sites. Thus, to achieve normal movement in the cells, regulation of ligand binding affinity is required of FLNA to integrin, migfilin to FLNA, and talin to integrin. It has been shown that excessive binding of FLNA to integrins β7 and β1A reduces cell migration, yet the adhesion and fibronectin matrix organization remain unaltered (191, 208, 211-213).

Furthermore, the role of FLNA in migration has been widely demonstrated and studied in a variety of cells. By degrading FLNA, filamin A-interacting protein (FILIP) regulates neuronal migration and cell polarity exclusively in the ventricular zone of the developing cortex (189, 214). In melanoma cells, *FLNA* deficiency has been shown to lead to reduced cell polarization and motility, an effect that can be rescued in vivo by addition of exogenous FLNA (202, 215-217). Neurons that lack *FLNA* also fail to migrate within the cerebral cortex (202, 218). In melanoma cells, *WNT5a* knockdown decreased *FLNA* expression and corresponded to reduced cell motility (219, 220). In *Dictyostelium discoideum* amoebae, a diminished *FLNA* level impaired locomotion and chemotaxis (221). In contrast, high levels of *FLNA* can also inhibit neural migration (189, 222).

Moreover, numerous studies have reported the role of *FLNA* in signaling transduction during migration and other regulatory processes in the cytoskeleton. It has been confirmed that the Rho family of small GTPases (Rac1, Cdc42, RalA, and RhoA) organize the cytoskeleton (223, 224). They are activated when integrins bind extracellular matrix ligands, which in turn leads to actin polymerization by FLNA (223, 224). In *FLNA*-null monocytes, the dynamic of the actin cytoskeleton and migration is impaired when the function of the small GTPases is abolished (224). More specifically, Rho GTPases rely on FLNA for signal transduction via binding the 23rd repeat of FLNA (181, 224-226). Furthermore, FLNA carries out essential cellular

functions by reacting with GTPases and their upstream factors (Trio, Lbc, FilGAP, RhoGAP) and downstream factors (ROCK, PAK1). For example, the interaction of FLNA with RalA in the cytoskeleton is essential for filopodial protrusion; similarly, ruffling of the cell membrane is mediated by FLNA interaction with PAK1. FLNA also interacts with FilGAP to inactivate Rac and CDC42, which promote cell retraction (190, 191, 225, 226).

3.1.2. Role of FLNA in bone development and cell mechanics

FLNA regulates TGF-β signaling by inducing phosphorylation and nuclear accumulation of SMAD2 and SMAD5. This phosphorylation leads to SMAD-mediated signaling which is essential for TGF-β signaling. *FLNA*-deficient human melanoma cells (i.e., M2 cells) have impaired TGF-β signaling; the deficiency was shown to be due to decreased SMAD2 phosphorylation. By transfecting the M2 cells with *FLNA*, however, TGF-β activity was restored (227).

TGF-β and BMP signaling play a main role in skeletal development, as both are indispensable in transcriptional regulation of osteogenic genes, and postnatal bone homeostasis (228, 229). TGF-βs and BMPs transduce signals to both the canonical SMAD-dependent signaling pathway, which includes BMP ligands and SMADs, and to the noncanonical-SMAD-independent signaling pathway, which includes p38 mitogen-activated protein kinase (MAPK14). MAPK14 regulates mesenchymal stem cell differentiation during skeletal development, bone formation, and bone homeostasis.

Both the SMAD and MAPK14 signaling pathways regulate transcription factors. For instance, they regulate *RUNX2* to promote osteoblast differentiation and chondrocyte differentiation of mesenchymal precursor cells. In bone formation, SMAD2 and SMAD3 respond to TGF-β and regulate TGF-β-mediated osteoblast and chondrocyte differentiation by interacting with SMAD4. TGF-β, BMPs and other binding factors induce phosphorylation of TGF-β

receptors leading to SMAD2/3 (Co-SMAD) phosphorylation. Then, phosphorylated Co-SMADs interact with SMAD4, and the entire complex (SMAD2/3/4) translocates to the nucleus to regulate gene transcription, including *RUNX2* inhibition (227, 230, 231). The BMP pathway utilizes SMAD1 and SMAD5 to mediate the BMP signaling in endochondral bone development. The BMP pathway is also involved in osteogenic differentiation. Although SMAD8 is a minor contributor to skeleton development, combined loss of SMAD1, 5, and 8 results in severe chondrodysplasia (228, 232). On the other hand, the inhibitory SMADs (SMAD6 and SMAD7) can inhibit BMP and TGF-β signals in several ways: a) by blocking chondrocyte differentiation via inhibiting SMAD1/5/8 and b) by inducing *RUNX2* degradation, which inhibits osteoblast differentiation. Thus, chondrocyte-specific Smad6 overexpression transgenic mice manifest with dwarfism, osteopenia, and delayed chondrocyte hypertrophy because of Smad1/5/8 signaling inhibition (228, 233). In all, *FLNA* affects essential proteins for endochondral ossification, which coordinate the growth of the skeleton.

In contrast, calvarial bones are formed by intramembranous ossification. MSCs in the calvaria directly differentiate to osteoblasts to produce bone matrix (234). *FLNA* contributes to calvarial bone development via mediating *FOXC1* transcriptional regulation when it transfers PBX1 into the nucleus and forms the FOXC1–PBX1 transcription-inhibitory complex (191, 196). *FOXC1* is primarily expressed in the calvaria and plays a pivotal role early in craniofacial development by regulating the initial stages of proliferation and differentiation of osteoprogenitor and chondrogenic cells as well as the meningeal tissue (235, 236). *FOXC1* expression precedes the onset of osteogenic differentiation, and its expression levels lessen progressively with the maturation of the bone matrix (235, 236). In mouse myoblasts, heterologous expression of *FOXC1* during differentiation results in differentiated osteoblasts with increased *MSX2* and *RUNX2* levels, which are considered to be early osteogenic markers. In contrast, the transcription factors *SP7*, *DLX5*, and *BGLAP*, which appear later in the differentiation process, do not show any significant increase (237). Consistent with other studies, *FOXC1* expression is

limited to the early stages of bone formation and controls the proliferation of the osteoprogenitor cells, with limited influence on differentiation (238).

FOXC1 mediates BMP signaling by regulating the expression of *MSX2* and *ALX4* in the calvarial mesenchyme (236). Knockdown of *FOXC1* in mouse cranial neural crest cells results in upregulation of the osteogenic markers *ALP*, *RUNX2*, and *BGLAP*; thus, reduced *FOXC1* could enhance the osteogenic activity in the cranial osteogenic precursor cells within the cranial tissues. Moreover, phosphorylated SMAD1/5/8 complex, which is downstream of the canonical BMP pathway, was increased supporting enhanced osteogenesis (56).
All these reported findings about *FOXC1* clearly indicate and confirm the involvement of *FLNA* in osteogenesis through *FOXC1* regulation.

In the noncanonical WNT5a-ROR2 pathway, *FLNA* interaction has a crucial role in inducing polarized cell migration. ROR2 is widely expressed in the craniofacial region during embryonic development, and its interaction with *FLNA* is essential for cell migration. ROR2 releases intracellular calcium, which cleaves *FLNA*. This interaction leads to rearrangement of the cytoskeleton, which in turn causes cell motility via formation of filopodia and lamellipodia (239). In addition, it has been reported that by applying stretching and mechanical stress to periosteum-derived cells, signals for osteoblast differentiation and osteogenesis are activated through the WNT pathway, and further analysis by microarray demonstrated that *WNT5a*, *ROR2*, and *FLNA* expressions are upregulated. In addition, the activation of the JNK molecule (downstream of *ROR2* and *MKK4/ SEK* in *WNT5a* signaling) is regulated by *FLNA*. In melanoma cells, *WNT5a* knockdown decreased *FLNA* expression and corresponded to reduced cell motility (219, 220). In sum, *FLNA* is essential in *WNT5a/ROR2/JNK* signaling.

FLNA regulates androgen receptor (AR) activity (191, 240, 241). It has been elucidated that androgen stimulates cell migration and motility through interacting with *FLNA*. The FLNA-AR interaction recruits integrin β1, which regulates focal adhesion (242). The effect of *FLNA* on AR in bone development has been shown during BMMSC differentiation. AR promotes

osteogenesis in BMMSCs via regulating the expression of osteogenic genes such as *SP7*, *IBSP*, *COL1A1*, *COL2A1*, *DMP1*, and *AKP2* (243).

Together, these studies and data about the involvement of *FLNA*—in various decisive signaling mechanisms that prompt regulation of mesenchymal stem cells, osteoprogenitor cells, and osteoblasts in calvarial development—suggest that dysregulation of FLNA expression represent a paramount role in bone formation.

3.1.3. Association of FLNA mutations and Craniosynostosis

The prominence of *FLNA* and its versatile functions in cell regulation are reflected by its role in numerous diseases and syndromes. *FLNA* missense and null mutations result in developmental defects to the bone, brain, and heart in humans and other organisms. Gain of function *FLNA* mutations have been described in a series of craniofacial and bone dysplastic syndromes referred to as otopalatodigital spectrum disorders (OPDS). This umbrella category includes otopalatodigital syndrome (OPD) types I and II, frontometaphyseal dysplasia (FMD), and Melnick–Needles syndrome (MNS). These syndromes all manifest in craniofacial and bone dysplasia (191, 244, 245). Although these syndromes each have different overall spectra of features, they share several overlapping skeletal phenotypes. Typically, OPD type I consists of generalized bone dysplasia, cleft palate, prominent forehead, short stature, supraorbital ridges, long metacarpals, broad thumbs, big toes, and dislocation of hips and knees. OPD type II also manifests with these features, but the skeletal phenotypes are more severe. OPD type I is observed primarily in males, while OPD type II occurs in both males and females at equal rates (173, 245-248). FMD is characterized by generalized skeletal dysplasia, increased density of the diaphysis, and a pronounced supraorbital ridge; more males than females are affected (247-249). In contrast, MNS affects females primarily (173, 250, 251) and is characterized by generalized bone dysplasia with micrognathia, abnormal facial appearance, flared metaphysis

of the humerus, fibula, and tibia, disproportionately tall vertebral bodies, and bowing of the radius and tibia, resulting in an S-shaped appearance (173, 247, 248, 252).

FLNA mutations associated with these disorders are spread over FLNA Ig repeats (Figure. 3.1). OPD type I mutations have been described in the CHD2 (actin binding domain), whereas OPD type II occurs in the CHD2 and Ig repeat 14 and 15. FMD mutations are more widespread and known to be in the CHD2, Ig repeats 3, 9–10, 14–15, and 22–23, while substitutions in Ig repeat 10 lead to MNS (173, 177, 245, 253, 254).

Interestingly, while other craniofacial phenotypes, such as micrognathia, supraorbital hyperostosis, and down-slanting palpebral fissures, are common among all OPDS, craniosynostosis has only recently been reported as a feature in some rare cases. To our knowledge, craniosynostosis has been reported in seven cases of OPDS (Table. 3.1): 1) MNS with multisuture synostosis (bicoronal, bilambdoid, and posterior sagittal) located on Ig repeat 14, 2) OPD II with sagittal synostosis located on the CHD2, 3) FMD with bicoronal synostosis located on the CHD2, 4) FMD with pansynostosis located on Ig repeat 9, 5) FMD with sagittal and bilambdoid synostosis located on Ig repeat 9, 6) FMD with sagittal and metopic synostosis located on Ig repeat 15, and lastly 7) FMD reported in 2021 with panosynostosis (premature fusion of all cranial sutures) located on Ig repeat 10 (255-258).

Table 3.1. OPDS & Craniosynostosis

Diagnosis	Exon	Nucleotide Change	Amino Acid Change	Sex	Inheritance	Domain position	Domain's interaction	Suture	Reference
FMD	5	c.C759G	p. D253E	M	Maternal	CHD2	F-actin	Bilateral coronal	Robertson et al. 2006
OPD2	5	c.G760A	p.E254K	F	De novo	CHD2	F-actin	Sagittal	Fennel et al. 2015
FMD	22	c.G3394T	p.G1132W	F	De novo	Ig repeat 9	F-actin/FOXC1	Pansynostosis	Fennel et al. 2015
FMD	22	c.C3467T	p.P1156L	M	De novo	Ig repeat 9	F-actin/FOXC1	Sagittal Bilateral lambdoid	Fennel et al. 2015
MNS	28	C4738_4755+10deL28	-	F	De novo	Ig repeat 14	F-actin	Bilateral coronal Bilateral lambdoid Posterior sagittal	Foley et al. 2010
FMD	29	c.T5169G	p.C1723W	M	Maternal	Ig repeat 15	F-actin	Metopic	Fennel et al. 2015
FMD	22	c.C3557T	p.S1186L	M	Maternal	Ig repeat 10	F-actin	Pansynostosis	Kim et al. 2021

Mouse models with *FLNA* deficiency have been well described; heterozygosity in female mice causes mild skeletal abnormalities. In contrast, hemizygous male mice manifest with severe cardiovascular, skeletal, and palate defects (191, 259-261). Complete loss of *FLNA* in mice results in lethality, with severe bone and cardiovascular defects (192, 202, 260-262). Loss of *FLNA* has also been shown to cause developmental defects in Drosophila and C. elegans (202, 263).

In addition to skeletal malformations, cardiovascular phenotypes associated with *FLNA* mutations include a rare form of heart disease, myxomatous valvular dystrophy (XMVD), defined by mitral and aortic regurgitation as well as mitral valve prolapse (191, 261). Moreover, a neurological disorder, periventricular nodular heterotopia (PVNH), is caused by a loss of function mutation in *FLNA*. PVNH is characterized by the failure of neuronal radial migration from the ventricular zone to the neocortex during fetal development. This X-linked disease affects primarily females, as it is associated with prenatal death in males. Patients with PVNH often experience cardiovascular defects such as premature stroke, aortic aneurysms, patent ductus arteriosus and minor cardiac malformations. Surviving males with PVNH have more severe cardiovascular defects, including intractable hemorrhage and lethal vascular defects (191, 218, 264). Further, none of the OPDS disorders display neuronal migration defects. Of

note, *FLNA* mutation associated with Ehlers-Danlos syndrome and PVNH has been reported. Ehlers-Danlos syndrome is characterized by joint hypermobility, aortic dilation early in adulthood, and connective tissue fragility (173, 265).

In all, mutation on *FLNA* causes various human diseases including the skeletal phenotypes, otopalatodigital spectrum disorders (OPDS). OPDS are characterized by skeletal and craniofacial malformations. In this dissertation, I will describe a newly identified rare *FLNA* variants associated with non-syndromic single suture craniosynostosis (SSC). Understanding these rare variants may shed light on the mechanisms and factors regulating premature ossification of cranial sutures.

Hypothesis

FLNA variants identified in patients with single suture craniosynostosis (SSC) have a gain of function effect and contribute to craniosynostosis through enhancing cellular proliferation and differentiation, and attenuating cell migration and contractility.

Aims

Aim1: To assess the contribution of FLNA in the pathogenesis of craniosynostosis through characterizing the impact of nine rare FLNA variants on primary calvarial mesenchymal stem cell (cMSC) and primary calvarial osteoblast (cOB) on development and cellular mechanics.

Aim 2: To determine the phenotype of cMSCs lacking FLNA, through a CRISPR/Cas9 knockout. Subsequently changes in a select set of genes associated with bone development will be identified.

3.2. Materials and Methods

3.2.1. Primary Calvarial Osteoblast culture

Calvarial bone samples that would have otherwise been discarded were collected from individuals undergoing surgery for single suture craniosynostosis (SSC) as well as from control individuals with no known skeletal disorders undergoing craniotomy for brain tumor, or hydrocephalus surgery or unaffected autopsy specimens. SSC and control samples collected from subjects who ranged in age from 3 months to 27 months. Bone fragments were transported in Waymouth's media (WM) (Sigma-Aldrich, St. Louis, MO) supplemented with 2% 100x antibiotic/antimycotic solution (Corning, Corning, NY) and 10% fetal bovine serum (FBS) (Invitrogen, Waltham, MA). Upon arrival in the laboratory, tissues were rinsed in WM and any remaining soft tissue was removed. A sterile scalpel was used to cut calvaria into 1–2 mm pieces. Two pieces per well were cultured in 12-well plates at 37°C and 5% CO_2. On reaching confluence, cells were washed with phosphate-buffered saline, trypsinized with 0.05% Trypsin-EDTA (Invitrogen, Waltham, MA) and passaged into T75 flasks. Upon confluency, cells were frozen in medium containing 90% FBS and 10% dimethyl sulfoxide and stored in liquid nitrogen.

Primary calvarial osteoblast (cOB) cell lines were developed from patients identified with SSC harboring *FLNA* variants (cases, n=9) and from patients who underwent cranial surgery but without a bone-related disease (controls, n=10) (Table 3.2). The chosen controls were matched with SSC patients of the same sex and similar age, and one additional female control was included as well, five females and five males, and their ages fall into the same range of the FLNA cases. The nine validated *FLNA* variants associated with SSC are missense variants and we have the inheritance information of 4 SSC patients only, 3 males and one female. They all inherited the variants from their healthy mothers who do not have craniosynostosis.

Table 3.2. SSC patients and controls

	Nucleotide Change	Inheritance	Age (months)	Sex	Age (months)	Sex
1	c.C842T	Het/ Unknown	4.37	M	7	M
2	c.A2319T	Hom/ Unknown	5	M	5	M
3	c.C7798T	Het/ Maternal	9.43	F	9	F
4	c.C3348A	Hom/ Maternal	15	F	14	F
5	c.C3755T	Hom/ Maternal	5	M	6	M
6	c.C4897T	Hom/ Maternal	3	F	4	F
7	c.C4625T	Hom/ Unknown	3	M	4	M
8	c.G1526A	Het/ Unknown	27.53	M	19	M
9	c.C5948T	Het/ Unknown	6.33	F	8	F
					10	F

3.2.2. RNA isolation

Cultured primary osteoblast cell lines (3.2.1) were thawed and cultured to confluency in T25 flasks. Upon confluency, cells were passaged to a density of 175,000 cells per T25. At 75% confluence, cells were dissociated from the flask, pelleted, and washed in cold phosphate-buffered saline. RNA was isolated using the Roche High Pure RNA Isolation Kit (Roche, Basel, Switzerland) according to the manufacturer's instructions. RNA integrity was assessed using the Agilent 2100 Bioanalyzer (Agilent Technologies, Santa Clara, CA) and only samples with RNA integrity number (RIN) scores above 8.6 were used for RNA Sequencing. RNA sequencing was performed by Genewiz (South Plainfield, NJ).

3.2.3. Identification of rare FLNA Variants in Single Suture Craniosynostosis

Variants were identified through RNA-Sequencing of the coding regions in 391 individuals with SSC. Using a strict approach, the variants were compared to 60,000 individual exomes sequenced in the Exome Aggregation Consortium (ExAC) database. Minor allele frequency (MAF) reported by the ExAC of ≤ 0.01 (266). Only variants that occur in less than 1% of the general population were considered. After that, scores for each variant were calculated for Polyphen, CADD, and GERP (267-269). Polyphen (Polymorphism Phenotyping) is a tool for predicting the possible impact of an amino acid substitution on the structure and function of a human protein. CADD (Combined Annotation Dependent Depletion) is a tool for scoring the harmful effect of single nucleotide variants. GERP (The Genomic Evolutionary Rate Profiling) measures the evolutionary conservation of a particular genetic sequence across species. Furthermore, variants had to be predicted as damaging by having high polyphen, CADD, and GERP scores (greater than 0.9, 15, and 3, respectively). Identified genes were further limited by meeting additional criteria of being significant at the gene level, meaning a higher proportion of predicted damaging variants are seen in patients compared to controls.

3.2.4. Variant validation

Nine FLNA variants which met all of the above criteria were validated and assessed for inheritance pattern by Sanger DNA sequencing of patient and parental genomic DNA. Parental DNA samples were from whole blood whereas patient DNA samples were extracted from calvarial grown cells.

Regions of interest were amplified with by polymerase chain reaction (PCR) using primers designed using Primer3 software (270) and sourced from (Sigma Aldrich, St. Louis, MO) (Table 3.3). Resulting Ab1 sequence files were analyzed in Sequencher® version 5.1 (GeneCodes Corporation, Ann Arbor, MI) by alignment to a reference *FLNA* sequence sourced from UCSC's Genome Browser (271). Chromatograms were visually inspected to confirm the existence and inheritance pattern of each *FLNA* variant.

Table 3.3. Chromosomal locations, nucleotide positions, amino acid change and primer sequences for Sanger sequencing of significant FLNA variants.

Chromosomal Location[a]	Variant[b]	Forward Primer (5'→3')	Reverse Primer (5'→3')
chrx:153591114	c.A2319T: p.K773N	GCGCAGTCCACAGTGAAGTA	TTGAGGATGAGCTTGCCTTT
chrx:153581714	c.C5948T: p.S1983L	CGAATGAAATCCCTGGACAC	CACTGGGAGCAGTGACAGAA
chrx:153595791	c.C842T: p.P281L	TCTTATGGGGAAGACGTTGG	CCTGTGTCCTGACTGGGACT
chrx:153577339	c.C7798T: p.H2608Y	AAGTGAAAGCCGAGAGGTCA	GTCACCCCAGAACTGGCTTA
chrx:153588815	c. C3348A: p.D1116E	CGAGCAGATCTCAATGGTCA	GGTGGAAAGTCAAGCAGGAG
chrX:153586697	c.C4625T: p.T1542I	TTTGCATCGATGGTGAACTC	CCCAGGAGACTAGCTGATGC
chrx:153585850	c. C4897T: p.R1633C	CAGCTTACCTAGCCCGTGAC	CAAGCCGAAGAAGACACACA
chrx:153588408	c. C3755T: p.A1252V	GTAGGTCTCCGTCAGGTTGC	CCAATTCCAAGTGGACTGCT
chrX:153593758	c.G1526A: p.G509D	GGACCATGGGGTAATACTCG	CCCTTCCAGTTCTGTCTTGC

[a] Human Reference Build GRCh37/hg19 [b] Coding DNA reference positions: protein reference sequence

3.2.5. Grouping FLNA variants based on their Ig repeat location

FLNA facilitates essential functional, signaling, and mechanical properties in the cell through interacting with various proteins. Each interaction regulates specific function (168, 173, 181, 188-197, 202, 272).

The nine rare *FLNA* variants we identified are scattered across FLNA Ig repeats (Figure. 3.1). Therefore, we sorted the nine rare *FLNA* variants into groups based on their Ig repeat interactions (Table. 3.4):

FLNA-ACT domain group: *FLNA* variants located on Ig repeats interact with F-actin, 9, 11, 14.

FLNA-VIM domain group: *FLNA* variants located on Ig repeats interact with Vimentin, 1, 3, 6.

FLNA-FOX domain group: *FLNA* variants located on Ig repeats interact with FOXC1, 6, 9, 18.

Since Ig repeat 9 interacts with both F-actin and FOXC-1, the variant was added to both groups. Likewise, the variant on Ig repeat 6 was added to the Vimentin and FOXC1 group. Only one variant is located on Ig repeat 24, therefore we didn't group this variant as a singular value might not be informative.

Table 3.4. Grouping FLNA Variants based on their domain location

	Nucleotide Change	Amino Acid Change	Sex	Domain Position	Domain's interactions	Fused Suture
FLNA-ACT	c.C3348A	p.D1116E	M	Ig Repeat 9	F-actin/FOXC1	Sagittal
	c.C3755T	p.A1252V	M	Ig Repeat 11	F-actin	Sagittal
	c.C4897T	p.R1633C	M	Ig Repeat 14	F-actin	Sagittal
	c.C4625T	p.T1542I	M	Ig Repeat 14	F-actin	Sagittal
FLNA-VIM	c.C842T	p.P281L	F	Ig Repeat 1	Vimentin	Sagittal
	c.A2319T	p.G509D	M	Ig Repeat 3	Vimentin	Sagittal
	c.C7798T	p.K773N	F	Ig Repeat 6	Vimentin/FOXC1	Coronal
FLNA-FOX	c.C7798T	p.K773N	F	Ig Repeat 6	Vimentin/FOXC1	Coronal
	c.C3348A	p.D1116E	M	Ig Repeat 9	F-actin/FOXC1	Sagittal
	c.G1526A	p.S1983L	F	Ig Repeat 18	FOXC1	Sagittal

3.2.6. Primary Calvarial MSC (cMSC) culture

cOB cell lines were passaged 6 times in culture (as described in 3.2.1). Cells were then sorted using FACS Aria II and fluorescent-conjugated antibodies against CD73, CD90, CD105, CD29 and CD34 (BD Biosciences, East Rutherford, NJ). Cells were gated for size and CD34 negative singlets sorted for expression of CD73, CD90, CD105 and CD29 (Figure. 2.1). Next, the sorted cells were expanded and grown in FN-coated culture flasks in StemXVivo serum-free (SF) media (R&D Systems, Minneapolis, MN). Cells were incubated at 37°C with 5% CO_2. At 90–100% confluence, cells were dissociated and passaged using TrypLE Express (Gibco, Grand Island, NY). Upon confluency at passage 3, cells were frozen using StemXVivo Serum-Free MSC Freezing Media (R&D Systems, Minneapolis, MN).

3.2.7. Proliferation

5-bromo-2-deoxyuridine (BrdU) (EMD Millipore, Billerica, MA) was used to assess the active proliferation of the cells. cMSCs and cOBs from FLNA SSC patients and controls were plated in triplicate in 96-well plates (1x10^5 cells/ well. The cMSCs were grown on FN-coated plate whereas cOBs were grown on non-coated plates. Twenty-four hours after plating, a BrdU cell proliferation assay was utilized per manufacturer's instructions.

The plate was read at the 24-hour timepoint using SpectraMax i3X at both 450nm (BrdU incorporation) and 550nm (background). The final reading for each well was obtained by subtracting 550 nm readings from 450 nm readings. The amount of BrdU incorporation is linearly correlated with the newly synthesized DNA strands of actively proliferating cells.

3.2.8. Migration

cMSCs and cOBs from each FLNA SSC patient and controls were seeded in 6-well plates at a density of 2x10^4 cells/well (cMSCs were on FN-coated wells). Twenty-three cells (number determined by power analysis) from each cell line were tracked and imaged every 5 minutes over a period of 15 hours using time-lapse, live-cell, phase contrast microscopy on an inverted microscope (Nikon TEi) with a 4× air objective in a 37°C, 5% CO_2 chamber. Subsequently, manual identification and labeling of the nucleus of each cell in ImageJ plugin, MTrackJ, (LOCI, University of Wisconsin) was used to track the spatial coordinates of each individual cell to determine migration speeds and distances.

3.2.9. Cell Contractility

A microcontact printed reference-free technique (black dots) (273) was used to measure cellular contractility force. cMSCs from FLNA SSC patients and controls were seeded at 30,000 cells/ substrate in a well of a 6-well plate. Cells were cultured and incubated at 37°C and 5% CO_2 for 24 hours. After that, cells on the black dots were fixed for 20 minutes with 4% paraformaldehyde and permeabilized with 0.5% Triton X-100. After fixing, substrates were washed with PBS and blocked with10% goat serum (Life Technologies Carlsbad, CA) diluted in PBS for 1 hour. Actin filaments were stained with Alexa-Fluor-488-conjugated phalloidin (Molecular Probes, Eugene, OR), and the nuclei was stained with Hoechst 33342 (Invitrogen, Waltham, MA). Substrates were mounted onto glass coverslips using Fluoromount-G mounting medium (Life Technologies, Carlsbad, CA) for microscopy. Imaging was carried out on an epi-fluorescent microscope (Nikon TEi; Nikon, Instruments) with a 40× oil objective. Traction forces were calculated using regularized Fourier Transform Traction Cytometry (FTTC) which measures the displacements of the surface (274, 275). To assess whole-cell contractility, the total force and net force were calculated for each cell to assess the whole cell contractility. The

calculation of total force was via summing the force magnitudes from each dot underneath the cell.

3.2.10. Alkaline Phosphate (ALP) assay

FLNA SSC and control cOBs were seeded into 12-well plates at a density of 2×10^5 cells/well. Each cell line was plated in a total of 6 wells; three sample wells and three control wells. Forty-eight hours after seeding, ALP activity was quantified using the Abcam ALP Assay Kit (ab83369) (Abcam, Waltham, MA) per manufacturer's protocol. In brief, 5mM of p-nitrophenyl phosphate (*p*NPP) was added to be dephosphorylated by the ALP generated in the samples. Samples were then incubated in the dark at 25 °C for 60 minutes. Stop solution was then added to each well and the absorbance of all wells was measured at 405 nm by SpectraMax i3X. The concentration of ALP activity (U/ml) of the samples was calculated as ALP activity (U/ml) = A / V / T where A is amount of p-nitrophenyl (*p*NP) generated by samples (in µmol), V is volume of sample added in the assay well (0.05 ml), and T is the reaction time (60 minutes).

To quantify normalized alkaline phosphatase activity per unit total protein, the amount of ALP activity was divided by the amount of total protein for normalization determined by BCA assay (3.2.11).

3.2.11. Protein quantification

Cells were lysed in 0.05ml Mammalian Protein Extraction Reagent (MPER) (Thermo Fisher Scientific, Waltham, MA). Total protein concentration was determined by Pierce BCA assay (Thermo Fisher Scientific, Waltham, MA) according to manufacturer's protocol. In brief, 25 µl of each sample and albumin BSA standards was added into a 96-well plate in triplicate. Then, 200 µl of BCA working reagent was added and mixed on a plate shaker for 30 seconds.

The plate was incubated in the dark at 37°C for 30 minutes. The plate was read at 562 nm by SpectraMax i3X. Triplicates were averaged and adjusted for blank measurements.

3.2.12. Osteogenic Differentiation of cMSCs

cMSCs from FLNA SSC patients and controls were seeded in SF media in duplicate for each of three time points in FN-coated 12-well plates at a density of 2x10^5 cells/well. Cells were grown for two days and then medium was replaced by osteogenic differentiation medium (StemPro, Life Technologies, Carlsbad, CA). Cells were incubated at 37 °C with 5% CO2 with osteogenic differentiation medium change every three days. Cells were assessed at day 0 (before adding differentiation medium), differentiation day 7, and differentiation day 21.

3.2.13. Analysis of osteogenic gene expression in osteogenically differentiated cMSCs

Bulk RNA was isolated from cMSCs at day 0 (before adding differentiation medium), differentiation day 7, and differentiation day 21 (3.2.12) by high pure RNA isolation kit (Roche, Basel, Switzerland). RNA concentration was measured on an ND-1000 NanoDrop spectrophotometer and 40 ng of total RNA from each sample was used for cDNA synthesis using Superscript IV VILO (Invitrogen, Waltham, MA) according to the manufacturer's instructions. Next, cDNA was combined with RT SYBR Green qPCR Mastermix (Qiagen, Germantown, MD) into a Qiagen custom RT^2 Profiler PCR Array (96- well plate) consisting of 11 curated osteogenic genes, 2 housekeeping (HK) genes, and 3 internal controls (Table. 3.5). qPCR was then performed using the CFX96 Touch real-time PCR detection system (BioRad, Hercules, CA) under the following parameters: 95 °C for 10 min, followed by 40 cycles of 95 °C for 15 s and 60 °C for 1 min. Gene expression data were analyzed where each osteogenic gene was normalized to the average of the housekeeping genes (276).

Table 3.5. Osteogenic gene list

Gene Bank	Symbol	Description
NM_002449	*MSX2*	Msh homebox 2
NM_001200	*BMP2*	Bone morphogenic protein 2
NM_000478	*ALP*	Alkaline phosphate
NM_152860	*SP7*	Sp7 transcription factor
NM_005221	*DLX5*	Distal-less homebox 5
NM_004348	*RUNX2*	Runt-related transcription factor
NM_000088	*COL1A1*	Collagen type 1 alpha
NM_003118	*SPARC*	Secreted protein acidic cystine rich (osteonectin)
NM_000582	*SPP1*	Secreted phosphoprotein 1
NM_199173	*BGLAP*	Bone gamma-carboxyglutamate (gla) protein
NM_025237	*SOST*	Sclerostin
NM_005877	*SF3A1*	Splicing factor 3a, subunit 1 (HK gene)
NM_002046	*GAPDH*	Glyceraldehyde-3-phosphate dehydrogenase (HK gene)
SA_00105	HGDC	Human genomic DNA contamination (control)
SA_00103	PPC	Positive PCR control (control)
SA_00104	RTC	Reverse transcription control (control)

3.2.14. X-inactivation test

cMSCs from female SSC patients with FLNA variants (Table. 3.6) were passaged three times post-FACS sorting. Bulk RNA was isolated by a high pure RNA isolation kit (Roche, Basel, Switzerland) per manufacturer's protocol. Intron-spanning PCR primers (Sigma Aldrich, St. Louis, MO) were designed for each FLNA variant using Primer3 software (270). Isolated mRNA was amplified by PCR with respective primers and amplicons were sent for Sanger sequencing (Genewiz, citation). Resultant Ab1 sequence files were analyzed using Sequencher® version 5.1 DNA (GeneCodes Corporation, Ann Arbor, MI) by aligning each sequence product to a corresponding reference sequence sourced from the UCSC Genome

Browser (271). Chromatograms were visually inspected to confirm the active expression of FLNA variants of interest in cMSCs from female patients.

Table 3.6. Chromosomal locations, nucleotide positions, amino acid change and primer sequences for Sanger sequences of Female FLNA variants.

Chromosomal Location[a]	Variant[b]	Forward Primer (5'→3')	Reverse Primer (5'→3')
chrx:153581714	c.C5948T: p.S1983L	ACCTAAAGGTCGGCTCTGCT	TGTAGTTGCCTGGCTCTGTG
chrx:153595791	c.C842T: p.P281L	CCTGTGTCCTGACTGGGACT	GGGTCCTCCACGTACACCAG
chrx:153577339	c.C7798T: p.H2608Y	CACAGTAGACTGCAGCAAAGCA	TGACCTCTCGGCTTTCACTT
chrX:153593758	c.G1526A: p.G509D	GGTCGAGGTTGTGATCCAGG	CGAGTATTACCCCATGGTCC

[a] Human Reference Build GRCh37/hg19 [b] Coding DNA reference position: Amino acid reference position

3.2.15. CRISPR/Cas9 gene editing

We used the CRISPR/Cas9-mediated gene disruption system to knockout *FLNA*. cMSCs from two control individuals, which had previously been passaged three times and frozen, were thawed and seeded in FN-coated T75 flasks with SF media for three days. Cells were then detached using TrypLE Express (Gibco, Grand Island, NY), and centrifuged for 5 minutes at 400 x g. Cells were then washed with PBS twice and resuspended in Neon Buffer R ($3x10^5$ cells in 5 µl) (Neon, Thermo Fisher Scientific, Waltham, MA).

Single guide RNA (sgRNA) targeting FLNA for Homology-directed repair (HDR) knock-in and non-homologous end joining (NHEJ) knockout was commercially synthesized (Synthego, Menlo Park, CA). sgRNA was resuspended to 100 µM (total sgRNA concentration) in RNase-free 1x TE buffer (10 mM Tris, 1 mM EDTA, pH 8). Prior to use, sgRNA stock diluted to 30 µM in RNase-free H_2O.

Single-stranded oligo DNA nucleotides (ssODNs) were commercially synthesized (Ultramer DNA Oligonucleotides; IDT) with phosphorothioate linkages between the first and final 3-bp sequences.

sgRNA: UCAGGGUCCAGAUGAGGCCC

ssODN: CACTCTTCTACTCACAGACAGCAAGGCCATCGTGGACGGGAACCTGAAG

CTGATCCTGGGTAAGTGACTAGAATAAACCTCATCTGGACCCTGATCCTGCACTACTCCAT CTCCATGCCCATGTGGGACGAG

Cas9-gRNA ribonucleoprotein (RNP) was assembled by complexing sgRNA with Cas9 nuclease (IDT, Coralville, IA) at a 9:1 ratio and delivered with ssODNs to cells by Neon electroporation (Thermo Fisher Scientific, Waltham, MA). 90 pmol of synthetic sgRNAs (Synthego, Menlo Park, CA) was combined with 10 pmol of Cas9, diluted to 7 µl in Neon R buffer, and the complex was incubated 10 min at room temperature. During this incubation, cells were harvested and counted. 5 µL of cell solution at a concentration of 3×10^5 cells/µl was added to the RNP and ssODN and gently mixed. The Cells+RNP+ssODN solution was electroporated (1300 V, 20 ms, one pulse) in 10 µl of Neon tips and then transferred into prewarmed SF medium without antibiotics. After editing, medium was exchanged to SF media with 1% SPF the next day. Cells were maintained for one week with medium change every 3 days. Cells were then split and expanded. Non-edited cells from the same two edited cMSC control lines were grown parallel and analyzed.

Gene disruption was analyzed using Inference of CRISPR Edits (ICE) analysis (Synthego, Menlo Park, CA). Total genomic DNA was isolated using QIAamp DNA mini kit (Qiagen, Germantown, MD). gRNA target genomic regions were first amplified using PCR with primers creating a 1348-bp amplicon containing the gRNA target site.

Forward primer: TGTATTTCCCAACCACCCAG

Reverse primer: CAAAAACCCACTCTTGTCTGAC.

PCR amplicons were purified with a NucleoSpin® PCR clean up kit. For ICE, 20 ng of purified PCR product was Sanger sequenced using GENEWIZ. The ab1 files were uploaded to https://ice.synthego.com for ICE analysis. Editing (null) was confirmed.

3.2.16. Western blotting for FLNA protein expression in CRISPR edited primary cMSCs

Western blotting was performed on gene-edited (3.2.15) and control cell lines. Cells were expanded one week after being split after electroporation in SF medium. Cells were then incubated in RIPA lysis buffer (Sigma, St. Louis, MO) on ice for 1 minute and then clarified by centrifugation for 15 minutes at 4°C. Concentration of clarified lysate was determined by Pierce BCA assay (3.2.11), diluted 1:1 with Laemmli 2x concentrate (Sigma, St. Louis, MO). Each protein/Laemmli solution was then boiled at 99°C for 5 minutes and put back on ice.

Ten micrograms of denatured lysate from each sample were run for 1 hour at room temperature at 150V, 55mA on a 3-8% Tris-Acetate NuPAGE gel (Invitrogen, Waltham, MA). Protein was transferred to a PVDF membrane using 1x transfer buffer (85% ddH2O, 10% methanol, 5% 20x NuPAGE transfer buffer). To achieve protein transfer, each PVDF membrane was run for 1 hour at room temperature at 30V and 220mA. Nonspecific binding was minimized with a one-hour room temperature incubation in Odyssey Blocking Buffer (LI-COR Biosciences, Lincoln, NE). The transfer membrane was incubated overnight at 4°C in (buffer) with 1:2000 FLNA antibody, rabbit polycolonal, product# TA349988 (Origene, Rockville, MD) and 1:10000 GAPDH antibody, mouse polyclonal, product# MA5-15738 (Invitrogen, Waltham, MA). After primary antibody incubation, the membrane was washed with PBS-T (0.1% Tween20) 4x for 5 minutes and incubated with secondary Abs at 1:10,000 for 30 min at RT. Secondary Abs were, IRDye® 800cw goat anti-rabbit (LI-COR Biosciences, Lincoln, NE), IRDye® 680RD goat anti-mouse (LI-COR Biosciences, Lincoln, NE). The membrane was then washed 4x for 5 minutes in PBS-T (0.1% Tween20).

The membrane was then washed and imaged on an Odyssey Infrared Imaging System (LI-COR Biosciences, Lincoln, NE). Western blot quantification was performed with ImageJ

software.

3.2.17. Analysis of *FLNA* and Osteogenic Gene expression in CRISPR-edited primary cMSCs

Bulk RNA was extracted from the two CRISPR-edited FLNA disrupted cMSC lines and two non-CRSIPR-edited controls using a high pure RNA isolation kit (Roche, Basel, Switzerland). RNA concentration was measured on an ND-1000 NanoDrop spectrophotometer and cDNA synthesis was performed as previously described (3.2.13).

1) FLNA expression:

In addition to assessing the protein level (3.2.16), we evaluated the mRNA expression of FLNA in CRISPR-edited cMSC lines and controls. Forward and reverse FLNA primers were designed using Primer3 software (270). Sequences were as follows: FLNA forward: CACAGCTTCCAGAGGAAAGG, FLNA reverse: GGTCCAGTAGGCGTCAATGT; Actin forward: CTACAATGAGCTGCGTGTGG, Actin reverse: GCTGGGGTGTTGAAGGTCT

Each reaction was done in technical triplicate. Data ere normalized with internal Actin control.

2) Osteogenic Genes Analysis:

cDNA was processed for qPCR analysis into a Qiagen's custom RT^2 Profiler PCR Array as described in (3.2.13).

3.2.18. Statistical Analysis

GraphPad Prism 9 (GraphPad Software, San Diego, CA) was used for all statistical analysis. All values are presented as the mean ± standard deviation (SD) in graphs and tables. Samples were analyzed for significance using Student's t-test. Data was considered significant at $P<0.05$. Replicates were considered during the analysis.

For analysis of CRISPR gene-edited cells, the p-values were calculated using paired t-tests.

3.3. Results

We identified 9 rare *FLNA* variants (Table.3.7) that we believe are associated with single suture craniosynostosis. Variants were identified through RNA-Sequencing of the coding regions in 391 patients with SSC. ExAC database was utilized to compare the identified rare *FLNA* variants to 60,000 individual exomes. ExAC provides the frequency of any variant in the public. Only variants that occur in less than 1% of the general population, have high polyphen, CADD, and GERP scores, and are significant at the gene level were considered.

Seven variants met the analysis criteria of having polyphen, CADD, GERP scores of (larger than 0.9, 15, and 3, respectively). Although the other two variants (marked by asterisks) only met two of these three cutoffs, they have been included due to their rarity and location within critical Ig repeats that interact with vimentin and FOXC1 (196, 277).

The identified *FLNA* variants were further validated by DNA Sanger sequencing (see methods), and the results confirmed the existence of all the variants at the DNA level.

Table 3.7. Characteristics of Selected Variants Identified Through RNA Sequencing

Chr	Exon	Nucleotide Change	Amino Acid Change	Exac_ALL	PolyP	CADD	GERP	Sex	Inheritance	Domain Position	Domain's interactions	Suture
X	5	c.C842T	p.P281L	0	0.971	33	4.99	F	Het/ Unknown	Ig Repeat 1	Vimentin	Sagittal
X	16	c.A2319T	p.G509D*	1.158E-05	0.511	19.53	4.44	M	Hom/ Unknown	Ig Repeat 3	Vimentin	Sagittal
X	47	c.C7798T	p.K773N*	0.0001606	0.97	24.7	2.09	F	Het/ Maternal	Ig Repeat 6	Vimentin/FOXC1	Coronal
X	22	c.C3348A	p.D1116E	3.502E-05	0.975	23.1	4.25	M	Hom/ Maternal	Ig Repeat 9	F-actin/FOXC1	Sagittal
X	22	c.C3755T	p.A1252V	1.184E-05	0.968	23.4	4.93	M	Hom/ Maternal	Ig Repeat 11	F-actin	Sagittal
X	29	c.C4897T	p.R1633C	4.655E-05	1	23.7	5.22	M	Hom/ Maternal	Ig Repeat 14	F-actin	Sagittal
X	28	c.C4625T	p.T1542I	3.499E-05	0.987	27.3	5.67	M	Hom/ Unknown	Ig Repeat 14	F-actin	Sagittal
X	10	c.G1526A	p.S1983L	0.0026	1	25.8	5.69	F	Het/ Unknown	Ig Repeat 18	FOXC1	Sagittal
X	36	c.C5948T	p.H2608Y	0.0002	1	29.6	5.74	F	Het/ Unknown	Ig Repeat 24	SMADs/Rho GTPases	Coronal

These FLNA variants are located on critical Ig repeats where cellular movement and intracellular signaling are carried out (Figure. 3.1).

Interestingly, all the identified *FLNA* variants that located on F-actin domains are in males. Two patients with sagittal SSC harbor variants on vimentin binding domains (Ig repeat 1 and 3) (277). Furthermore, one patient with coronal SSC has a variant located on Ig repeat 6, where it binds vimentin and FOXC1 (191, 196). Two additional cases with sagittal SSC were found to have variants on other distinct FOXC1 and F-actin binding domains (Ig repeats 9 and 18). Moreover, two reported cases of frontometaphyseal dysplasia (FMD) with craniosynostosis (pansynostosis, sagittal and bilateral lambdoid) had missense variants located on Ig repeat 9 too (255). Ig repeats (9 -15) of FLNA bind to F-actin and promote filament branching (176, 191). Three male sagittal SSC patients harbor missense variants in this region: one on Ig repeat 11, and two on Ig repeat 14. In addition, one reported female patient with Melnick–Needles syndrome syndrome (MNS) who has bilateral coronal, bilateral lambdoid, and posterior sagittal synostosis has a variant located on Ig repeat 14 of FLNA (256). FLNA Ig repeat 24 interacts with the Rho family of GTPases and SMAD proteins. A missense variant in a female patient with coronal synostosis is located on Ig repeat 24 (Figure. 3.1), (Table. 3.1).

3.3.1. X-chromosome inactivation and FLNA variants in Female SSC patients

Because FLNA is located on the X-chromosome (181), it was important to know if the variants seen in our female patients impacted allelic skewing. In this study, cMSC cell lines harboring *FLNA* variants were subjected to multiple passaging. Therefore, we decided to evaluate the pattern of *FLNA* variant expression in female cell lines. Confirming the maintenance of the variants is crucial to proceed to further characterization of the cell lines.

We performed Sanger sequencing of PCR amplicons of cDNA and saw the maintenance of the variant's alleles in all the female cell lines (Figure. 3.2). The heterozygous *FLNA* variant at C5948T maintains equal dosage of the normal and variant alleles. However, heterozygous *FLNA* variants at C7798T, C842T, and G1526A demonstrate skewing toward the variant alleles,

as variants' dosages were higher than wild-type alleles. The position of the variants of interest are depicted in red circles (Figure. 3.2). The observed predominant expression of the variant alleles suggest some kind of selection for the variant allele in vitro. In order to further clarify the upcoming results of the performed tests, values were colored in figures based on their sex identity: pink (female), orange (skewed female), and blue (male) (Figure. 3.3 - 3.4, Figure. 3.6 - 3.11).

3.3.2. Characterization of cMSCs and cOBs harboring FLNA variants

We have chosen to study both cMSCs and cOBs because cMSCs present during an early stage whereas cOBs represent a mature stage of bone development in vitro. We assumed that the effect of the *FLNA* variants on the tested process may vary between the undifferentiated state (cMSCs) and differentiated state (cOBs).

Proliferation

The BrdU assay was performed on cMSCs and cOBs harboring *FLNA* variants of interest and controls to assess whether *FLNA* variants affect cellular proliferation. Overall, no significant difference was found in proliferation rate in the cMSCs in *FLNA* variants compared to controls, whereas cOBs from some *FLNA* variants showed a significantly higher proliferation rate compared to controls (Fig 3.3, A).

However, when cell lines were assessed based on the functional domains of the variants, significant patterns emerged. Both cMSCs and cOBs from individuals with *FLNA* variants in the FLNA-ACT domains had a statistically significant higher proliferation rate ($P<0.05$) compared to controls (Fig 3.3, B). No significant change was seen in the proliferation rate of cMSCs or cOBs with variants in FLNA-VIM domains as compared to controls (Fig 3.3,

C). Among individuals with variants in FLNA-FOX domains, cMSCs did not show a significant difference while cOBs had a higher proliferation rate compared to controls (Fig 3.3, D).

Migration

To investigate the effect of *FLNA* variants on the migration of cMSCs and cOBs, we utilized a cell-tracking assay with time-lapse microscopy over a 15-hour period to trace the migration paths of cells from individuals with *FLNA* variants of interest and controls. Collecting and analyzing the migration of the cells showed that cMSCs and cOBs from SSC patients with *FLNA* variants migrated at a significantly slower speed compared to controls at $P \leq 10e4$ (Figure. 3.4, A).

We've assessed the SSC cell lines based on *FLNA* functional domains. The results revealed that in the FLNA-ACT domain group, cMSC migration rate had no significant difference compared to controls. In contrast, cOBs migrated a significantly shorter distance compared to controls (P=1x10^-4) (Figure. 3.4, B). In the FLNA-VIM domain group, both cMSCs and cOBs had a significantly lower migration rate compared to controls (Figure. 3.4, C). Lastly, a significantly lower migration rate was shown in cMSCs from the FLNA-FOX domain group while no significant change was noted in cOBs (Figure. 3.4, D).

Contractility

To examine the effect of *FLNA* variants on cell contractility, cMSCs harboring variants of interest and controls were seeded onto flexible microcontact prints with fluorescent micropatterning (Figure. 3.5). The traction force of the cells was measured by analyzing the displacement of each dot underlying the cell. Results showed that there was no significant difference (P=0.22) in the generated force between cMSCs with *FLNA* variants and controls

(Figure. 3.6, A). The cell spreading area was analyzed to determine if *FLNA* variants affect the cell area in cMSCs. cMSCs with *FLNA* variants had a significantly smaller cell area as compared to controls (P <0.01). In order to estimate the actual strength of the cell's mechanical protein, we divided total calculated force over the number of associated analyzed dots (points of contact). No changes were found between cMSCs between *FLNA* variants and controls.

When the results were analyzed based on the functional domain of the *FLNA* variants, difference in total exerted force were detected for some domain groups. In the FLNA-ACT domain group, no significant difference was identified in the total force (P=0.33), cell area (P=0.64), nor force/ dot (P=0.48) (Figure. 3.6, B). Force/dot represents the ratio of force to the surface area; the number of dots underneath each contracting cell are known, see (3.2.9). In the FLNA-VIM domain group, cMSC showed a higher force/ dot ratio (P=0.02) compared to controls whereas no significant difference was found in the generated force (P=0.89) nor the cell area (P=0.17) (Figure. 3.6, C). However, the cell area was significantly reduced in the FLNA-FOX domain group (P=0.02) while no significant change was noted in the total force (P=0.16) or the force/ dot ratio (P=0.7) (Figure. 3.6, D).

ALP Activity

The amount of relative ALP activity in cOBs harbouring FLNA variants and controls was examined. ALP activity was determined through cellular dephosphorylation of pNPP over a period of two days. No significant difference was found in ALP activiity between cOBs with *FLNA* variants and controls (Figure. 3.7, A). Likewise, the subgroups, FLNA-ACT domain, FLNA-VIM domain , and FLNA-FOX domain, did not show a significant change in ALP activity compared to controls (Figure. 3.7, B, C, D).

Expression of osteogenic marker genes by qPCR

We have examined the expression profile of early and late osteogenic genes in cMSC harboring *FLNA* variants from patients with SSC and controls at *in vitro* osteogenic differentiation days 0, 7, and 21. The relative expression of *MSX2*, *BMP2*, *ALP*, *SP7*, *DLX5*, *RUNX2*, *COL1A1*, *SPARC*, *SPP1*, *BGLAP*, and *SOST* were determined by qPCR using the average of *SF3A1* and *GAPDH* as a reference. At day 0 (Figure. 3.8, G), *BGLAP* expression was lower in FLNA cMSCs compared to control cMSCs (*P*=0.006), while no significant difference in the expression of the other tested genes was observed.

SP7 and *BGLAP* were significantly reduced in cMSCs with FLNA variants at day 7 of osteogenic differentiation (SP7, *P*=0.01), (BGLAP, *P*=0.01) (Figure. 3.8, B, H). At day 21, *SPARC* expression was upregulated (Figure. 3.8, F) (*P*=0.04) whereas no significant change was noted in the other genes.

Assessing the expression of the osteogenic genes based on the functional domain of the *FLNA* variants revealed distinct results. In the FLNA-ACT domain group, *BMP2* (*P*=0.001), *RUNX2* (*P*=0.02), *SPP1* (*P*=0.0001), and *BGLAP* (*P* =0.006) had a significant reduction in their expression compared to controls at day 0 (Figure. 3.9, A, G, J, M). Moreover, the expression of *BMP2*, *SP7*, and *SPP1* was significantly reduced in cMSCs in comparison to controls, (*P* =0.03, *P* =0.03, and *P* =0.002 respectively) at day 7 (Figure. 3.9, B, E, K). *BMP2* and *SP7* were downregulated in SSC cMSCs (Figure. 3.9, C, F), at day 21 compared to controls (*P* =0.02, *P* =0.04 respectively).

In the FLNA-VIM domain group, *SP7* expression was downregulated at day 7 (*P* =0.05) (Figure. 3.10, B). By contrast, both *SPARC* and *SPP1* expression were upregulated in the FLNA-VIM domain group compared to controls, (*P*=0.05 and *P*=0.04) respectively) (Figure. 3.10, F, I).

In FLNA-FOX domain group, a significant decrease in the expression of *BMP2* (*P* =0.05) and *BGLAP* (*P*=0.003) was observed on day 0 of differentiation (Figure. 3.11, A, J). At day 7, *SP7* and *BGLAP* were downregulated (Figure. 3.11, E, K), (*P*=0.02 and *P*=0.03 respectively). However, *SPARC* expression was increased compared to controls (*P*=0.05) (Figure. 3.11, I).

Near complete *FLNA* Knockout:

Using modified CRISPR/Cas9 method, we designed a workflow for editing primary human calvarial MSCs (cMSCs). We successfully disrupted the expression of *FLNA* in cMSCs. We used chemically synthesized sgRNA targeting exon 2 (a required region for gene expression) to interrupt successful translation of a functional protein product. We enhanced CRISPR/Cas9 gene disruption via promoting two mechanisms (NHEJ and HDR). This process was accomplished by the codelivery of HDR template (132-bp) with stop codons for all potential reading frames.

To our knowledge, this is the first model of *FLNA* loss in cMSCs that have elucidated the effect of FLNA loss on the expression of master osteogenic genes in cMSCs.

To confirm the *FLNA* knockout (KO), each cell line was genotyped and *FLNA* mRNA expression and FLNA protein levels analyzed. Western blot analysis consistently demonstrated significant reduction of FLNA protein expression in the two *FLNA* KO cell lines (cell line 1 and 2) compared to controls with this approach (Figure. 3.12, A). We showed consistent data from qPCR analysis, *FLNA* mRNA levels were downregulated (Figure. 3.12, B) in KO 1 and 2 compared to controls, respectively.

Loss of *FLNA* reduced the expression of osteogenic genes

In parallel with assessing and verifying *FLNA* KO in cMSCs, we sought to investigate the consequences of *FLNA* loss on the expression of osteogenic genes: *MSX2*, *BMP2*, *ALP*, *SP7*, *DLX5*, *RUNX2*, *COL1A1*, *SPARC*, *SPP1*, *BGLAP*, and *SOST*. These genes are vital in intramembranous ossification and calvarial development (19, 149-155, 237, 278-282). Their expression is regulated by transcription factors and proteins that directly interact with *FLNA* (191, 196, 227). We performed qPCR on cDNA from the two different *FLNA* KO (edited) cell lines and two controls (non-edited). The gene expression profile of the two KO cell lines was similar. Thus, we averaged the results from KOs and compared them to controls. *SPP1* expression was lacked in the KO cell lines while presents in controls. The expression of (*MSX2*, *BMP2*, *ALP*, *SP7*, *DLX5*, *RUNX2*, *COL1A1*, *SPARC*, *SPP1*, and *BGLAP*) was lower in KOs compared to controls, whereas *SOST* expression was higher (Figure. 3.13).

Together, these results show that human cMSCs lacking FLNA demonstrate reduction in most of the osteogenic genes in comparison to controls.

Osteogenic gene expression in *FLNA* Variants and *FLNA* KO

We have demonstrated the osteogenic gene expression of cMSCs harboring *FLNA* variants from each domain group and FLNA KO cell lines compared to controls, before adding the osteogenic media. The goal was to evaluate whether *FLNA* variants mimic the loss of function *FLNA* KO. We evaluated the mRNA expression of osteogenic genes (3.2.13) in *FLNA* variants and *FLNA* KO compared to controls (Figure 3.14). Each of the genes were similarly downregulated in the FLNA-ACT group and *FLNA* KOs with the exception of *SOST*, which was upregulated in *FLNA* KO compared to controls. In FLNA-VIM group, ALP and BMP2 were upregulated compared to controls, unlike *FLNA* KO. However, the rest of the genes investigated (*MSX2*, *SPARC*, *DLX5*, *RUNX2*, *SP7*, *COL1A1*, *SPP1*, *BGLAP*, and *SOST*) were similarly

expressed in FLNA-VIM and *FLNA* KO when compared controls. In FLNA-FOX group, *MSX2*, *SPARC*, *BMP2*, *RUNX2*, *SP7*, *COL1A1*, *BGLAP*, and *SOST* showed a similar expression to *FLNA* KO. These observations indicate the possibility that all FLNA variants investigated demonstrate a loss of function as most of the osteogenic genes in these variants showed a similar mRNA expression to the *FLNA* KO.

3.4. Discussion

In this study, we characterized the effect of nine rare *FLNA* variants on cellular proliferation, differentiation, mechanobiology, and gene expression of primary calvarial MSCs (cMSCs) and osteoblasts (cOBs) from patients with SSC. *FLNA* is on the X chromosome, thus it is expected that phenotypes of *FLNA* mutations would vary between sexes. We observed skewed X-inactivation in three of the female *FLNA* variants whereas only one showed random X-inactivation. X-inactivation skewing could be responsible for altering phenotypes in females harboring the same mutation (283). X- chromosome inactivation is a random epigenetic mechanism in mammals to equalize the gene dosage of X-linked genes between males and females (284, 285). The X-inactivation process can be skewed toward one allele. This can modify the phenotypes in females with X-linked diseases or alter cell behaviors in vitro (286-288). Skewing of X allele expression in OPDS was associated with more severe phenotypes (245, 283, 289). Therefore, considering and estimating the degree of skewing could help us understand the behavior of the cells in vitro.

Moreover, diseases associated with a *FLNA* mutations demonstrate a more severe phenotype than females (191, 218, 247-249, 264). Thus, we considered the fact that male cell lines harboring *FLNA* variants might behave in a distinct way. Incidentally, all male variants occurred in the FLNA-ACT domain group as we described previously.

To explore the specific role of the *FLNA* variants, we grouped and analyzed them based on their locations within known functional domains (Ig repeats).

A myriad of cellular mechanisms inform the regulation of proliferation, differentiation, and migration patterns of MSCs and osteoblasts in the development and growth of the calvarial bones and sutures (290, 291). Thus, altering the states of proliferation and differentiation can disrupt normal growth and result in structural defects including the premature fusion of the cranial sutures. The role of these regulatory mechanisms has been demonstrated in both mouse and human models of craniosynostosis (292-294).

The role of *FLNA* in bone formation and skeletal phenotypes is most clearly demonstrated by OPDS, a wide range of skeletal disorders associated with calvarial dysplasia and craniosynostosis (255-257). *FLNA* contributes to the development of calvarial MSCs and osteoblasts as it acts on pivotal signaling pathways. It affects osteogenic gene expression by binding FOXC1 and mediating BMP signaling (196). FLNA also binds SMAD2 and SMAD5 to regulate both TGF-β and BMP signaling (227). Both processes are fundamental in bone formation as they regulate the expression of osteogenic genes (236, 237).

We started by analyzing the characteristics of all the cell lines with *FLNA* variants together as compared to controls. We first demonstrated that cOBs with *FLNA* variants had a significant increase in the overall proliferation rate compared to controls. Data from syndromic craniosynostosis demonstrated parallel supportive results. Mutations in *MSX2* and *AXIN2* showed increased levels of cell proliferation in the fused sutures (295-298). Craniosynostosis with enhanced PDGFRα also showed enhanced cellular proliferation (299). Additionally, increased cell proliferation was shown in caA3 mutants, where craniosynostosis associated with enhanced BMP (300). Thus, increased cellular proliferation would be expected to exacerbate syndromic craniosynostosis.

However, reduced cellular proliferation was also reported in non-syndromic (292) and syndromic forms of craniosynostosis, in osteoblasts from patients with Apert Syndrome (293). Nevertheless, proliferation rate appeared normal in osteoblasts with the *FGFR2* mutation that causes an Apert phenotype (301).

Changes in mechanical forces and matrix features are believed to be associated with craniosynostosis (302-306). FLNA, through interacting with several binding proteins in the cytoskeleton, can trigger biochemical responses that reorganize the cytoskeletal main elements to resist strain. As a result, signaling pathways can induce cellular changes leading to generating focal adhesion sites that control migration and contraction forces (209, 214, 307).

Cell migration is fundamental in the growth of cranial bones. The normal expansion and patterning of the of the calvaria is regulated by the migration of osteoprogenitors within the suture area (302). We demonstrated that both cMSCs and cOBs with *FLNA* variants have slower migration rates than controls. We then showed that cMSCs with *FLNA* variants did not generate a significantly different contractile forces than controls. However, they manifested a small cell area compared to controls.

Our data supports evidence from previous observations. In humans, osteoblasts with high levels of *IGF1* expression from patients with SSC had reduced migration and enhanced intracellular force generation (308). It also has been shown that impaired migration in osteogenic precursor cells leads to craniosynostosis in mice (309). Previous studies have also reported the effect of *FLNA* in migration. Neurons that lack *FLNA* fail to migrate within the cerebral cortex (202, 218). In melanoma cells, *FLNA* deficiency leads to reduced cell motility, and the effect can be rescued in vivo by exogenous FLNA (202, 215-217). Moreover, *WNT5a* knockdown decreased *FLNA* expression and corresponds with reduced cell motility (219, 220). In *Dictyostelium* amoebae, diminished *FLNA* levels impair locomotion and chemotaxis (221). The dynamics of the actin cytoskeleton and migration were impaired in *FLNA*-null monocytes (224).

The combination of findings, increased proliferation and decreased migration provide some support that *FLNA* variants could be associated with premature suture fusion in SSC.

Furthermore, FLNA is required for normal contractility and stiffness in various cell types (185-187, 310, 311) and high contractile force has been reported in osteoblasts from patients with SSC (308). Based on reported studies, the relationship between contractility and *FLNA* is well-defined. FLNA generates contractile forces upon binding to the actin filaments (312). FLNA facilitates contractility by reducing the tension in the cytoskeleton and shortening the contractile apparatus (313).

Despite the supporting literature, we found no significant difference in contractility between

cMSCs with *FLNA* variants and controls. This could be due to the limited sampling size (9 cMSCs from patients with SSC and 10 controls) or to the fact that the cells were growing in SF medium, and the effect might rise during osteogenic induction or with supplemented media that mimic in vivo environment. It has been shown that different types of culture media can have a significant impact on MSC growth, contraction potential, surface marker expression, and ECM properties (314, 315). SF media has been shown to inhibit BMMSC contraction and ECM production. (316, 317).

Our findings suggest that the identified rare *FLNA* variants could affect the cytoskeleton organization leading to restricted spreading and small area.

Taken together, *FLNA* variants could contribute to the development of SSC through altering the cytoskeleton, migration, and proliferation.

The correlation between dysregulation of differentiation and premature fusion of the cranial sutures has been investigated previously (278, 318-320). The osteogenic differentiation of cMSCs revealed altered *SP7*, *BGLAP*, and *SPARC* expression between cMSCs with *FLNA* variants and controls. *SP7* is a well-established osteogenic gene and is essential for bone development; it demonstrates a role in specifying MSCs commitment toward an osteoblastic lineage (19, 149). Moreover, it regulates the expression of osteoblast differentiation and matrix mineralization genes such as: *COL1A1*, *BGLAP*, *SPP1*, *SPARC*, *RUNX2* (150-152). *BGLAP* is a late osteogenic marker expressed by mature osteoblasts during mineralization and it makes up 20% of the total protein in the bone (153-155). *SPARC* regulates prominent cellular activities with the ECM through interacting with several matrix proteins. It can modulate proliferation, migration, adhesion, and cell shape (321, 322). The altered expression of these genes indicates dysregulated ossification mechanism in the calvarial tissues of SSC patients with *FLNA* variants.

In this study, we focused on assessing the expression of genes directly associated with intramembranous ossification. We demonstrated that *SP7* and *BGLAP* were downregulated whereas *SPARC* was upregulated in cMSC with *FLNA* variants compared to controls. The under-expression of *SP7* and *BGLAP* is contrary to previous studies which have confirmed the association between increased osteogenic differentiation and craniosynostosis through upregulation of master osteogenic genes (318-320). However, hypomineralization (280) and chondrogenesis (323-330) have been reported with premature suture fusion. Constant upregulation of *SOX9*, a master regulator of chondrogenesis (331, 332) has been reported with *BGLAP* downregulation in the suture (333). Furthermore, *SPARC,* is a downstream target for *SOX9* (334), and their co-expression has been reported in ectopic calcification of atherosclerotic tissues (335-337). *SPARC* is required for cartilage formation and is directly involved in chondrocyte differentiation and inhibiting its translation and splicing, resulting in cartilage defects similar to *SOX9* mutant defects (338). *SPARC* was the only gene that showed high expression in cMSCs with FLNA variants compared to controls. Though the low expression of *SP7* and *BGLAP* is rather difficult to interpret because they are fundamental in osteogenic process, the increased expression of *SPARC* suggests that cranial fusion in SSC patients with *FLNA* variant could be carried out through endochondral ossification.

Previous works has established an association between craniosynostosis and chondrogenesis (323-330). Ectopic cartilage formation and chondrogenesis in the sutures have been described in various human and mice models of craniosynostosis (323-330). *Axin2* knockout, *FGFR1* heterozygosity (339) and *Twist1*+/− haploinsufficiency in mice lead to premature suture fusion (330, 340). In addition to that, chondrogenic synostosis of the cranial suture has also been associated with Apert syndrome (325), Crouzon syndrome (341-343), and with dysregulated PDGFRα signaling (299). These studies have shown that craniosynostosis can develop through endochondral ossification.

Cyclic tensile strain on human MSCs significantly enhanced the expression of *SOX9*, *RUNX2*, *SPARC*, *SPP1*, and *ALP* (344). Compressive strain induced chondrogenic differentiation and significantly increased *SOX9* expression (345). Mechanical stimuli could affect early osteogenic and chondrogenic differentiation in the suture (344, 346). It can also affect FLNA interaction with partner proteins leading to altered function (173, 177, 245, 253, 254). Moreover, *FLNA* mutations have been attributed to early obliteration of the cranial sutures (4, 255). Since *FLNA* is a mechanoresponsive gene (173), altered FLNA function in SSC patients with *FLNA* variants, along with mechanical stimuli could have affected the normal growth of the calvarial bone and sutures. External force during fetal life could have led to upregulation of *SPARC* expression and synostosis in SSC patients with *FLNA* variants.

Taken together, these results suggest that the normal bone formation process is altered in cMSCs harboring *FLNA* variants as depicted by the possible late upregulation of *SPARC* and downregulation of *SP7* and *BGLAP* in comparison to controls. It also suggests that the mechanism governing craniosynostosis in patients harboring *FLNA* variants might be distinct from intramembranous ossification. The *FLNA* variants could have adopted a different fate, an alternative way of ossification in the fused sutures. Our data provides the possibility that *FLNA* associated craniosynostosis may occur through endochondral ossification.

The *FLNA* variants of interest that we identified in individuals with SSC are not localized/clustered in one functional domain. Therefore, we decided to take a specific approach and group them based on their domain's interactions: FLNA-ACT, FLNA-VIM, and FLNA-FOX. This perspective could illustrate further cellular and biomechanical features of each group.

FLNA-ACT domain group

All individuals with variants in this group were males who inherited the variants from their healthy mothers suggesting an X-linked recessive pattern (Table. 3.4). Previously-reported missense *FLNA* mutations associated with craniosynostosis in OPDS are clustered within F-actin domains (177, 255-258). These reported mutations were seen in four males and three females where three of the males showed a maternal inheritance pattern and one male and all the three females were de novo.

FLNA crosslinking of actin filaments relies on a delicate ratio of FLNA to F-actin concentration, required for diverse biomechanical processes (185-187). Disrupting this balance by a genetic factor or external force may have a substantial impact on the cytoskeleton, demonstrated by altered migration, adhesion, and/or contractility (184, 191, 203, 204). Additionally, it has been shown that *FLNA* mutations on the F-actin domains enhance FLNA-F-actin binding affinity that disorganizes the actin filaments, leading to altered processes in the cytoskeleton (177). Altered mechanical processes like contractility and migration have been associated with craniosynostosis (308). In this study, we observed higher proliferation in cMSCs and cOBs with FLNA-ACT variants, along with impaired migration in cOBs with *FLNA* variants. This is consistent with studies showing increased proliferation (293, 295-300, 347-349) and reduced migration rate (308) as being correlated with craniosynostosis.

Moreover, dysregulated FLNA interactions can initiate or restrict subsequent signaling cascade involved in bone development (191, 196, 227, 235, 236). The gene expression pattern of the cMSCs from patients with SSC during differentiation was altered in the FLNA-ACT domain group as compared to controls. The expression of *BMP2*, *SP7*, *RUNX2*, *SPP1*, and *BGLAP* were markedly reduced compared to controls. *BMP2* is expressed in calvarial bones and can regulate bone formation and eventually lead to osteogenesis in the suture (126, 278,

318, 350). *RUNX2* is an early marker of osteogenesis, and its expression is coupled with *ALP* downregulation (351, 352). It is vital for osteoblast differentiation and calvarial bone development, as it regulates the proliferation of MSCs and osteoprogenitors in the sutures (156-158). This change suggests that cells harboring FLNA-ACT variants are exhibiting impaired osteogenic differentiation, indicated by downregulation of main osteogenic genes. Nonetheless, these variants could have pursued a distinct ossification process (endochondral) in the fused sutures. However, further investigations are needed to prove this claim.

In all, our identified FLNA-ACT variants exhibited altered proliferation, migration, and osteogenesis. These results indicate that these variants could be disrupting the interaction between FLNA and F-actin leading to enhanced binding resulting in reduced migration. The recurrence of our *FLNA* variants' location and the consistency of our findings with previous reports suggests that these variants contribute to craniosynostosis. Additional investigation will further our understanding of the correlation between FLNA and F-actin interactions and cranial suture fusion.

FLNA-VIM domain group

In this group, one of the individuals is male and two are females (Table. 3.4). Both females demonstrated skewed X-inactivation toward the variant allele. We have the inheritance information of one female only who inherited the variant from her mother, who did not have craniosynostosis. This pattern suggests an X-linked dominant inheritance with incomplete penetrance.

Vimentin is an intermediate filament constructing the cytoskeleton along with FLNA and F-actin to mediate interaction with partner proteins, contractility, migration, and cell shape (277, 353-355). FLNA and vimentin are known to be co-expressed in MSCs and osteoblasts. Their

expression is upregulated in osteoblasts during shear stress events as they act as mechano-protectors (356). cMSC and cOB cells in this group had a lower migration rate than controls. Assessment of the proliferation rate showed that cMSCs did not demonstrate a significant difference whereas cOBs had a higher proliferation rate compared to controls. Although these variants didn't impact contractility force and cell area in cMSCs, they exhibited an increase in force/ dot ratio. This finding suggests that the actual strength of the mechanical protein is higher in FLNA-VIM domain group compared to controls.

Along with maintaining the cytoskeleton integrity, vimentin plays a fundamental role in osteogenic differentiation of MSCs and osteoprogenitors. It has an inhibitory role during osteoblast differentiation as it suppresses *BGLAP* transcription; vimentin expression has shown to be downregulated in the terminal osteoblast differentiation stage (357, 358). Simultaneously, vimentin mRNA level also decreases overtime during differentiation of primary calvarial osteoblasts (358). Furthermore, vimentin determines the osteogenic fate of MSCs through regulating the FA contact size where small FA sizes induce cell motility and facilitate osteogenesis (359). Therefore, disrupting vimentin regulation could contribute to craniosynostosis through affecting osteogenesis in the suture.

We have demonstrated that during osteogenic differentiation of cMSCs with FLNA-VIM variants, *SPARC* and *SPP1* expressions were upregulated whereas *SP7* was downregulated.

SPP1 and *SPARC* are main components of the bone matrix. There are similarities between the expression of *SPP1* and *SPARC* in the FLNA-VIM domain group and previous observations. During chondrogenesis, both *SPP1* and *SPARC* are co-expressed with *SOX9* in ectopic calcification in atherosclerotic lesions (335, 336). *SPARC* is required for cartilage formation and directly involved in chondrocyte differentiation. Inhibiting its translation and splicing results in cranial cartilage defects similar to *SOX9* mutant (338). *SOX9* regulates the expression of *SPARC*, *SPP1*, and vimentin (334).

Interestingly, the reported correlation between *SPP1* and vimentin (360, 361) has emerged from the FLNA-VIM domain group, since *SPP1* was only found upregulated in this group. Previous study has shown that *SPP1* and vimentin colocalize in MSCs at bone formation and remodeling sites in mouse models of osteogenesis imperfecta (360). *SPP1* also works to increase vimentin stability through impeding the degradation of the vimentin protein (361).

Taken together, supportive studies along with our findings suggest that overexpression of *SPP1* and *SPARC* is associated with chondrogenesis; indicating that ectopic cartilage formation caused craniosynostosis in SSC patients harboring FLNA-VIM variants.

Fundamentally, *SPP1* and *SPARC* are major matricellular proteins, in addition to playing critical role in bone and cartilage mineralization (362, 363). They have a major structural role as they regulate cell's mechanics. *SPP1* regulates cell responses through several integrin receptors and affects actin filaments interactions and binding, through modulating the intracellular levels of Ca2+ (321). These diverse activities mediate chemotaxis, cell motility, and migration (321) which are important for suture mesenchyme homeostasis. Additionally, *SPARC* expression is positively correlated with vimentin expression (364). Furthermore, mechanical stimuli could affect early chondrogenic differentiation (344, 345) and upregulate vimentin and FLNA expressions (356). In support of that, cyclic tensile strain on human MSCs also significantly enhanced the expression of *SOX9*, *RUNX2*, *SPARC*, *SPP1*, and *ALP*.

These findings support our results via highlighting the association between FLNA, vimentin and bone or cartilage formation. The results from FLNA-VIM group emphasize the potential effect of *FLNA* variants on cranial suture fusion. Two variants exhibited skewed X-inactivation, which indicates that the variants are expressed in most cMSCs. These results suggest that variants could have have triggered the concurrent expression of *SPP1* and *SPARC*, along with reduced migration, enhanced proliferation, and altered cells mechanics exhibited in a higher force/ dot ratio. In support of previous studies (361, 364), the results

suggest that vimentin concentration could be higher in cells harboring these *FLNA* variants. Disrupted vimentin could alter FLNA function and subsequently the cytoskeleton's interactions. These changes are implicated in disrupted biomechanical features and bone formation leading to craniosynostosis.

FLNA-FOX domain group

In this group (Table. 3.4), two of the individuals are males and one is female expressing the X variant at an approximate equal level to the normal allele. One male and the female showed maternal inheritance. This suggests an X-linked recessive pattern in the male and X-linked dominant pattern with incomplete penetrance in the female.

FOXC1 regulates proliferation and differentiation during osteogenesis and chondrogenesis and is substantially expressed in the calvaria during the early stages of development (235, 236). It mainly influences the proliferation phase in calvarial bone development through regulating *MSX2* and *ALX4* (237).

FLNA negatively regulates FOXC1 transcription by binding and inhibiting *FOXC1* in the nucleus (191, 196). *FOXC1* knockdown is correlated with enhanced *ALP*, *RUNX2* and *BGLAP* expression (238). Therefore, FOXC1-FLNA interaction mediates the expression of osteogenic gene markers. In FLNA-FOX domain group, we showed marked increase in *SPARC* expression compared to controls, where *BMP2*, *SP7*, and *BGLAP* expressions were decreased. Enhanced proliferation and impaired migration compared to controls were observed in this group as well. These findings combined suggest that variants in the FLNA-FOX domains could contribute to craniosynostosis via altering gene expression, proliferation, and migration. Previous studies also have correlated craniosynostosis with dysregulated osteogenesis, increased proliferation and reduced migration (280, 295-300, 308, 318, 347-349).

Our results suggest that chondrogenesis might be the process governing

craniosynostosis in SSC patients harboring variants in the FLNA-FOX domain group. In this group, only *SPARC* showed higher expression in cMSCs compared to controls. *SPARC* plays an essential role in chondrogenic differentiation by acting downstream of *SOX9* (334-338). *SOX9* positively regulates *SPARC* expression during chondrogenesis (365). Moreover, constant upregulation of *SOX9* (331, 332) has been reported with *BGLAP* downregulation in the suture (333). This finding is confirmed in our results as *BGLAP* expression was downregulated and *SPARC* was upregulated in FLNA-FOX group.

In light of the suggestion that variants in the FLNA-FOX domain group lead to suture fusion via chondrogenesis, FOXC1 directly affects endochondral ossification. Overexpression of *FOXC1* in chondrocytes significantly upregulated *COL10A1* expression (366). The occurrence of the variants on functional domains where *FOXC1* interacts with *FLNA* could have altered FOXC1 regulation leading to ectopic chondrogenesis.

In addition to characterizing the identified rare FLNA variants, we wanted to further elucidate the role of FLNA in calvarial mesenchyme by knocking out FLNA; then evaluating the expression of a subset of critical osteogenic genes in FLNA KOs and controls. FLNA loss has been extensively studied in heart, skeletal muscle, and neurons (224, 260, 367-373), but little is known about FLNA's role in the calvaria. FLNA is a critical upstream element of the signaling cascade governing bone formation (191, 196, 227, 228, 230, 236).

The primary goal of these experiments was to achieve a near complete KO of FLNA. We successfully established FLNA KO to address the consequences of FLNA loss in human cMSCs. Using CRISPR/ Cas9, we obtained efficient gene disruption (Figure. 3.12).

FLNA KOs showed an altered expression of osteogenic genes as compared to controls (Figure. 3.13). *RUNX2* and *COL1A1* expressions were significantly reduced in *FLNA* KOs compared to controls. *RUNX2* tightly controls skull patterning and growth, as it is essential for calvarial osteoprogenitor and osteoblast differentiation (164). It regulates signaling molecules

and transcription factors during osteogenesis and calvarial development (159). *Runx2* -/- (total KO) mice completely lack calvarial osteoblasts (374). Moreover, Runx2 deficiency in mice is associated with reduction in *DLX5, SP7, SPP1, COL1A1* and *BGLAP* expression in the intramembranous regions of the skull (calvaria and mandible) (159, 164, 375, 376).

COL1A1 is an early marker of osteogenesis (377) and it is upregulated during calvarial suture osteogenesis and osteoblastic differentiation (161). It positively regulates the expression of *ALP* and *BGLAP* (378). *COL1A1* mRNA expression was increased in cranial suture osteoblasts isolated from patients with Apert's syndrome (301). Moreover, mutations in *COL1A1* result in decreased bone mineral density and associated with osteoporotic fractures (379).

Taken together, we showed that *FLNA* positively regulates the expression of *RUNX2* and *COL1A1* in cMSCs suggesting the involvement of *FLNA* in calvarial bone development. The downregulation of the tested osteogenic genes in *FLNA* KOs compared to controls provides tentative evidence that *FLNA* affect their expression.

Our data suggests that *FLNA* is essential for early stages of osteogenesis. *FLNA* loss in cMSCs could dysregulate the osteogenic process and impair bone formation in the calvaria. These findings are consistent with reported studies of *FLNA* knockout in mice (260). Complete *FLNA* knockout is lethal to males due to major cardiac and skeletal defects. However, hemizygous females exhibited skeletal abnormalities (260). *FLNA*- null female mice represented delay in bone development exhibited in cleft palate and failure in the sternum fusion (260).

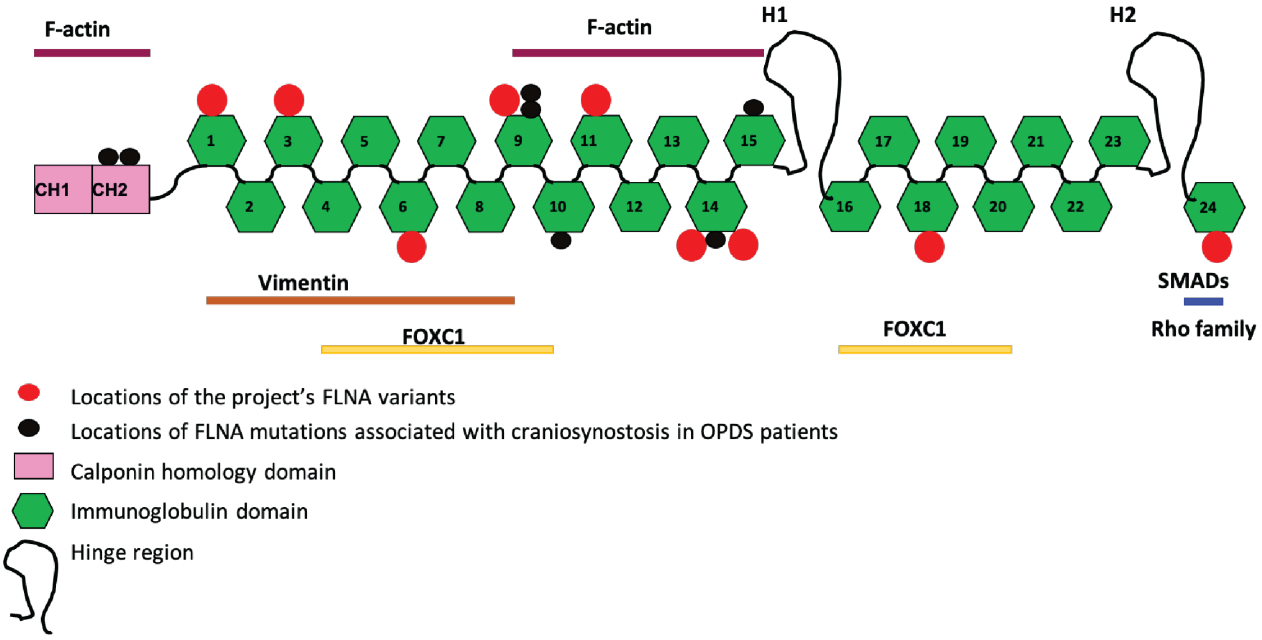

Figure 3.1. Schematic representation of FLNA structure (monomer) and location of the rare, identified variants and reported mutations.
Filamin-A is a homodimer. Each monomer contains 24 tandem repeats. Filamin-A can be divided into 5 major domains: (CH1 and CH2), Rod1 (Ig domain 1-15), hinge 1 (between Ig domain 15-16), hinge 2 (between Ig domain 23 and 24), C-terminal domain in Ig domain 24.

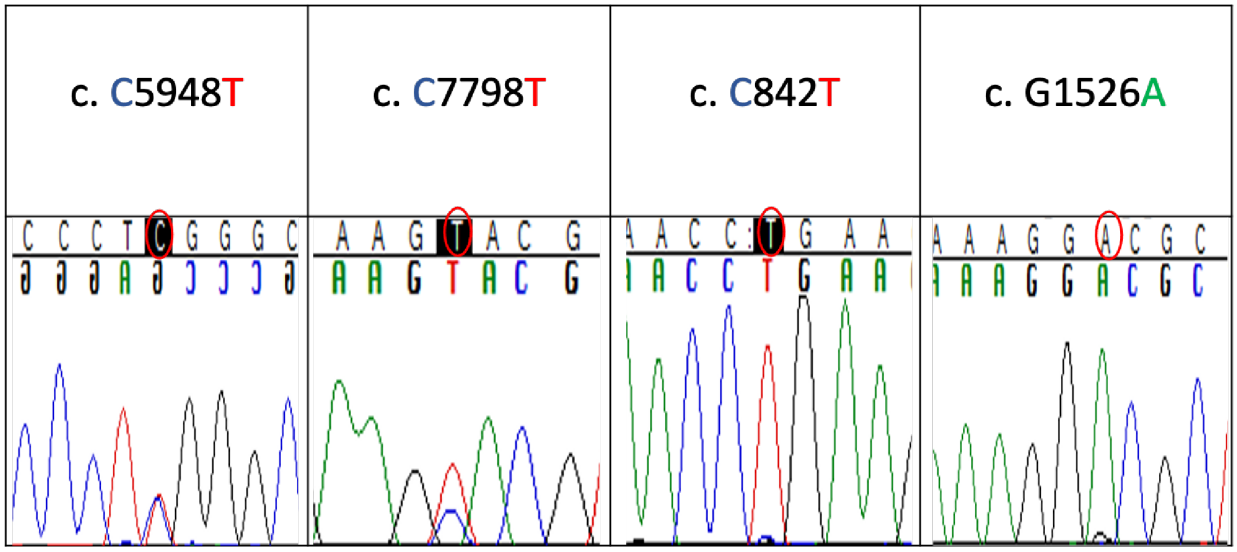

Figure 3.2. Sequence traces from cDNA of SSC cMSCs females with FLNA variants. Sequences showing heterozygous exchange position, 5948, 7798, 842, and 1526.

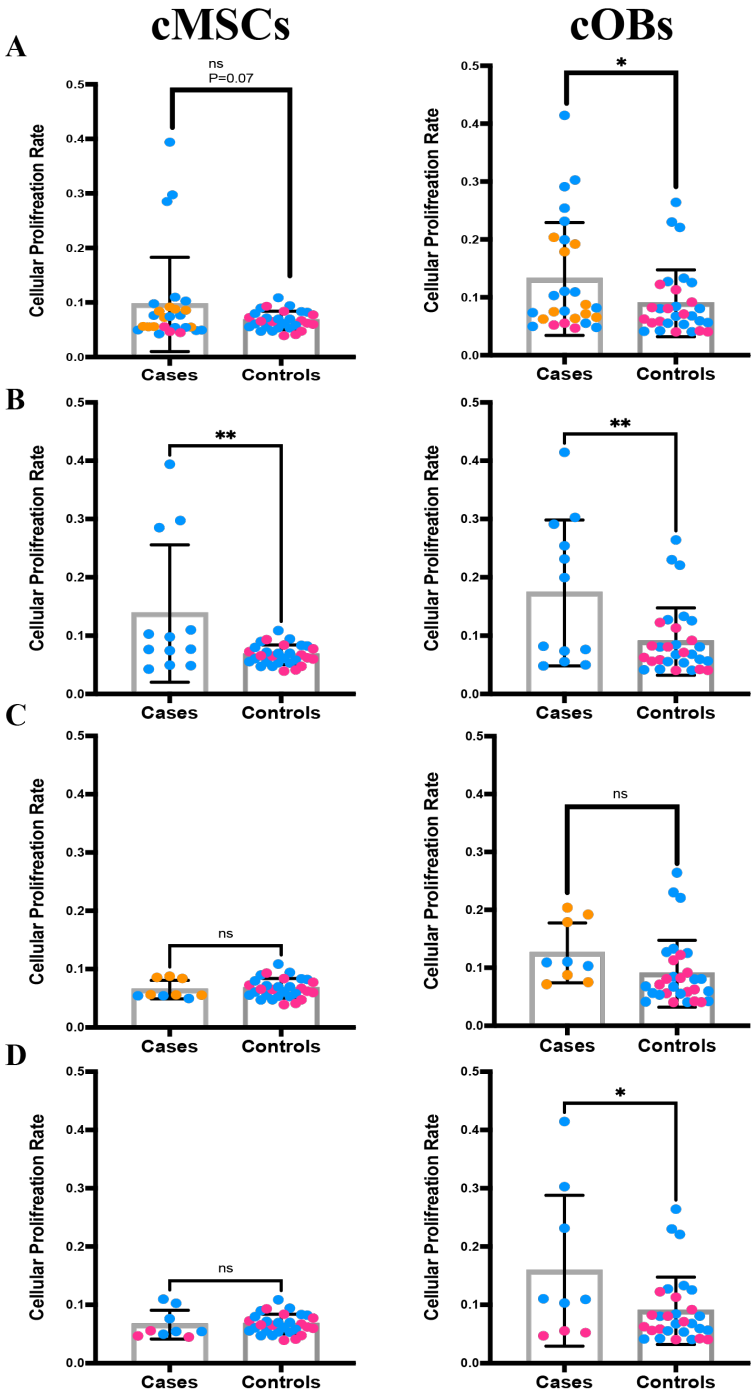

Figure 3.3. BrdU incorporation by SSC cMSCs with FLNA variants and cOBs.
No difference was found between SSC cMSC and controls whereas SSC cOBs had significant enhanced proliferation compared to controls (*P*=0.05) (A). Both SSC cMSCs and cOBs from the FLNA-ACT group (B) had a significant increase in proliferation compared to controls (*P*=0.002), (*P*=0.004) respectively. Proliferation was not significant in SSC cMSCs and cOBs of FLNA-VIM group (*P*=0.7), (*P*=0.1) (C). In FLNA-FOX group, SSC cMSCs didn't show a difference (*P*=0.8) while SSC cOBs had a significantly higher proliferation compared to controls (*P*=0.02) (D). Data shown as mean±sd from three experimental replicates ns *P*> 0.05, *$P \leq 0.05$, **$P \leq 0.01$ (Student's t-test).
Pink= female, Orange= skewed female, and Blue= male.

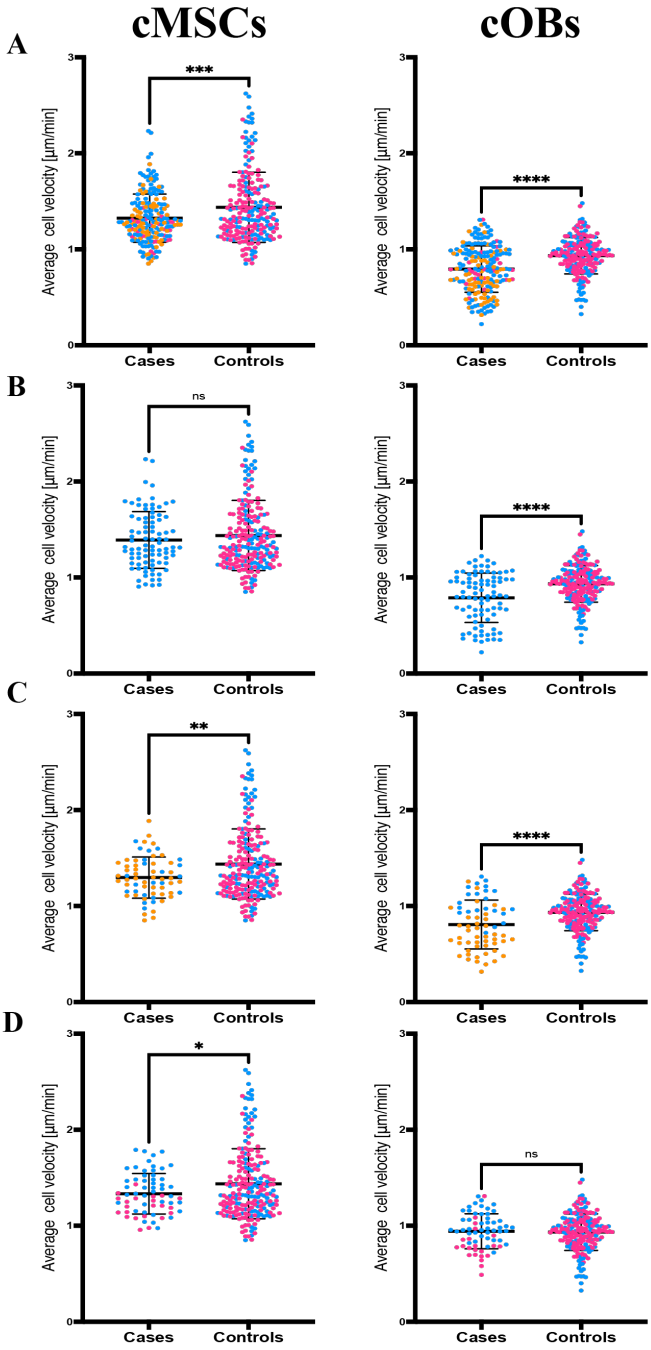

Figure 3.4. Reduced Migration rate observed in SSC cMSC and cOBs harboring FLNA variants.

Migration speed was significantly reduced in cMSCs and cOBs in FLNA cases compared to controls (*P*=3x10−4), (*P*=1x10−4) respectively (A). In FLNA-ACT group, only cOBs showed a significant lower migration compared to controls (*P*=1x10−4) while no difference was found in cMSCs (*P*=0.28) (B). Both cMSCs and cOBs in FLNA-VIM group exhibited reduced migration rate compared to controls (*P*=3x10−3), (*P*=1x10−4) respectively (C). cMSCs from FLNA-FOX group had a significant low migration rate compared to controls (*P*=0.02) whereas cOBs didn't show any difference (D). Data shown as mean±sd from 23 biological replicates.
ns *P*> 0.05, **P*≤ 0.05, ***P*≤ 0.01, ****P*≤ 0.001, ****P*≤ 0.001 (Student t-test).
Pink= female, Orange= skewed female, and Blue= male.

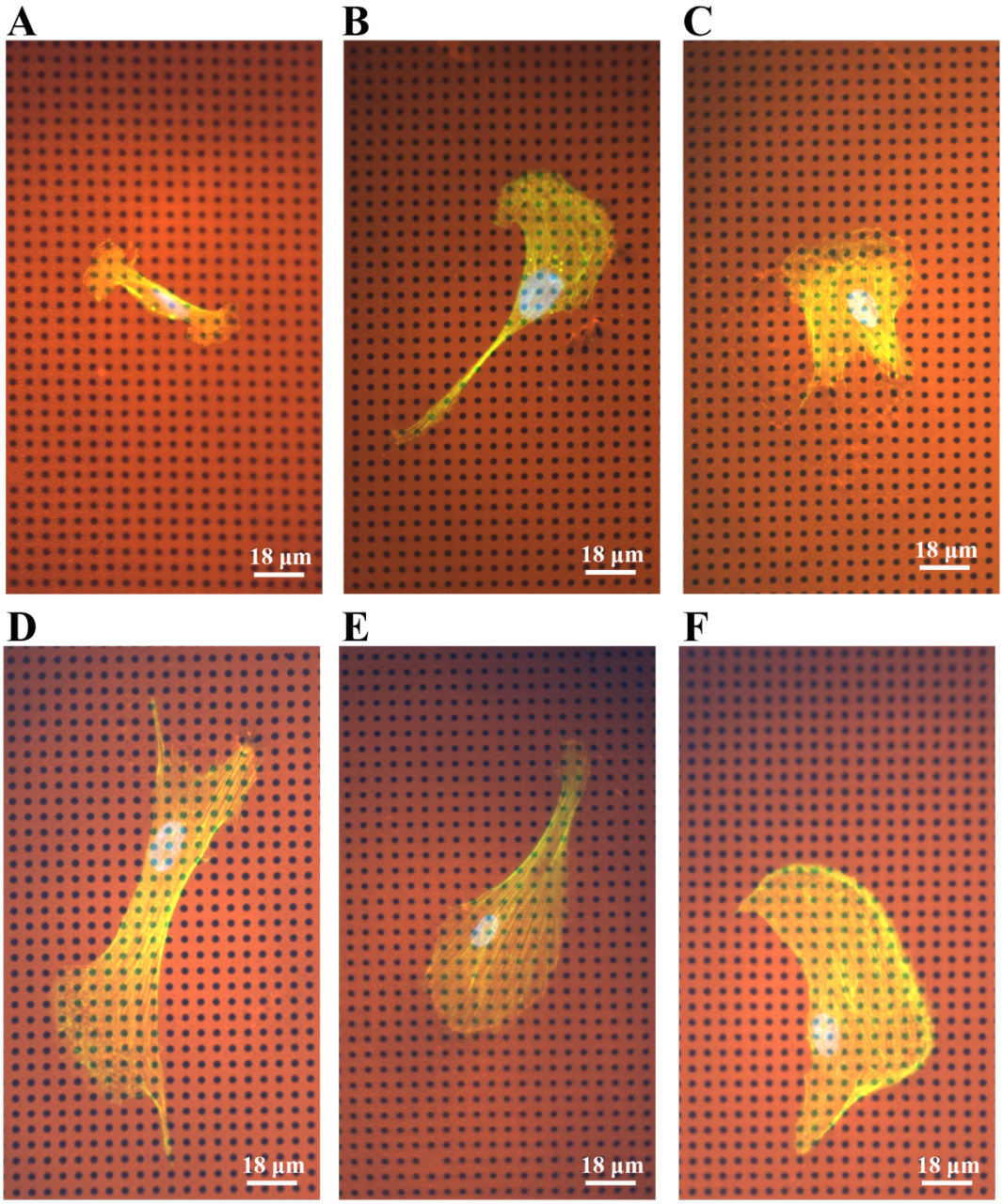

Figure 3.5. Black dots used to measure contractile force of SSC cMSCs with FLNA variants.
Substrates made using fluorescent BSA-Alexa Fluor 594 and cells are stained for both F-actin (green) and nucleus (blue). The cells adhere and deform the black dots substrate when contracting. Contractile forces are calculated from the displacement of the dots in FLNA cases (A, B, C) and controls (D, E, F).

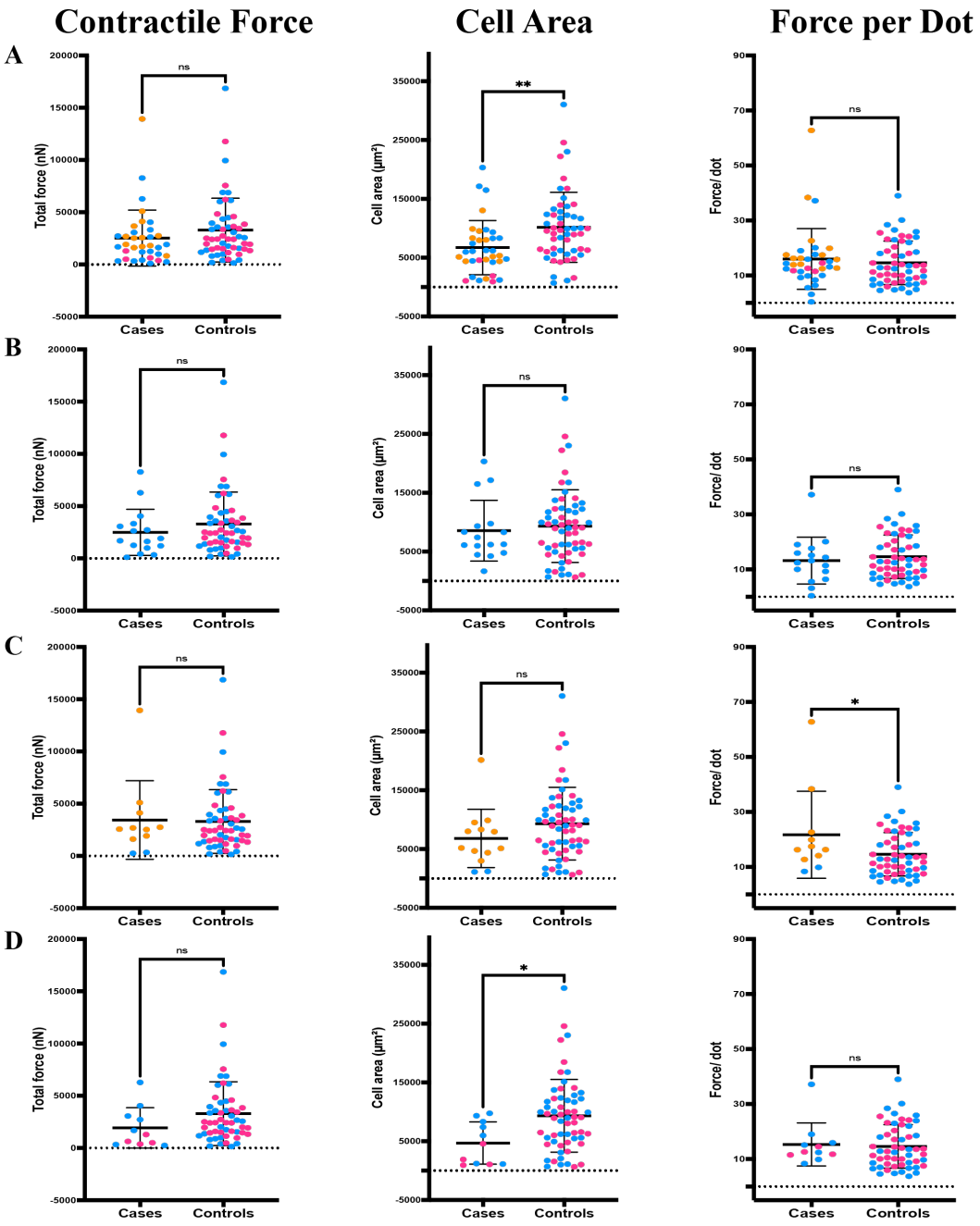

Figure 3.6. Contractility, cell area, and force/ dot in SSC cMSCs with FLNA variants.
No significant change in generated cell force was observed in all FLNA cases (*P*=0.22) (A), FLNA-ACT (*P*=0.33) (B), FLNA-VIM (*P*=0.89) (C), and FLNA-FOX (*P*=0.16) (D). Spread area was smaller in all FLNA cases (*P*=4x10−3) (A), and in FLNA-FOX group (*P*=0.02) (D), compared to controls; while no difference was found in FLNA-ACT (*P*=0.64) (B) and FLNA-VIM (*P*=0.17) (C). Force per dot (estimation of the protein's strength in the cell) was significant in FLNA-VIM group only (*P*=0.02) (C) whereas no change was observed in all FLNA cases (*P*=0.48) (A), FLNA-ACT (*P*=0.54) (B), and FLNA-FOX (*P*=0.7) (D).
Data shown as mean±sd. ns *P*> 0.05, **P*≤ 0.05, ***P*≤ 0.01 (Student's t-test).
Pink= female, Orange= skewed female, and Blue= male.

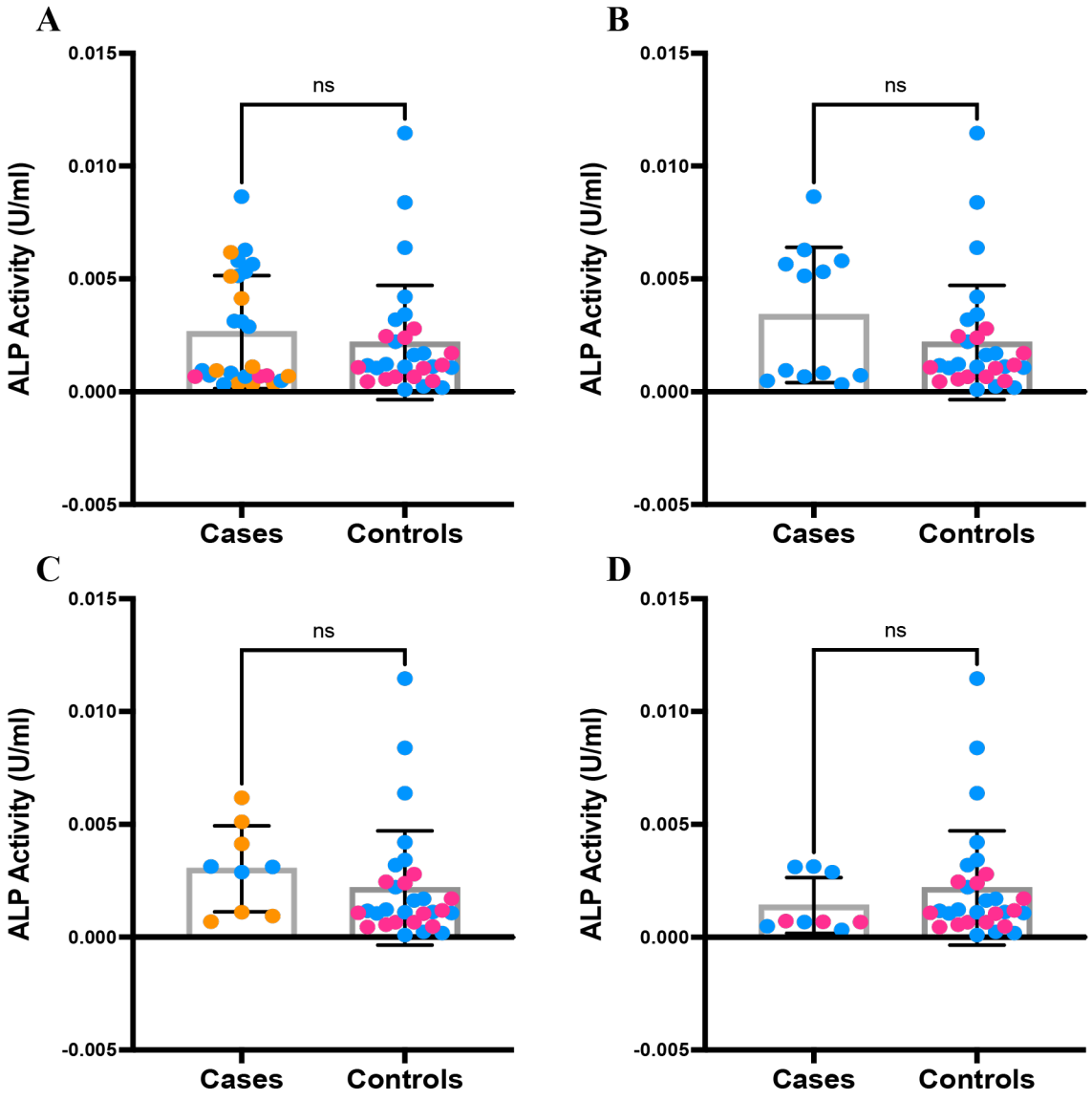

Figure 3.7. ALP Activity in SSC cOBs with FLNA variant.
Calculating ALP activity (OD405)/(BCA total protein) didn't reveal significant difference between all FLNA cases and controls (*P*=0.49) (A), FLNA-ACT (*P*=0.18) (B), FLNA-VIM (*P*=0.35) (C), and FLNA-FOX (*P*=0.38) (D). Data shown as mean±sd from 3 experimental replicates. ns *P*> 0.05 (Student's t-test).
Pink= female, Orange= skewed female, and Blue= male.

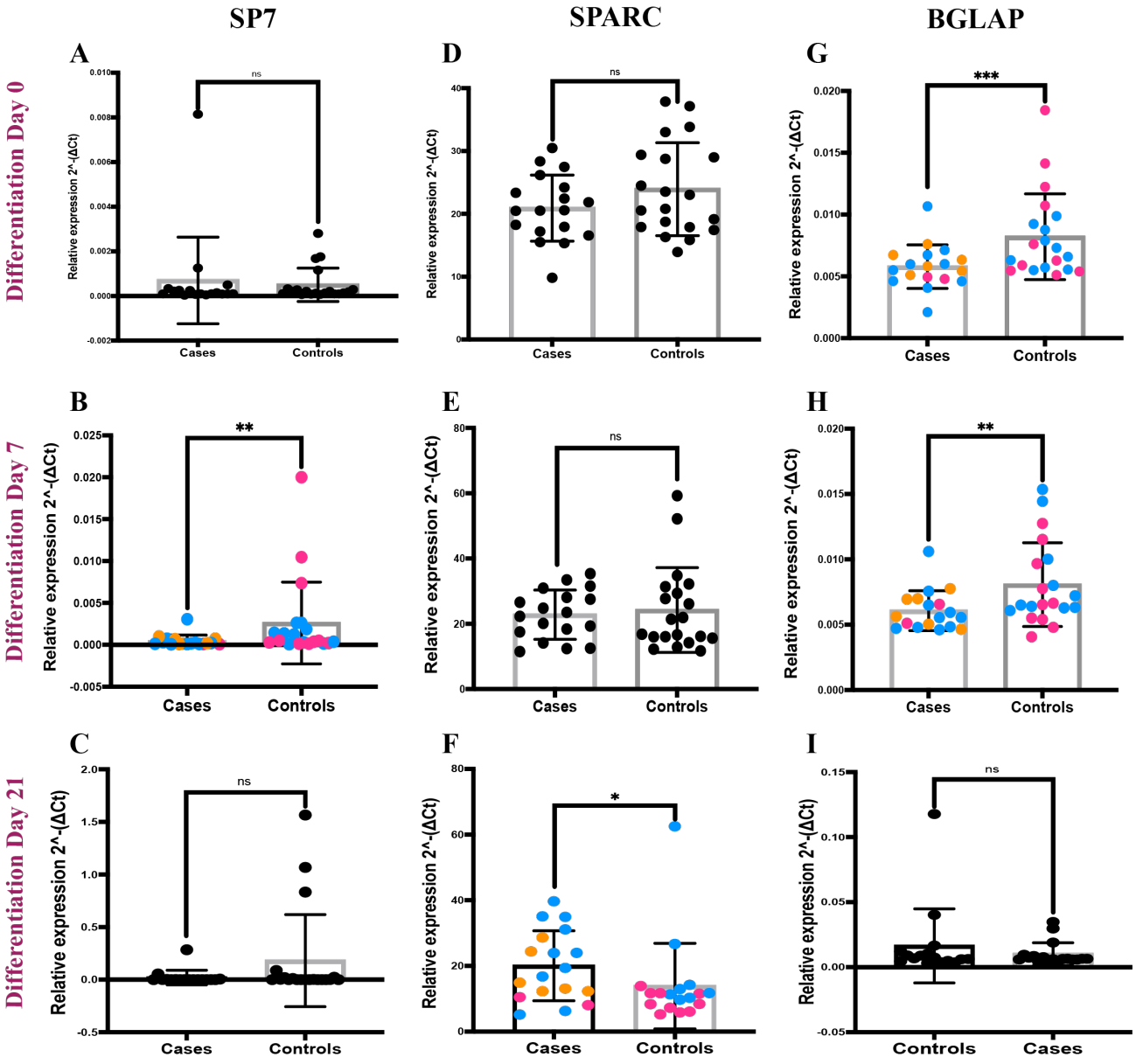

Figure 3.8. qPCR expression analysis of osteoblast marker genes at various time points during osteogenic differentiation of SSC cMSCs with FLNA variants.
SP7 mRNA expression was significantly reduced (*P*=0.01) at day 7 compared to controls (B) while no change was observed at day 0 (*P*=0.5) (A) and day 21 (*P*=0.08) (C). No significant difference was observed in the SPARC mRNA expression at day 0 (*P*=0.1) (D) and day 7 (*P*=0.9) (E), whereas the expression was significantly upregulated at day 21 (*P*=0.04) compared to controls (F). BGLAP mRNA expression had a significant reduction at day 0 (*P*=0.006) (G) and day 7 (*P*=0.01) (H), but no change was found at day 21 (*P*=0.6) (I).
Data shown as mean±sd. ns *P*> 0.05, **P*≤ 0.05, ***P*≤ 0.01 (Student's t-test).
Pink= female, Orange= skewed female, and Blue= male.

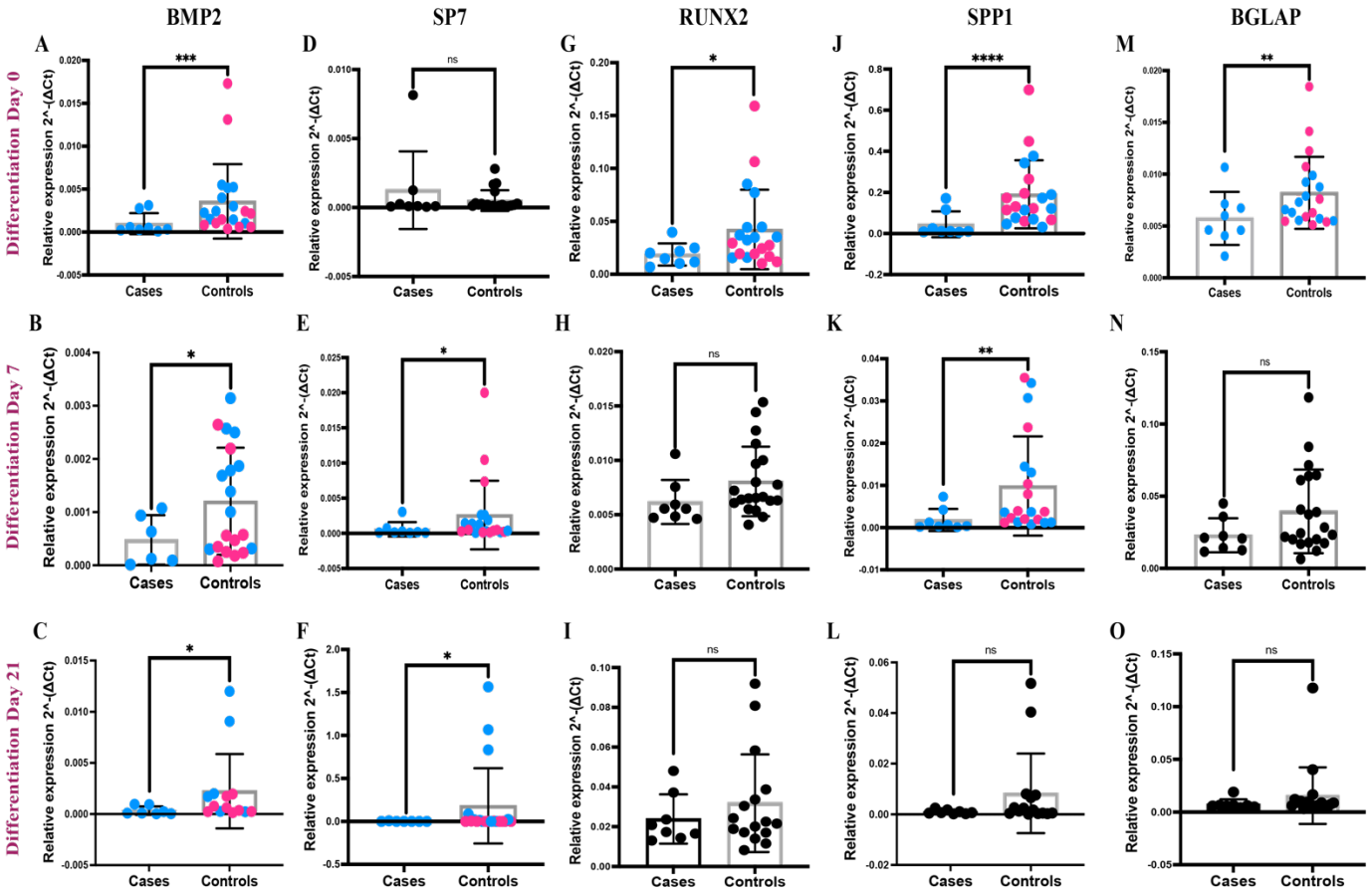

Figure 3.9. qPCR expression analysis of osteoblast marker genes at various time points during osteogenic differentiation of SSC cMSCs with FLNA-ACT variants.
BMP2 mRNA expression was downregulated at all the three time points (day 0, day 7, and day21) compared to controls (*P*=0.001) (A), (*P*=0.03) (B), and (*P*=0.02) (C) respectively. SP7 mRNA expression showed no difference at day 0 (*P*=0.9) (D), though day 7 (*P*=0.03) (D) and day 21 (*P*=0.04) (F) were significantly reduced compared to controls. RUNX2 mRNA expression had a significant reduction at day 0 (*P*=0.02) (G), but no difference in the expression was observed at day 7 (*P*=0.1) (H) and day 21 (*P*=0.5) (I). SPP1 mRNA expression was significantly lower than controls at day 0 (*P*=0.0001) (J) and day 7 (*P*=0.002) (K) while no change was observed at day 21 (*P*=0.2) (L). At day 0, BGLAP expression was significantly reduced compared to controls (*P*=0.006) (M) while the expression was not significantly different at day 7 (*P*=0.08) (N) and day 21 (P=0.4) (O).
Data shown as mean±sd. ns *P*> 0.05, **P*≤ 0.05, ***P*≤ 0.01, ****P*≤ 0.001, *****P*≤ 0.0001 (Student's t-test).
Pink= female, Blue= male.

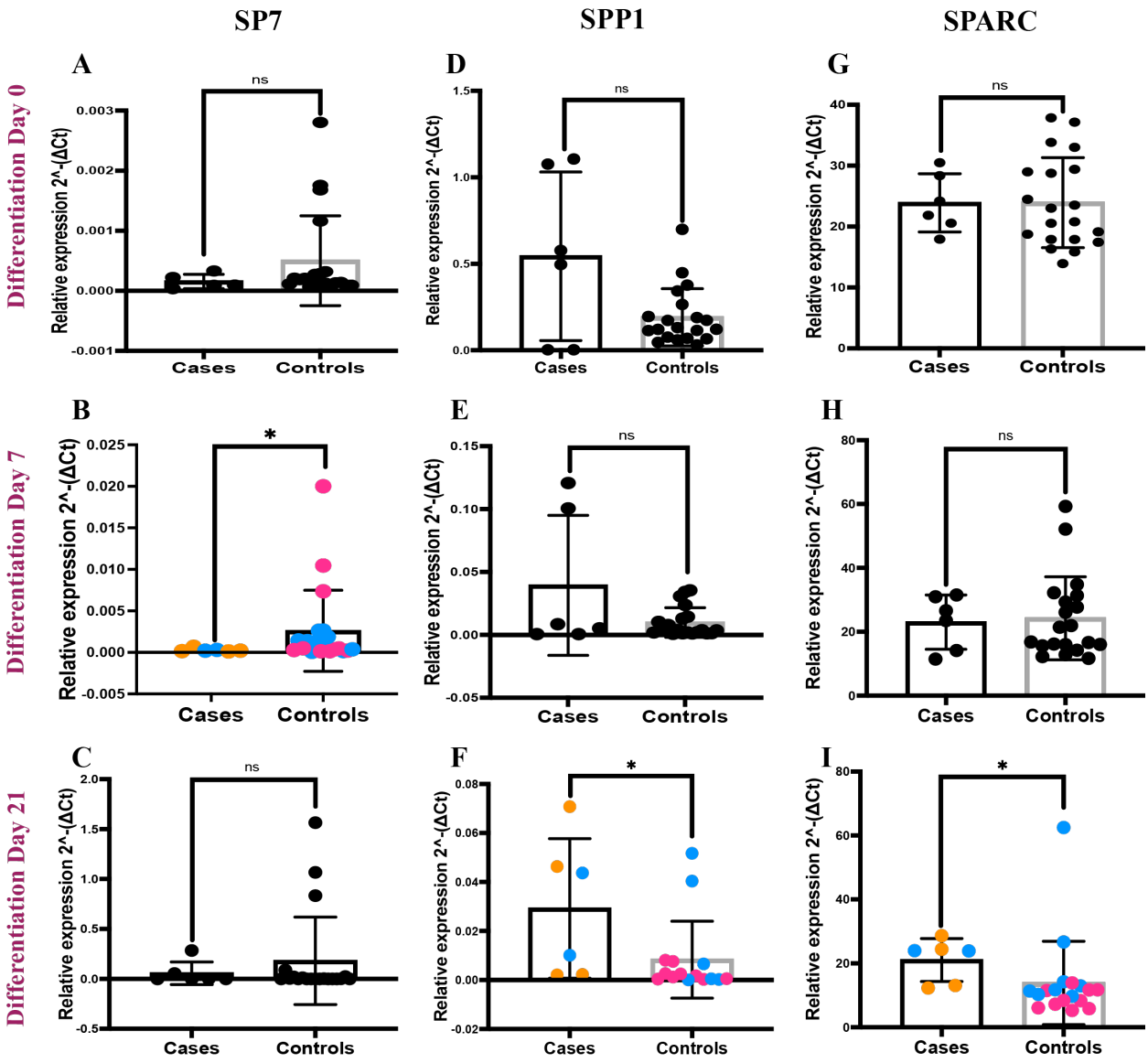

Figure 3.10. qPCR expression analysis of osteoblast marker genes at various time points during osteogenic differentiation of SSC cMSCs with FLNA-VIM variants.
SP7 mRNA expression was significantly downregulated at day 7(*P*=0.05) (B), but no significant change was observed at day 0 (*P*=0.2) (A) and day 21(*P*=0.5) (C). SPP1 mRNA expression didn't exhibit significant difference at day 0 (P=0.8) (D) and day 7 (*P*=0.5) (E) whereas it was significantly upregulated at day 21 compared to controls (*P*=0.04) (F). SPARC mRNA expression had a significant increase at day 21 (*P*=0.0.05) (I) compared to controls while no change was observed at day 0 (*P*=0.9) (G) and day 7 (*P*=0.8) (H).
Data shown as mean±sd. ns *P*> 0.05, **P*≤ 0.05 (Student's t-test).
Pink= female, Orange= skewed female, and Blue= male.

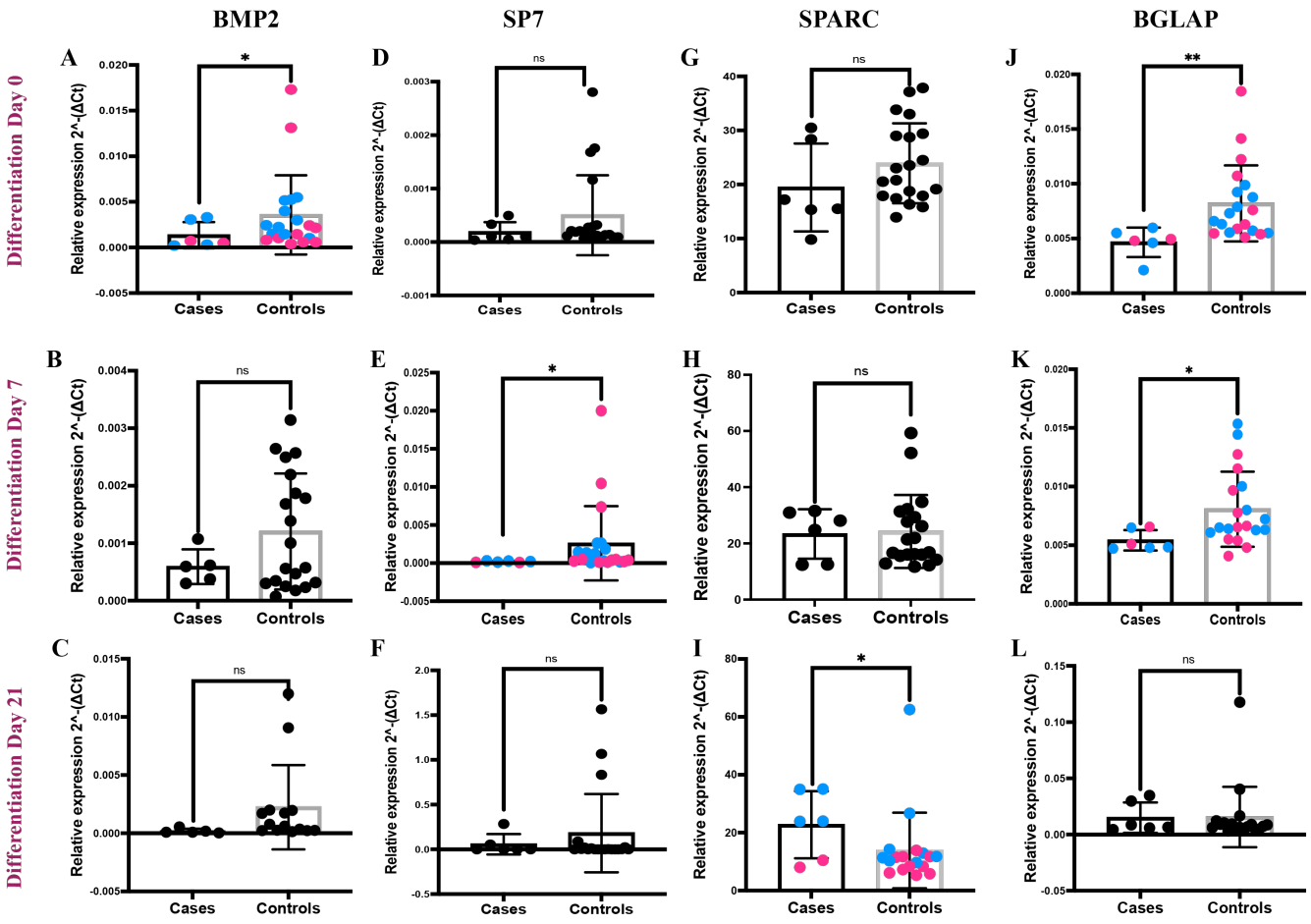

Figure 3.11. qPCR expression analysis of osteoblast marker genes at various time points during osteogenic differentiation of SSC cMSCs with FLNA-FOX variants.
BMP2 mRNA expression had a significant reduction at day 0 (*P*=0.05) (A), whereas no significant change was found at day 7 (*P*=0.6) (B) and day 21(*P*=0.5) (C). SP7 mRNA expression was significantly reduced at day 7 (*P*=0.02) (E) compared to controls; at day 0 (*P*=0.1) (D) and day 21 (*P*=0.6) (F), no significant change was observed. SPARC mRNA expression didn't exhibit significant difference at day 0 (*P*=0.1) (G) and day 7 (*P*=0.9) (H) whereas it was significantly upregulated at day 21 compared to controls (*P*=0.05) (I). BGLAP mRNA expression was significantly reduced at day 0 (*P*=0.003) (J) and day 7 (*P*=0.03) (K) while no significant change was observed at day 21 (*P*=0.6) (L).
Data shown as mean±sd. ns *P*> 0.05, **P*≤ 0.05, ***P*≤ 0.01 (Student's t-test).
Pink= female, Blue= male.

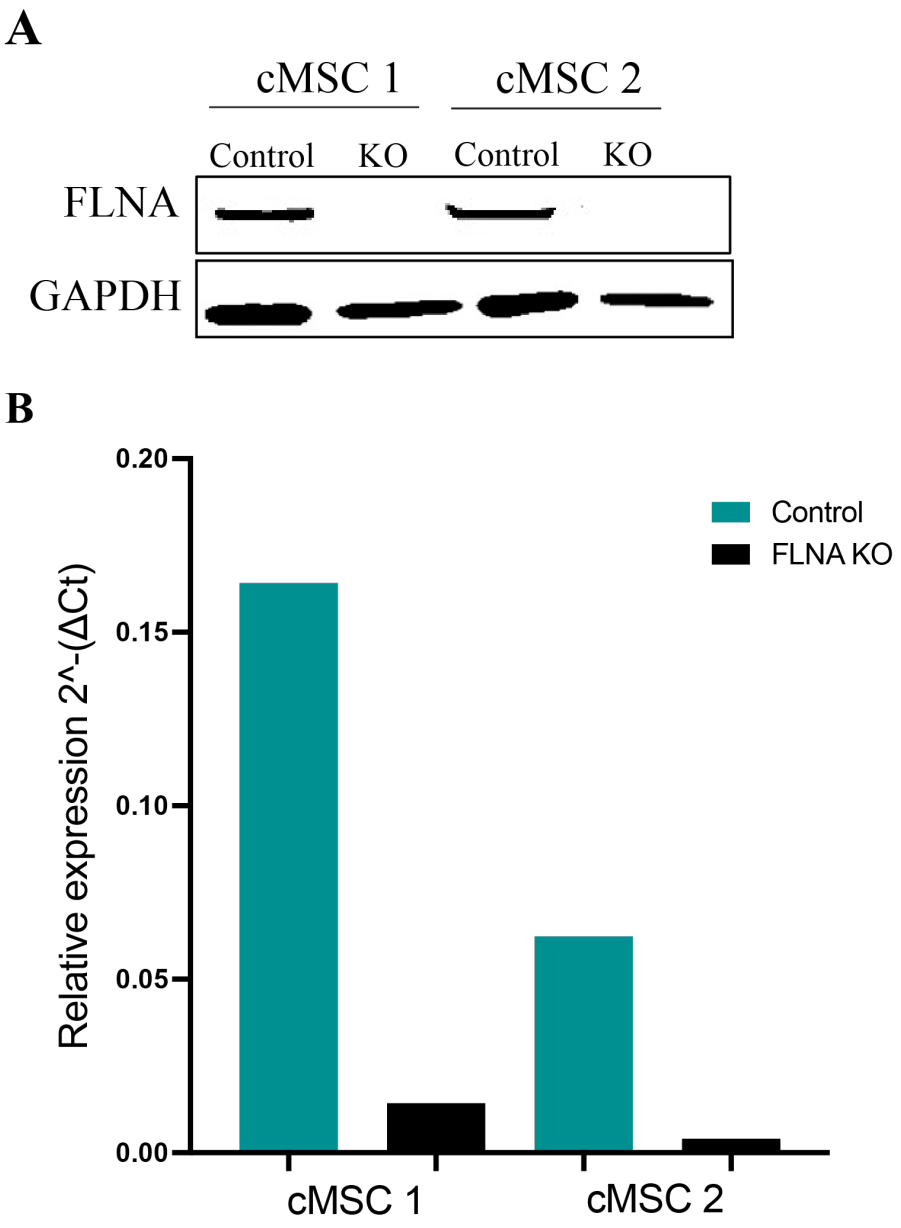

Figure 3.12. Assessment of CRISPR/Cas9. Representative western blot of FLNA protein levels knockout and control (A). FLNA expression at mRNA level of knockout and control cMSCs (B). All data are from two biological replicates.

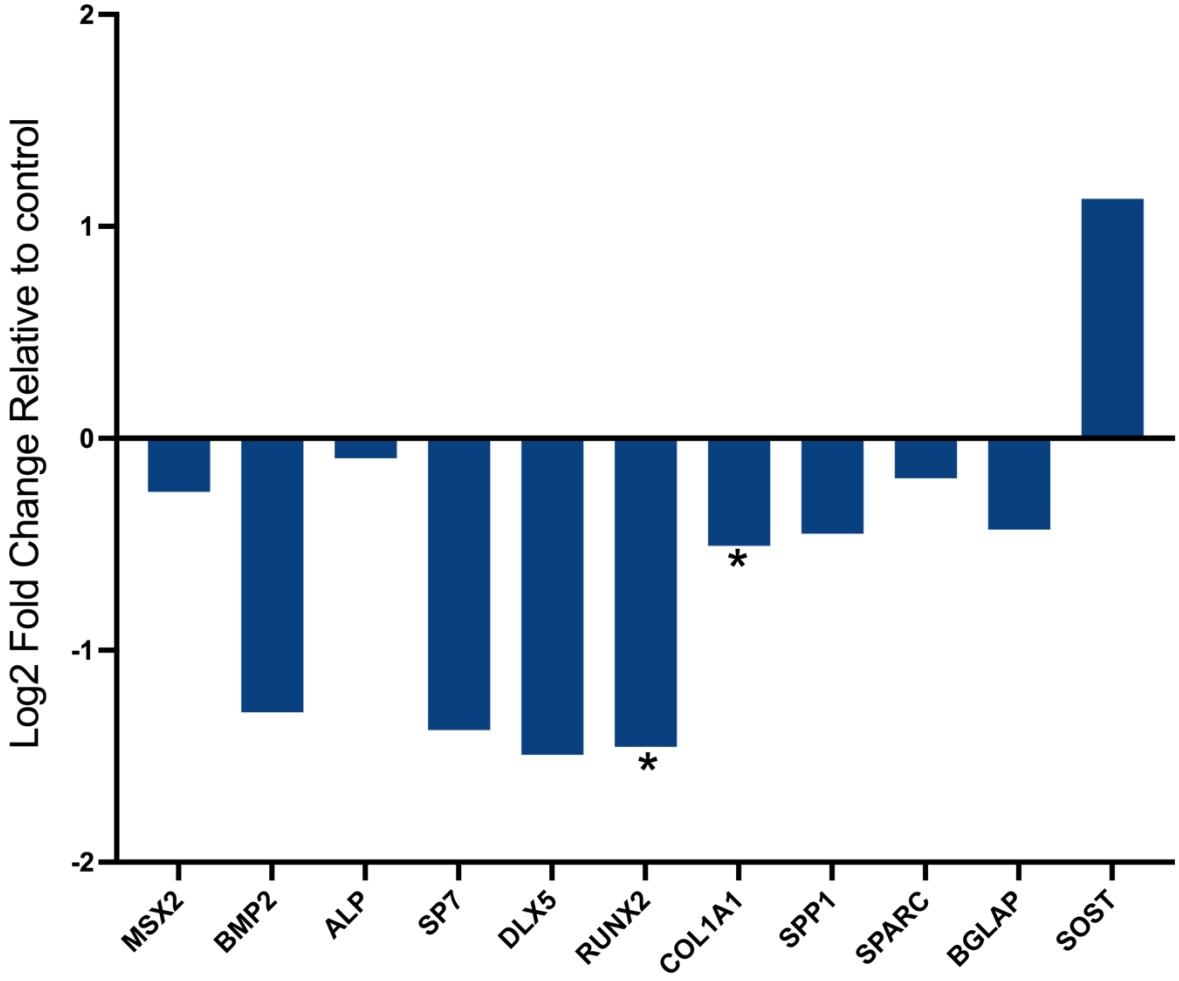

Figure 3.13. qPCR expression analysis of osteoblast marker genes in FLNA KO cMSCs compared to control cMSCs.
mRNA expression of all the tested genes was downregulated in *FLNA* KO compared to controls. However, only RUNX2 and COL1A1 were statistically significant resp. *$P \leq 0.05$ (paired t-test).

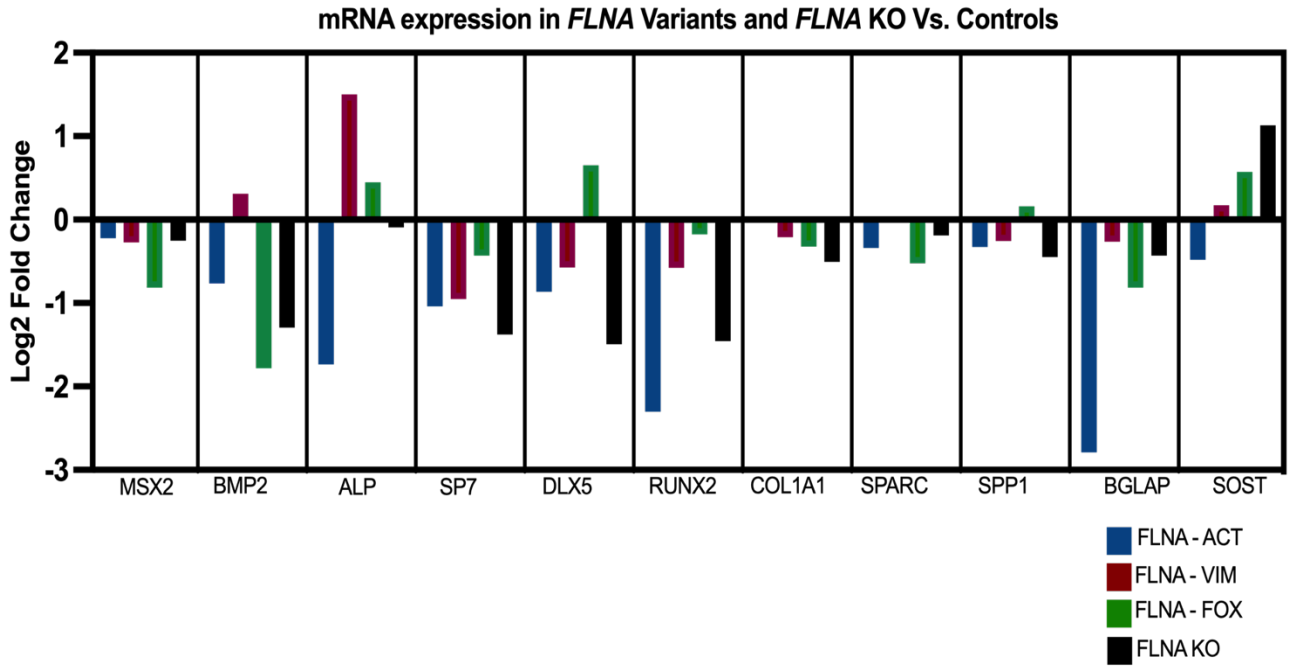

Figure 3.14. qPCR expression analysis of osteoblast marker genes in cMSCs with FLNA variants and FLNA KO cMSCs.
Log2 Fold changes in mRNA levels are shown relative to control cMSCs.

4. Conclusions and Future directions

Single suture craniosynostosis (SSC) is one of the common significant birth defects of the skull, occurring with an incidence of approximately 1 in ~2500 live births globally. It is described by the early fusion of one of the cranial sutures (2-4, 23), affecting males more than females (24-27). Patients with SSC can present with a wide spectrum of defects including dental anomalies, craniofacial deformities, and various medical problems (29-34). Varity of genes have been identified and associated with the etiology of syndromic craniosynostosis (3, 4, 37). However, the etiology of SSC is not yet identified.

In this research, we identified and studied nine rare variants in the X-linked gene, *FLNA* in patients with SSC, using RNA-Seq. The premature ossification of the cranial is commonly thought to arise from dysregulated activity of the calvarial osteoprogenitors and osteoblasts. Therefore, our overall goal was to assess the effect of these variants on bone development. We proposed that the identified *FLNA* variants will impact biological properties, affect cellular mechanics, and alter osteogenic gene expression in SSC patients. To test this hypothesis, we developed a system for isolating primary calvarial MSCs from osteoblasts. We demonstrated that our isolation method is reproducible and the isolated calvarial MSCs possess proliferation and differentiation potential and present a distinct genetic profile when compared to commercial BMMSC line. To our knowledge, our study is the first to report MSCs isolated from human calvaria. We then thoroughly characterized calvarial osteoblast and MSC lines harboring the nine *FLNA* variants. The experiments we described attempt to elucidate the effect of these variants on osteogenesis and cell mechanics of the cells. Our current findings suggest that the identified variants may have a significant impact on the cytoskeleton structure. The data provide evidence that *FLNA* variants may cause SSC through acting on different modes of ossification. These variants could be inducing ectopic cartilage. However, the precise mechanisms leading to premature suture fusion are not entirely understood.

Strikingly, grouping the *FLNA* variants based on the specific functional domains of FLNA

Ig repeats revealed compelling results. The most significant differences were observed in *FLNA* variants located on domains interacting with F-actin and vimentin. We found that variants on FLNA-ACT domains were in males suggesting an X-linked recessive inheritance pattern. In FLNA-ACT domain variants, cells exhibited higher proliferation rates in both cMSCs (early stage of development) and cOBs (late stage of development) as well as impaired migration and altered osteogenesis. Similar osteogenic expression patterns of FLNA KOs and FLNA-ACT and FLNA-FOX domain groups indicate a loss of function pattern. However, in the FLNA-VIM domain group, the some of the main osteogenic/ chondrogenic were highly expressed compared to controls at some osteogenic differentiation time point. These genes are also involved in regulating cell mechanical properties.

Moreover, our findings imply that FLNA variants mediate changes in the cytoskeleton and migration in SSC cMSC and cOBs although the mechanism is not established. Our findings complement earlier studies on the role of FLNA in cellular migration (202, 215-217); we provide supporting evidence that our rare identified FLNA variants might affect migration through mechanotransduction.

We also aimed to knockout *FLNA* in human cMSC line to study the effect of *FLNA* loss on osteogenesis. To our knowledge, we are the first to successfully create a model of *FLNA* loss in human MSC line. The *FLNA* KO data suggests a requirement of *FLNA* in cMSC development. Our modified CRISPR/ Cas9 approach could enable further clarification of the role of *FLNA* on calvarial bone development. Future work could evaluate the expression of critical osteogenic genes and additional candidate molecules and growth factors in *FLNA* knockdown/knockout cMSCs. In addition to that, further investigation in the migration, contraction, and adhesive properties of undifferentiated and osteogenically differentiated *FLNA* KO cMSCs will provide critical information.

More significantly, the discovery of FLNA's effect on cMSCs is useful and helped us

understand the contribution of the rare *FLNA* variants we identified in SSC patients. The expression pattern of *FLNA* KOs was similar to the ACT, VIM and FOX *FLNA* domain groups. We speculate that variants of the FLNA-ACT, FLNA-VIM and FLNA-FOX groups are loss of function, however, further investigation should test our claim.

Future studies could also uncover the link between the male predominance and craniosynostosis on FLNA-ACT domain variants. This could be done through generating the variants of interest and assessing their rates in male and female mice models and patient cell lines. In addition, future work could generate and study isogenic cell models of the nine *FLNA* variants. Studying cMSCs harboring FLNA variants growing in different culture media (serum free, MSC conditioned, osteogenic induction, and chondrogenic induction) will help in understanding the variants' effect on bone and cartilage development. Moreover, future studies could also investigate the mode of ossification and type of bone generated by *FLNA* variants through studying the expression profile of a wide array of genes involved in bone development including growth factors, ECM molecules, transcription factors, and master osteogenic and chondrogenic genes.

Since FLNA is a mechano-responsive gene, future work could study, in depth, the role of mechanical forces in the induction of craniosynostosis in individuals harboring *FLNA* variants. Future work can study the effect of cyclic stretch on these variants and demonstrate the mechanobiological responses compared to controls. This could be carried out through utilizing human osteoblast cell lines or mouse models. Further investigation of FLNA and interacting proteins will provide deeper insights into the mechanisms that regulate the premature cranial suture fusion in SSC patients.

5. Appendix

List of 61 genes associated with syndromic craniosynostosis (380).

Gene	Disease	Inheritance	OMIM # (Gene)
ADAMTSL4	Ectopia lentis	AR	610113
ALPL	Hypophosphatasia	AR/AD	171760
ALX4	Frontonasal dysplasia 2, Parietal foramina 2, susceptibility to Craniosynostosis 5	AR/AD	605420
ASXL1	Bohring-Opitz syndrome	AD	612990
ATR	Seckel syndrome 1	AR	601215
CDC45	Meier-Gorlin syndrome 7	AR	603465
COLEC11	3MC syndrome 2	AR	612502
CTSK	Pycnodysostosis	AR	601105
CYP26B1	CS with radiohumeral fusions and other skeletal and craniofacial anomalies	AR	605207
EFNA4	——	AD	601380

Gene	Disease	Inheritance	OMIM # (Gene)
EFNB1	Craniofrontonasal dysplasia	XLD	300035
ERF	Craniosynostosis 4, Chitayat syndrome	AD	611888
ESCO2	Roberts syndrome, SC phocomelia syndrome	AR	609353
FAM20C	Raine syndrome	AR	611061
FBN1	Marfan syndrome, Weill-Marchesani syndrome 2	AD	134797
FGFR1	Pfeiffer syndrome, Osteoglophonic dysplasia, Trigonocephaly 1	AD	136350
FGFR2	Apert syndrome, Crouzon syndrome, Beare-Stevenson syndrome, Bent bone dysplasia	AD	176943
FGFR3	Muenke syndrome, Crouzon syndrome with acanthosis nigricans	AD	134934
FLNA	Otopalatodigital syndrome, type I and II; frontometaphyseal dysplasia	XLR/XLD	300017
FREM1	Trigonocephaly 2	AD	608944

Gene	Disease	Inheritance	OMIM # (Gene)
GLI3	Greig cephalopolysyndactyly syndrome	AD	165240
GNAS	Osseous heteroplasia, pseudohypoparathyroidism	AD	139320
GNPTAB	Mucolipidosis IIIA/B	AR	607840
GPC3	Simpson-Golabi-Behmel syndrome, type 1	XLR	300037
HUWE1	Intellectual disability, X-linked syndromic, Turner type	XLR	300697
IDS	Mucopolysaccharidosis II	XLR	300823
IDUA	Hurler, Scheie, and Hurler/Scheie syndromes	AR	252800
IFT122	Cranioectodermal dysplasia 1	AR	606045
IFT43	Cranioectodermal dysplasia 3	AR	614068
IGF1R	——	unk	147370
IHH	Acrocapitofemoral dysplasia, Brachydactyly, type A1	AR/AD	600726

Gene	Disease	Inheritance	OMIM # (Gene)
IL11RA	Craniosynostosis and dental anomalies	AR	600939
IRX5	Hamamy syndrome	AR	606195
JAG1	Alagille syndrome 1	AD	601920
KAT6A	Intellectual disability, autosomal dominant 32	AD	601408
KMT2D	Kabuki syndrome 1	AD	602113
KRAS	Cardiofaciocutaneous syndrome 2, Noonan syndrome 3	AD	190070
LMX1B	Nail-patella syndrome	AD	602575
LRP5	Osteopetrosis, autosomal dominant 1; Osteosclerosis	AD	603506
MASP1	3MC syndrome 1	AR	600521
MEGF8	Carpenter syndrome 2	AR	604267
MSX2	Craniosynostosis 2, Parietal foramina 1, Parietal foramina with cleidocranial dysplasia	AD	123101

Gene	Disease	Inheritance	OMIM # (Gene)
PHEX	Hypophosphatemic rickets, X-linked dominant	XLD	300550
POR	Antley-Bixler syndrome with genital anomalies and disordered steroidogenesis	AR	124015
RAB23	Carpenter syndrome	AR	606144
RECQL4	Baller-Gerold syndrome, RAPADILINO syndrome, Rothmund-Thomson syndrome	AR	603780
RUNX2	Cleidocranial dysplasia	AD	600211
SCARF2	Van den Ende-Gupta syndrome	AR	613619
SH3PXD2B	Frank-ter Haar syndrome	AR	613293
SKI	Shprintzen-Goldberg syndrome	AD	164780
SPECC1L	Opitz GBBB syndrome, type II	AD	614140
STAT3	Hyper-IgE recurrent infection syndrome	AD	102582
TCF12	Craniosynostosis 3	AD	600480

Gene	Disease	Inheritance	OMIM # (Gene)
TGFBR1	Loeys-Dietz syndrome 1	AD	190181
TGFBR2	Loeys-Dietz syndrome 2	AD	190182
TMCO1	Craniofacial dysmorphism, skeletal anomalies, and Intellectual disability syndrome	AR	614123
TWIST1	Craniosynostosis 1, Saethre-Chotzen syndrome	AD	601622
WDR19	Sensenbrenner syndrome	AR	614378
WDR35	Cranioectodermal dysplasia 2	AR	613602
ZEB2	Mowat-Wilson syndrome	AD	605802
ZIC1	Craniosynostosis 6	AD	600470

6. Bibliography

1. Jin SW, Sim KB, Kim SD. Development and Growth of the Normal Cranial Vault : An Embryologic Review. J Korean Neurosurg Soc. 2016;59(3):192-6.
2. Morriss-Kay GM, Wilkie AO. Growth of the normal skull vault and its alteration in craniosynostosis: insights from human genetics and experimental studies. J Anat. 2005;207(5):637-53.
3. Katsianou MA, Adamopoulos C, Vastardis H, Basdra EK. Signaling mechanisms implicated in cranial sutures pathophysiology: Craniosynostosis. BBA Clin. 2016;6:165-76.
4. Twigg SR, Wilkie AO. A Genetic-Pathophysiological Framework for Craniosynostosis. Am J Hum Genet. 2015;97(3):359-77.
5. Bradley JP, Levine JP, Roth DA, McCarthy JG, Longaker MT. Studies in cranial suture biology: IV. Temporal sequence of posterior frontal cranial suture fusion in the mouse. Plast Reconstr Surg. 1996;98(6):1039-45.
6. Jiang X, Iseki S, Maxson RE, Sucov HM, Morriss-Kay GM. Tissue origins and interactions in the mammalian skull vault. Dev Biol. 2002;241(1):106-16.
7. Yoshida T, Vivatbutsiri P, Morriss-Kay G, Saga Y, Iseki S. Cell lineage in mammalian craniofacial mesenchyme. Mech Dev. 2008;125(9-10):797-808.
8. Hay ED. The mesenchymal cell, its role in the embryo, and the remarkable signaling mechanisms that create it. Dev Dyn. 2005;233(3):706-20.
9. Rodeck CH, Whittle MJ. Fetal medicine : basic science and clinical practice. Edinburgh: Churchill Livingstone; 2009. xii, 780 : ill. ; 29 cm. p.
10. Adeeb N, Mortazavi MM, Tubbs RS, Cohen-Gadol AA. The cranial dura mater: a review of its history, embryology, and anatomy. Childs Nerv Syst. 2012;28(6):827-37.
11. Caetano-Lopes J, Canhao H, Fonseca JE. Osteoblasts and bone formation. Acta Reumatol Port. 2007;32(2):103-10.
12. Ishii M, Merrill AE, Chan YS, Gitelman I, Rice DP, Sucov HM, et al. Msx2 and Twist cooperatively control the development of the neural crest-derived skeletogenic mesenchyme of the murine skull vault. Development. 2003;130(24):6131-42.
13. Sperber GH, Sperber SM, Guttmann GD. Craniofacial embryogenetics and development. Shelton, CT: People's Medical Pub; 2010. 250 : ill. ; 28 cm. p.
14. Tubbs RS, Bosmia AN, Cohen-Gadol AA. The human calvaria: a review of embryology, anatomy, pathology, and molecular development. Childs Nerv Syst. 2012;28(1):23-31.
15. Eley KA, Thomas GP, Sheerin F, Cilliers D, Wall S, Johnson D. The Significance of Squamosal Suture Synostosis. J Craniofac Surg. 2016;27(6):1543-9.
16. Opperman LA. Cranial sutures as intramembranous bone growth sites. Dev Dyn. 2000;219(4):472-85.
17. Slater BJ, Lenton KA, Kwan MD, Gupta DM, Wan DC, Longaker MT. Cranial sutures: a brief review. Plast Reconstr Surg. 2008;121(4):170e-8e.
18. Beederman M, Farina EM, Reid RR. Molecular basis of cranial suture biology and disease: Osteoblastic and osteoclastic perspectives. Genes Dis. 2014;1(1):120-5.
19. Lana-Elola E, Rice R, Grigoriadis AE, Rice DP. Cell fate specification during calvarial bone and suture development. Dev Biol. 2007;311(2):335-46.
20. Moss ML. Growth of the calvaria in the rat; the determination of osseous morphology. Am J Anat. 1954;94(3):333-61.

21. Markens IS. Embryonic development of the coronal suture in man and rat. Acta Anat (Basel). 1975;93(2):257-73.
22. Nagaraja S, Anslow P, Winter B. Craniosynostosis. Clin Radiol. 2013;68(3):284-92.
23. Wilkie AO. Craniosynostosis: genes and mechanisms. Hum Mol Genet. 1997;6(10):1647-56.
24. French LR, Jackson IT, Melton LJ, 3rd. A population-based study of craniosynostosis. J Clin Epidemiol. 1990;43(1):69-73.
25. Shuper A, Merlob P, Grunebaum M, Reisner SH. The incidence of isolated craniosynostosis in the newborn infant. Am J Dis Child. 1985;139(1):85-6.
26. Singer S, Bower C, Southall P, Goldblatt J. Craniosynostosis in Western Australia, 1980-1994: a population-based study. Am J Med Genet. 1999;83(5):382-7.
27. Cornelissen M, Ottelander B, Rizopoulos D, van der Hulst R, Mink van der Molen A, van der Horst C, et al. Increase of prevalence of craniosynostosis. J Craniomaxillofac Surg. 2016;44(9):1273-9.
28. Kimonis V, Gold JA, Hoffman TL, Panchal J, Boyadjiev SA. Genetics of craniosynostosis. Semin Pediatr Neurol. 2007;14(3):150-61.
29. Magge SN, Westerveld M, Pruzinsky T, Persing JA. Long-term neuropsychological effects of sagittal craniosynostosis on child development. J Craniofac Surg. 2002;13(1):99-104.
30. Shimoji T, Tomiyama N. Mild trigonocephaly and intracranial pressure: report of 56 patients. Childs Nerv Syst. 2004;20(10):749-56.
31. Shipster C, Hearst D, Somerville A, Stackhouse J, Hayward R, Wade A. Speech, language, and cognitive development in children with isolated sagittal synostosis. Dev Med Child Neurol. 2003;45(1):34-43.
32. Thompson DN, Malcolm GP, Jones BM, Harkness WJ, Hayward RD. Intracranial pressure in single-suture craniosynostosis. Pediatr Neurosurg. 1995;22(5):235-40.
33. Johnson D, Wilkie AO. Craniosynostosis. Eur J Hum Genet. 2011;19(4):369-76.
34. de La Dure-Molla M, Fournier BP, Manzanares MC, Acevedo AC, Hennekam RC, Friedlander L, et al. Elements of morphology: Standard terminology for the teeth and classifying genetic dental disorders. Am J Med Genet A. 2019;179(10):1913-81.
35. Passos-Bueno MR, Serti Eacute AE, Jehee FS, Fanganiello R, Yeh E. Genetics of craniosynostosis: genes, syndromes, mutations and genotype-phenotype correlations. Front Oral Biol. 2008;12:107-43.
36. Chumas PD, Cinalli G, Arnaud E, Marchac D, Renier D. Classification of previously unclassified cases of craniosynostosis. J Neurosurg. 1997;86(2):177-81.
37. Wilkie AO, Morriss-Kay GM. Genetics of craniofacial development and malformation. Nat Rev Genet. 2001;2(6):458-68.
38. Loeys BL, Chen J, Neptune ER, Judge DP, Podowski M, Holm T, et al. A syndrome of altered cardiovascular, craniofacial, neurocognitive and skeletal development caused by mutations in TGFBR1 or TGFBR2. Nat Genet. 2005;37(3):275-81.
39. Sood S, Eldadah ZA, Krause WL, McIntosh I, Dietz HC. Mutation in fibrillin-1 and the Marfanoid-craniosynostosis (Shprintzen-Goldberg) syndrome. Nat Genet. 1996;12(2):209-11.
40. Jenkins D, Seelow D, Jehee FS, Perlyn CA, Alonso LG, Bueno DF, et al. RAB23 mutations in Carpenter syndrome imply an unexpected role for hedgehog signaling in cranial-suture development and obesity. Am J Hum Genet. 2007;80(6):1162-70.

41. Kamath BM, Stolle C, Bason L, Colliton RP, Piccoli DA, Spinner NB, et al. Craniosynostosis in Alagille syndrome. Am J Med Genet. 2002;112(2):176-80.
42. Van Maldergem L, Siitonen HA, Jalkh N, Chouery E, De Roy M, Delague V, et al. Revisiting the craniosynostosis-radial ray hypoplasia association: Baller-Gerold syndrome caused by mutations in the RECQL4 gene. J Med Genet. 2006;43(2):148-52.
43. Sirmaci A, Walsh T, Akay H, Spiliopoulos M, Sakalar YB, Hasanefendioglu-Bayrak A, et al. MASP1 mutations in patients with facial, umbilical, coccygeal, and auditory findings of Carnevale, Malpuech, OSA, and Michels syndromes. Am J Hum Genet. 2010;87(5):679-86.
44. Iqbal Z, Cejudo-Martin P, de Brouwer A, van der Zwaag B, Ruiz-Lozano P, Scimia MC, et al. Disruption of the podosome adaptor protein TKS4 (SH3PXD2B) causes the skeletal dysplasia, eye, and cardiac abnormalities of Frank-Ter Haar Syndrome. Am J Hum Genet. 2010;86(2):254-61.
45. Vissers LE, Cox TC, Maga AM, Short KM, Wiradjaja F, Janssen IM, et al. Heterozygous mutations of FREM1 are associated with an increased risk of isolated metopic craniosynostosis in humans and mice. PLoS Genet. 2011;7(9):e1002278.
46. Yagnik G, Ghuman A, Kim S, Stevens CG, Kimonis V, Stoler J, et al. ALX4 gain-of-function mutations in nonsyndromic craniosynostosis. Hum Mutat. 2012;33(12):1626-9.
47. Doyle AJ, Doyle JJ, Bessling SL, Maragh S, Lindsay ME, Schepers D, et al. Mutations in the TGF-beta repressor SKI cause Shprintzen-Goldberg syndrome with aortic aneurysm. Nat Genet. 2012;44(11):1249-54.
48. Blumel R, Zink M, Klopocki E, Liedtke D. On the traces of tcf12: Investigation of the gene expression pattern during development and cranial suture patterning in zebrafish (Danio rerio). PLoS One. 2019;14(6):e0218286.
49. Opperman LA, Passarelli RW, Morgan EP, Reintjes M, Ogle RC. Cranial sutures require tissue interactions with dura mater to resist osseous obliteration in vitro. J Bone Miner Res. 1995;10(12):1978-87.
50. Lin E, Kuo PH, Liu YL, Yang AC, Tsai SJ. Transforming growth factor-beta signaling pathway-associated genes SMAD2 and TGFBR2 are implicated in metabolic syndrome in a Taiwanese population. Sci Rep. 2017;7(1):13589.
51. Grafe I, Alexander S, Peterson JR, Snider TN, Levi B, Lee B, et al. TGF-beta Family Signaling in Mesenchymal Differentiation. Cold Spring Harb Perspect Biol. 2018;10(5).
52. Hunenko O, Karmacharya J, Ong G, Kirschner RE. Toward an understanding of nonsyndromic craniosynostosis: altered patterns of TGF-beta receptor and FGF receptor expression induced by intrauterine head constraint. Ann Plast Surg. 2001;46(5):546-53; discussion 53-4.
53. Seo HS, Serra R. Tgfbr2 is required for development of the skull vault. Dev Biol. 2009;334(2):481-90.
54. Pizette S, Niswander L. BMPs are required at two steps of limb chondrogenesis: formation of prechondrogenic condensations and their differentiation into chondrocytes. Dev Biol. 2000;219(2):237-49.
55. Han J, Ishii M, Bringas P, Jr., Maas RL, Maxson RE, Jr., Chai Y. Concerted action of Msx1 and Msx2 in regulating cranial neural crest cell differentiation during frontal bone development. Mech Dev. 2007;124(9-10):729-45.

56. Sun J, Ishii M, Ting MC, Maxson R. Foxc1 controls the growth of the murine frontal bone rudiment by direct regulation of a Bmp response threshold of Msx2. Development. 2013;140(5):1034-44.
57. Kanatani N, Fujita T, Fukuyama R, Liu W, Yoshida CA, Moriishi T, et al. Cbf beta regulates Runx2 function isoform-dependently in postnatal bone development. Dev Biol. 2006;296(1):48-61.
58. Most D, Levine JP, Chang J, Sung J, McCarthy JG, Schendel SA, et al. Studies in cranial suture biology: up-regulation of transforming growth factor-beta1 and basic fibroblast growth factor mRNA correlates with posterior frontal cranial suture fusion in the rat. Plast Reconstr Surg. 1998;101(6):1431-40.
59. Rice DP, Aberg T, Chan Y, Tang Z, Kettunen PJ, Pakarinen L, et al. Integration of FGF and TWIST in calvarial bone and suture development. Development. 2000;127(9):1845-55.
60. Warren SM, Brunet LJ, Harland RM, Economides AN, Longaker MT. The BMP antagonist noggin regulates cranial suture fusion. Nature. 2003;422(6932):625-9.
61. Szepesi A, Matula Z, Szigeti A, Varady G, Szalma J, Szabo G, et al. In Vitro Characterization of Human Mesenchymal Stem Cells Isolated from Different Tissues with a Potential to Promote Complex Bone Regeneration. Stem Cells Int. 2016;2016:3595941.
62. Xie L, Zhang N, Marsano A, Vunjak-Novakovic G, Zhang Y, Lopez MJ. In vitro mesenchymal trilineage differentiation and extracellular matrix production by adipose and bone marrow derived adult equine multipotent stromal cells on a collagen scaffold. Stem Cell Rev Rep. 2013;9(6):858-72.
63. Hass R, Kasper C, Bohm S, Jacobs R. Different populations and sources of human mesenchymal stem cells (MSC): A comparison of adult and neonatal tissue-derived MSC. Cell Commun Signal. 2011;9:12.
64. Giovannini S, Brehm W, Mainil-Varlet P, Nesic D. Multilineage differentiation potential of equine blood-derived fibroblast-like cells. Differentiation. 2008;76(2):118-29.
65. Heidari B, Shirazi A, Akhondi MM, Hassanpour H, Behzadi B, Naderi MM, et al. Comparison of proliferative and multilineage differentiation potential of sheep mesenchymal stem cells derived from bone marrow, liver, and adipose tissue. Avicenna J Med Biotechnol. 2013;5(2):104-17.
66. Rentsch C, Hess R, Rentsch B, Hofmann A, Manthey S, Scharnweber D, et al. Ovine bone marrow mesenchymal stem cells: isolation and characterization of the cells and their osteogenic differentiation potential on embroidered and surface-modified polycaprolactone-co-lactide scaffolds. In Vitro Cell Dev Biol Anim. 2010;46(7):624-34.
67. Baghaei K, Hashemi SM, Tokhanbigli S, Asadi Rad A, Assadzadeh-Aghdaei H, Sharifian A, et al. Isolation, differentiation, and characterization of mesenchymal stem cells from human bone marrow. Gastroenterol Hepatol Bed Bench. 2017;10(3):208-13.
68. Meirelles Lda S, Nardi NB. Murine marrow-derived mesenchymal stem cell: isolation, in vitro expansion, and characterization. Br J Haematol. 2003;123(4):702-11.
69. Lennon DP, Caplan AI. Isolation of rat marrow-derived mesenchymal stem cells. Exp Hematol. 2006;34(11):1606-7.
70. Ringe J, Kaps C, Schmitt B, Buscher K, Bartel J, Smolian H, et al. Porcine mesenchymal stem cells. Induction of distinct mesenchymal cell lineages. Cell Tissue Res. 2002;307(3):321-7.

71. Caterson EJ, Nesti LJ, Danielson KG, Tuan RS. Human marrow-derived mesenchymal progenitor cells: isolation, culture expansion, and analysis of differentiation. Mol Biotechnol. 2002;20(3):245-56.
72. Kasten P, Luginbuhl R, van Griensven M, Barkhausen T, Krettek C, Bohner M, et al. Comparison of human bone marrow stromal cells seeded on calcium-deficient hydroxyapatite, beta-tricalcium phosphate and demineralized bone matrix. Biomaterials. 2003;24(15):2593-603.
73. Stich S, Loch A, Park SJ, Haupl T, Ringe J, Sittinger M. Characterization of single cell derived cultures of periosteal progenitor cells to ensure the cell quality for clinical application. PLoS One. 2017;12(5):e0178560.
74. Ringe J, Leinhase I, Stich S, Loch A, Neumann K, Haisch A, et al. Human mastoid periosteum-derived stem cells: promising candidates for skeletal tissue engineering. J Tissue Eng Regen Med. 2008;2(2-3):136-46.
75. Trautvetter W, Kaps C, Schmelzeisen R, Sauerbier S, Sittinger M. Tissue-engineered polymer-based periosteal bone grafts for maxillary sinus augmentation: five-year clinical results. J Oral Maxillofac Surg. 2011;69(11):2753-62.
76. Zhu SJ, Choi BH, Huh JY, Jung JH, Kim BY, Lee SH. A comparative qualitative histological analysis of tissue-engineered bone using bone marrow mesenchymal stem cells, alveolar bone cells, and periosteal cells. Oral Surg Oral Med Oral Pathol Oral Radiol Endod. 2006;101(2):164-9.
77. Duchamp de Lageneste O, Julien A, Abou-Khalil R, Frangi G, Carvalho C, Cagnard N, et al. Periosteum contains skeletal stem cells with high bone regenerative potential controlled by Periostin. Nat Commun. 2018;9(1):773.
78. Schimming R, Schmelzeisen R. Tissue-engineered bone for maxillary sinus augmentation. J Oral Maxillofac Surg. 2004;62(6):724-9.
79. Schmelzeisen R, Schimming R, Sittinger M. Soft tissue and hard tissue engineering in oral and maxillofacial surgery. Ann R Australas Coll Dent Surg. 2002;16:50-3.
80. Kong L, Wang Y, Ji Y, Chen J, Cui J, Shen W. Isolation and Characterization of Human Suture Mesenchymal Stem Cells In Vitro. Int J Stem Cells. 2020;13(3):377-85.
81. Dominici M, Le Blanc K, Mueller I, Slaper-Cortenbach I, Marini F, Krause D, et al. Minimal criteria for defining multipotent mesenchymal stromal cells. The International Society for Cellular Therapy position statement. Cytotherapy. 2006;8(4):315-7.
82. Boxall S, Jones E. The use of multiparameter flow cytometry and cell sorting to characterize native human bone marrow mesenchymal stem cells (MSC). Methods Mol Biol. 2015;1235:121-30.
83. Huang S, Xu L, Sun Y, Wu T, Wang K, Li G. An improved protocol for isolation and culture of mesenchymal stem cells from mouse bone marrow. J Orthop Translat. 2015;3(1):26-33.
84. Caroti CM, Ahn H, Salazar HF, Joseph G, Sankar SB, Willett NJ, et al. A Novel Technique for Accelerated Culture of Murine Mesenchymal Stem Cells that Allows for Sustained Multipotency. Sci Rep. 2017;7(1):13334.
85. Thompson DL, Sabbagh Y, Tenenhouse HS, Roche PC, Drezner MK, Salisbury JL, et al. Ontogeny of Phex/PHEX protein expression in mouse embryo and subcellular localization in osteoblasts. J Bone Miner Res. 2002;17(2):311-20.
86. Deng M, Mei T, Hou T, Luo K, Luo F, Yang A, et al. TGFbeta3 recruits endogenous mesenchymal stem cells to initiate bone regeneration. Stem Cell Res Ther. 2017;8(1):258.

87. Kaji H, Naito J, Sowa H, Sugimoto T, Chihara K. Smad3 differently affects osteoblast differentiation depending upon its differentiation stage. Horm Metab Res. 2006;38(11):740-5.
88. Liu X, Liang Z, Gao K, Li H, Zhao G, Wang S, et al. MicroRNA-128 inhibits EMT of human osteosarcoma cells by directly targeting integrin alpha2. Tumour Biol. 2016;37(6):7951-7.
89. Wilk K, Yeh SA, Mortensen LJ, Ghaffarigarakani S, Lombardo CM, Bassir SH, et al. Postnatal Calvarial Skeletal Stem Cells Expressing PRX1 Reside Exclusively in the Calvarial Sutures and Are Required for Bone Regeneration. Stem Cell Reports. 2017;8(4):933-46.
90. Huang Y, Kong Y, Zhang L, He T, Zhou X, Yan Y, et al. High Expression of ITGA3 Promotes Proliferation and Cell Cycle Progression and Indicates Poor Prognosis in Intrahepatic Cholangiocarcinoma. Biomed Res Int. 2018;2018:2352139.
91. Chang W, Kim R, Park SI, Jung YJ, Ham O, Lee J, et al. Enhanced Healing of Rat Calvarial Bone Defects with Hypoxic Conditioned Medium from Mesenchymal Stem Cells through Increased Endogenous Stem Cell Migration via Regulation of ICAM-1 Targeted-microRNA-221. Mol Cells. 2015;38(7):643-50.
92. Ullah M, Liu DD, Thakor AS. Mesenchymal Stromal Cell Homing: Mechanisms and Strategies for Improvement. iScience. 2019;15:421-38.
93. Xu FF, Zhu H, Li XM, Yang F, Chen JD, Tang B, et al. Intercellular adhesion molecule-1 inhibits osteogenic differentiation of mesenchymal stem cells and impairs bio-scaffold-mediated bone regeneration in vivo. Tissue Eng Part A. 2014;20(19-20):2768-82.
94. Kevorkova O, Martineau C, Martin-Falstrault L, Sanchez-Dardon J, Brissette L, Moreau R. Low-bone-mass phenotype of deficient mice for the cluster of differentiation 36 (CD36). PLoS One. 2013;8(10):e77701.
95. Quarles LD. FGF23, PHEX, and MEPE regulation of phosphate homeostasis and skeletal mineralization. Am J Physiol Endocrinol Metab. 2003;285(1):E1-9.
96. Behr B, Sorkin M, Lehnhardt M, Renda A, Longaker MT, Quarto N. A comparative analysis of the osteogenic effects of BMP-2, FGF-2, and VEGFA in a calvarial defect model. Tissue Eng Part A. 2012;18(9-10):1079-86.
97. Duan X, Bradbury SR, Olsen BR, Berendsen AD. VEGF stimulates intramembranous bone formation during craniofacial skeletal development. Matrix Biol. 2016;52-54:127-40.
98. Moenning A, Jager R, Egert A, Kress W, Wardelmann E, Schorle H. Sustained platelet-derived growth factor receptor alpha signaling in osteoblasts results in craniosynostosis by overactivating the phospholipase C-gamma pathway. Mol Cell Biol. 2009;29(3):881-91.
99. Mitlak BH, Finkelman RD, Hill EL, Li J, Martin B, Smith T, et al. The effect of systemically administered PDGF-BB on the rodent skeleton. J Bone Miner Res. 1996;11(2):238-47.
100. Sasaki T, Ito Y, Bringas P, Jr., Chou S, Urata MM, Slavkin H, et al. TGFbeta-mediated FGF signaling is crucial for regulating cranial neural crest cell proliferation during frontal bone development. Development. 2006;133(2):371-81.
101. Chen J, Deng S, Zhang S, Chen Z, Wu S, Cai X, et al. The role of miRNAs in the differentiation of adipose-derived stem cells. Curr Stem Cell Res Ther. 2014;9(3):268-79.
102. Shi C, Iura A, Terajima M, Liu F, Lyons K, Pan H, et al. Deletion of BMP receptor type IB decreased bone mass in association with compromised osteoblastic differentiation of bone marrow mesenchymal progenitors. Sci Rep. 2016;6:24256.

103. Fujii M, Takeda K, Imamura T, Aoki H, Sampath TK, Enomoto S, et al. Roles of bone morphogenetic protein type I receptors and Smad proteins in osteoblast and chondroblast differentiation. Mol Biol Cell. 1999;10(11):3801-13.
104. Sahni V, Mukhopadhyay A, Tysseling V, Hebert A, Birch D, McGuire TL, et al. BMPR1a and BMPR1b signaling exert opposing effects on gliosis after spinal cord injury. J Neurosci. 2010;30(5):1839-55.
105. Pauk M, Bordukalo-Niksic T, Brkljacic J, Paralkar VM, Brault AL, Dumic-Cule I, et al. A novel role of bone morphogenetic protein 6 (BMP6) in glucose homeostasis. Acta Diabetol. 2019;56(3):365-71.
106. Mundy GR. Directions of drug discovery in osteoporosis. Annu Rev Med. 2002;53:337-54.
107. Battula VL, Bareiss PM, Treml S, Conrad S, Albert I, Hojak S, et al. Human placenta and bone marrow derived MSC cultured in serum-free, b-FGF-containing medium express cell surface frizzled-9 and SSEA-4 and give rise to multilineage differentiation. Differentiation. 2007;75(4):279-91.
108. Devireddy LR, Myers M, Screven R, Liu Z, Boxer L. A serum-free medium formulation efficiently supports isolation and propagation of canine adipose-derived mesenchymal stem/stromal cells. PLoS One. 2019;14(2):e0210250.
109. Gottipamula S, Muttigi MS, Kolkundkar U, Seetharam RN. Serum-free media for the production of human mesenchymal stromal cells: a review. Cell Prolif. 2013;46(6):608-27.
110. Wang Q, Huang C, Zeng F, Xue M, Zhang X. Activation of the Hh pathway in periosteum-derived mesenchymal stem cells induces bone formation in vivo: implication for postnatal bone repair. Am J Pathol. 2010;177(6):3100-11.
111. Wang X, Wang Y, Gou W, Lu Q, Peng J, Lu S. Role of mesenchymal stem cells in bone regeneration and fracture repair: a review. Int Orthop. 2013;37(12):2491-8.
112. Liu G, Shu C, Cui L, Liu W, Cao Y. Tissue-engineered bone formation with cryopreserved human bone marrow mesenchymal stem cells. Cryobiology. 2008;56(3):209-15.
113. Livingston TL, Gordon S, Archambault M, Kadiyala S, McIntosh K, Smith A, et al. Mesenchymal stem cells combined with biphasic calcium phosphate ceramics promote bone regeneration. J Mater Sci Mater Med. 2003;14(3):211-8.
114. Mankani MH, Kuznetsov SA, Robey PG. Formation of hematopoietic territories and bone by transplanted human bone marrow stromal cells requires a critical cell density. Exp Hematol. 2007;35(6):995-1004.
115. Brennan MA, Renaud A, Amiaud J, Rojewski MT, Schrezenmeier H, Heymann D, et al. Pre-clinical studies of bone regeneration with human bone marrow stromal cells and biphasic calcium phosphate. Stem Cell Res Ther. 2014;5(5):114.
116. He J, Yan J, Wang J, Zhao L, Xin Q, Zeng Y, et al. Dissecting human embryonic skeletal stem cell ontogeny by single-cell transcriptomic and functional analyses. Cell Res. 2021.
117. Volk SW, Shah SR, Cohen AJ, Wang Y, Brisson BK, Vogel LK, et al. Type III collagen regulates osteoblastogenesis and the quantity of trabecular bone. Calcif Tissue Int. 2014;94(6):621-31.
118. Silver MH, Foidart JM, Pratt RM. Distribution of fibronectin and collagen during mouse limb and palate development. Differentiation. 1981;18(3):141-9.

119. Bretaud S, Guillon E, Karppinen SM, Pihlajaniemi T, Ruggiero F. Collagen XV, a multifaceted multiplexin present across tissues and species. Matrix Biol Plus. 2020;6-7:100023.
120. Wu J, Ren W, Zheng Z, Huang Z, Liang T, Li F, et al. Mmu_circ_003795 regulates osteoblast differentiation and mineralization in MC3T3E1 and MDPC23 by targeting COL15A1. Mol Med Rep. 2020;22(3):1737-46.
121. Berendsen AD, Pinnow EL, Maeda A, Brown AC, McCartney-Francis N, Kram V, et al. Biglycan modulates angiogenesis and bone formation during fracture healing. Matrix Biol. 2014;35:223-31.
122. Holmes G, Gonzalez-Reiche AS, Lu N, Zhou X, Rivera J, Kriti D, et al. Integrated Transcriptome and Network Analysis Reveals Spatiotemporal Dynamics of Calvarial Suturogenesis. Cell Rep. 2020;32(1):107871.
123. Tao H, Han Z, Han ZC, Li Z. Proangiogenic Features of Mesenchymal Stem Cells and Their Therapeutic Applications. Stem Cells Int. 2016;2016:1314709.
124. Murphy MP, Quarto N, Longaker MT, Wan DC. (*) Calvarial Defects: Cell-Based Reconstructive Strategies in the Murine Model. Tissue Eng Part C Methods. 2017;23(12):971-81.
125. Han A, Bandyopadhyay B, Jayaprakash P, Lua I, Sahu D, Chen M, et al. The anti-motility signaling mechanism of TGFbeta3 that controls cell traffic during skin wound healing. Biol Open. 2012;1(12):1169-77.
126. Chen G, Xu H, Yao Y, Xu T, Yuan M, Zhang X, et al. BMP Signaling in the Development and Regeneration of Cranium Bones and Maintenance of Calvarial Stem Cells. Front Cell Dev Biol. 2020;8:135.
127. Zhou H, Zou S, Lan Y, Fei W, Jiang R, Hu J. Smad7 modulates TGFbeta signaling during cranial suture development to maintain suture patency. J Bone Miner Res. 2014;29(3):716-24.
128. Tholpady SS, Ogle RC. Expression of transforming growth factor-beta-responsive smads in cranial suture development and closure. J Craniofac Surg. 2011;22(1):324-8.
129. Loeys BL, Schwarze U, Holm T, Callewaert BL, Thomas GH, Pannu H, et al. Aneurysm syndromes caused by mutations in the TGF-beta receptor. N Engl J Med. 2006;355(8):788-98.
130. Boyce BF, Yao Z, Xing L. Functions of nuclear factor kappaB in bone. Ann N Y Acad Sci. 2010;1192:367-75.
131. Takase O, Yoshikawa M, Idei M, Hirahashi J, Fujita T, Takato T, et al. The role of NF-kappaB signaling in the maintenance of pluripotency of human induced pluripotent stem cells. PLoS One. 2013;8(2):e56399.
132. Tamama K, Fan VH, Griffith LG, Blair HC, Wells A. Epidermal growth factor as a candidate for ex vivo expansion of bone marrow-derived mesenchymal stem cells. Stem Cells. 2006;24(3):686-95.
133. Belluoccio D, Grskovic I, Niehoff A, Schlotzer-Schrehardt U, Rosenbaum S, Etich J, et al. Deficiency of annexins A5 and A6 induces complex changes in the transcriptome of growth plate cartilage but does not inhibit the induction of mineralization. J Bone Miner Res. 2010;25(1):141-53.
134. Genge BR, Wu LN, Wuthier RE. In vitro modeling of matrix vesicle nucleation: synergistic stimulation of mineral formation by annexin A5 and phosphatidylserine. J Biol Chem. 2007;282(36):26035-45.

135. Passanha FR, Geuens T, Konig S, van Blitterswijk CA, LaPointe VL. Cell culture dimensionality influences mesenchymal stem cell fate through cadherin-2 and cadherin-11. Biomaterials. 2020;254:120127.
136. Robubi A, Berger C, Schmid M, Huber KR, Engel A, Krugluger W. Gene expression profiles induced by growth factors in in vitro cultured osteoblasts. Bone Joint Res. 2014;3(7):236-40.
137. Alimperti S, Andreadis ST. CDH2 and CDH11 act as regulators of stem cell fate decisions. Stem Cell Res. 2015;14(3):270-82.
138. Yao GQ, Wu JJ, Ovadia S, Troiano N, Sun BH, Insogna K. Targeted overexpression of the two colony-stimulating factor-1 isoforms in osteoblasts differentially affects bone loss in ovariectomized mice. Am J Physiol Endocrinol Metab. 2009;296(4):E714-20.
139. Byrne PV, Guilbert LJ, Stanley ER. Distribution of cells bearing receptors for a colony-stimulating factor (CSF-1) in murine tissues. J Cell Biol. 1981;91(3 Pt 1):848-53.
140. Guo L, Bertola DR, Takanohashi A, Saito A, Segawa Y, Yokota T, et al. Bi-allelic CSF1R Mutations Cause Skeletal Dysplasia of Dysosteosclerosis-Pyle Disease Spectrum and Degenerative Encephalopathy with Brain Malformation. Am J Hum Genet. 2019;104(5):925-35.
141. Hatzistergos KE, Quevedo H, Oskouei BN, Hu Q, Feigenbaum GS, Margitich IS, et al. Bone marrow mesenchymal stem cells stimulate cardiac stem cell proliferation and differentiation. Circ Res. 2010;107(7):913-22.
142. Xiong Q, Ye L, Zhang P, Lepley M, Tian J, Li J, et al. Functional consequences of human induced pluripotent stem cell therapy: myocardial ATP turnover rate in the in vivo swine heart with postinfarction remodeling. Circulation. 2013;127(9):997-1008.
143. Brodeur MR, Brissette L, Falstrault L, Luangrath V, Moreau R. Scavenger receptor of class B expressed by osteoblastic cells are implicated in the uptake of cholesteryl ester and estradiol from LDL and HDL3. J Bone Miner Res. 2008;23(3):326-37.
144. Ruchon AF, Marcinkiewicz M, Siegfried G, Tenenhouse HS, DesGroseillers L, Crine P, et al. Pex mRNA is localized in developing mouse osteoblasts and odontoblasts. J Histochem Cytochem. 1998;46(4):459-68.
145. Robinson ME, AlQuorain H, Murshed M, Rauch F. Mineralized tissues in hypophosphatemic rickets. Pediatr Nephrol. 2020;35(10):1843-54.
146. Kamiya N, Ye L, Kobayashi T, Mochida Y, Yamauchi M, Kronenberg HM, et al. BMP signaling negatively regulates bone mass through sclerostin by inhibiting the canonical Wnt pathway. Development. 2008;135(22):3801-11.
147. Zhu F, Friedman MS, Luo W, Woolf P, Hankenson KD. The transcription factor osterix (SP7) regulates BMP6-induced human osteoblast differentiation. J Cell Physiol. 2012;227(6):2677-85.
148. Yakar S, Rosen CJ, Beamer WG, Ackert-Bicknell CL, Wu Y, Liu JL, et al. Circulating levels of IGF-1 directly regulate bone growth and density. J Clin Invest. 2002;110(6):771-81.
149. Nakashima K, Zhou X, Kunkel G, Zhang Z, Deng JM, Behringer RR, et al. The novel zinc finger-containing transcription factor osterix is required for osteoblast differentiation and bone formation. Cell. 2002;108(1):17-29.
150. Ducy P, Zhang R, Geoffroy V, Ridall AL, Karsenty G. Osf2/Cbfa1: a transcriptional activator of osteoblast differentiation. Cell. 1997;89(5):747-54.
151. Karsenty G. Bone formation and factors affecting this process. Matrix Biol. 2000;19(2):85-9.

152. Zhang X, Schwarz EM, Young DA, Puzas JE, Rosier RN, O'Keefe RJ. Cyclooxygenase-2 regulates mesenchymal cell differentiation into the osteoblast lineage and is critically involved in bone repair. J Clin Invest. 2002;109(11):1405-15.
153. Kulterer B, Friedl G, Jandrositz A, Sanchez-Cabo F, Prokesch A, Paar C, et al. Gene expression profiling of human mesenchymal stem cells derived from bone marrow during expansion and osteoblast differentiation. BMC Genomics. 2007;8:70.
154. Maeda S, Nobukuni T, Shimo-Onoda K, Hayashi K, Yone K, Komiya S, et al. Sortilin is upregulated during osteoblastic differentiation of mesenchymal stem cells and promotes extracellular matrix mineralization. J Cell Physiol. 2002;193(1):73-9.
155. Nohe A, Hassel S, Ehrlich M, Neubauer F, Sebald W, Henis YI, et al. The mode of bone morphogenetic protein (BMP) receptor oligomerization determines different BMP-2 signaling pathways. J Biol Chem. 2002;277(7):5330-8.
156. Qin X, Jiang Q, Miyazaki T, Komori T. Runx2 regulates cranial suture closure by inducing hedgehog, Fgf, Wnt and Pthlh signaling pathway gene expressions in suture mesenchymal cells. Hum Mol Genet. 2019;28(6):896-911.
157. Huang LF, Fukai N, Selby PB, Olsen BR, Mundlos S. Mouse clavicular development: analysis of wild-type and cleidocranial dysplasia mutant mice. Dev Dyn. 1997;210(1):33-40.
158. Lou Y, Javed A, Hussain S, Colby J, Frederick D, Pratap J, et al. A Runx2 threshold for the cleidocranial dysplasia phenotype. Hum Mol Genet. 2009;18(3):556-68.
159. Komori T. Regulation of Proliferation, Differentiation and Functions of Osteoblasts by Runx2. Int J Mol Sci. 2019;20(7).
160. Dacic S, Kalajzic I, Visnjic D, Lichtler AC, Rowe DW. Col1a1-driven transgenic markers of osteoblast lineage progression. J Bone Miner Res. 2001;16(7):1228-36.
161. Greenwald JA, Mehrara BJ, Spector JA, Warren SM, Crisera FE, Fagenholz PJ, et al. Regional differentiation of cranial suture-associated dura mater in vivo and in vitro: implications for suture fusion and patency. J Bone Miner Res. 2000;15(12):2413-30.
162. Yen HY, Ting MC, Maxson RE. Jagged1 functions downstream of Twist1 in the specification of the coronal suture and the formation of a boundary between osteogenic and non-osteogenic cells. Dev Biol. 2010;347(2):258-70.
163. Yu M, Ma L, Yuan Y, Ye X, Montagne A, He J, et al. Cranial Suture Regeneration Mitigates Skull and Neurocognitive Defects in Craniosynostosis. Cell. 2021;184(1):243-56 e18.
164. Veistinen LK, Mustonen T, Hasan MR, Takatalo M, Kobayashi Y, Kesper DA, et al. Regulation of Calvarial Osteogenesis by Concomitant De-repression of GLI3 and Activation of IHH Targets. Front Physiol. 2017;8:1036.
165. Joeng KS, Long F. The Gli2 transcriptional activator is a crucial effector for Ihh signaling in osteoblast development and cartilage vascularization. Development. 2009;136(24):4177-85.
166. Abzhanov A, Rodda SJ, McMahon AP, Tabin CJ. Regulation of skeletogenic differentiation in cranial dermal bone. Development. 2007;134(17):3133-44.
167. Fischer RS, Fowler VM. Thematic Minireview Series: The State of the Cytoskeleton in 2015. J Biol Chem. 2015;290(28):17133-6.
168. Popowicz GM, Schleicher M, Noegel AA, Holak TA. Filamins: promiscuous organizers of the cytoskeleton. Trends Biochem Sci. 2006;31(7):411-9.

169. Chou SZ, Pollard TD. Mechanism of actin polymerization revealed by cryo-EM structures of actin filaments with three different bound nucleotides. Proc Natl Acad Sci U S A. 2019;116(10):4265-74.
170. Ito T, Suzuki A, Stossel TP. Regulation of water flow by actin-binding protein-induced actin gelatin. Biophys J. 1992;61(5):1301-5.
171. Tseng Y, An KM, Esue O, Wirtz D. The bimodal role of filamin in controlling the architecture and mechanics of F-actin networks. J Biol Chem. 2004;279(3):1819-26.
172. Wang K, Ash JF, Singer SJ. Filamin, a new high-molecular-weight protein found in smooth muscle and non-muscle cells. Proc Natl Acad Sci U S A. 1975;72(11):4483-6.
173. Feng Y, Walsh CA. The many faces of filamin: a versatile molecular scaffold for cell motility and signalling. Nat Cell Biol. 2004;6(11):1034-8.
174. Gorlin JB, Yamin R, Egan S, Stewart M, Stossel TP, Kwiatkowski DJ, et al. Human endothelial actin-binding protein (ABP-280, nonmuscle filamin): a molecular leaf spring. J Cell Biol. 1990;111(3):1089-105.
175. Hartwig JH, Stossel TP. Isolation and properties of actin, myosin, and a new actinbinding protein in rabbit alveolar macrophages. J Biol Chem. 1975;250(14):5696-705.
176. Nakamura F, Osborn TM, Hartemink CA, Hartwig JH, Stossel TP. Structural basis of filamin A functions. J Cell Biol. 2007;179(5):1011-25.
177. Clark AR, Sawyer GM, Robertson SP, Sutherland-Smith AJ. Skeletal dysplasias due to filamin A mutations result from a gain-of-function mechanism distinct from allelic neurological disorders. Hum Mol Genet. 2009;18(24):4791-800.
178. Lorenzi M, Gimona M. Synthetic actin-binding domains reveal compositional constraints for function. Int J Biochem Cell Biol. 2008;40(9):1806-16.
179. Fucini P, Koppel B, Schleicher M, Lustig A, Holak TA, Muller R, et al. Molecular architecture of the rod domain of the Dictyostelium gelation factor (ABP120). J Mol Biol. 1999;291(5):1017-23.
180. Fucini P, Renner C, Herberhold C, Noegel AA, Holak TA. The repeating segments of the F-actin cross-linking gelation factor (ABP-120) have an immunoglobulin-like fold. Nat Struct Biol. 1997;4(3):223-30.
181. Stossel TP, Condeelis J, Cooley L, Hartwig JH, Noegel A, Schleicher M, et al. Filamins as integrators of cell mechanics and signalling. Nat Rev Mol Cell Biol. 2001;2(2):138-45.
182. Himmel M, Van Der Ven PF, Stocklein W, Furst DO. The limits of promiscuity: isoform-specific dimerization of filamins. Biochemistry. 2003;42(2):430-9.
183. Pudas R, Kiema TR, Butler PJ, Stewart M, Ylanne J. Structural basis for vertebrate filamin dimerization. Structure. 2005;13(1):111-9.
184. Glogauer M, Arora P, Chou D, Janmey PA, Downey GP, McCulloch CA. The role of actin-binding protein 280 in integrin-dependent mechanoprotection. J Biol Chem. 1998;273(3):1689-98.
185. Brotschi EA, Hartwig JH, Stossel TP. The gelation of actin by actin-binding protein. J Biol Chem. 1978;253(24):8988-93.
186. Dabrowska R, Goch A, Osinska H, Szpacenko A, Sosinski J. Dual effect of filamin on actomyosin ATPase activity. J Muscle Res Cell Motil. 1985;6(1):29-42.
187. Niederman R, Amrein PC, Hartwig J. Three-dimensional structure of actin filaments and of an actin gel made with actin-binding protein. J Cell Biol. 1983;96(5):1400-13.

188. Gardel ML, Nakamura F, Hartwig JH, Crocker JC, Stossel TP, Weitz DA. Prestressed F-actin networks cross-linked by hinged filamins replicate mechanical properties of cells. Proc Natl Acad Sci U S A. 2006;103(6):1762-7.
189. Nagano T, Morikubo S, Sato M. Filamin A and FILIP (Filamin A-Interacting Protein) regulate cell polarity and motility in neocortical subventricular and intermediate zones during radial migration. J Neurosci. 2004;24(43):9648-57.
190. Ohta Y, Suzuki N, Nakamura S, Hartwig JH, Stossel TP. The small GTPase RalA targets filamin to induce filopodia. Proc Natl Acad Sci U S A. 1999;96(5):2122-8.
191. Zhou AX, Hartwig JH, Akyurek LM. Filamins in cell signaling, transcription and organ development. Trends Cell Biol. 2010;20(2):113-23.
192. Zhou X, Boren J, Akyurek LM. Filamins in cardiovascular development. Trends Cardiovasc Med. 2007;17(7):222-9.
193. Travis MA, van der Flier A, Kammerer RA, Mould AP, Sonnenberg A, Humphries MJ. Interaction of filamin A with the integrin beta 7 cytoplasmic domain: role of alternative splicing and phosphorylation. FEBS Lett. 2004;569(1-3):185-90.
194. Wu C. Migfilin and its binding partners: from cell biology to human diseases. J Cell Sci. 2005;118(Pt 4):659-64.
195. Kiema T, Lad Y, Jiang P, Oxley CL, Baldassarre M, Wegener KL, et al. The molecular basis of filamin binding to integrins and competition with talin. Mol Cell. 2006;21(3):337-47.
196. Berry FB, O'Neill MA, Coca-Prados M, Walter MA. FOXC1 transcriptional regulatory activity is impaired by PBX1 in a filamin A-mediated manner. Mol Cell Biol. 2005;25(4):1415-24.
197. Yuan Y, Shen Z. Interaction with BRCA2 suggests a role for filamin-1 (hsFLNa) in DNA damage response. J Biol Chem. 2001;276(51):48318-24.
198. Kumar A, Shutova MS, Tanaka K, Iwamoto DV, Calderwood DA, Svitkina TM, et al. Filamin A mediates isotropic distribution of applied force across the actin network. J Cell Biol. 2019;218(8):2481-91.
199. Sutherland-Smith AJ. Filamin structure, function and mechanics: are altered filamin-mediated force responses associated with human disease? Biophys Rev. 2011;3(1):15-23.
200. Barry NP, Bretscher MS. Dictyostelium amoebae and neutrophils can swim. Proc Natl Acad Sci U S A. 2010;107(25):11376-80.
201. Lammermann T, Bader BL, Monkley SJ, Worbs T, Wedlich-Soldner R, Hirsch K, et al. Rapid leukocyte migration by integrin-independent flowing and squeezing. Nature. 2008;453(7191):51-5.
202. Nakamura F, Stossel TP, Hartwig JH. The filamins: organizers of cell structure and function. Cell Adh Migr. 2011;5(2):160-9.
203. Jiang P, Campbell ID. Integrin binding immunoglobulin type filamin domains have variable stability. Biochemistry. 2008;47(42):11055-61.
204. Pentikainen U, Ylanne J. The regulation mechanism for the auto-inhibition of binding of human filamin A to integrin. J Mol Biol. 2009;393(3):644-57.
205. Loo DT, Kanner SB, Aruffo A. Filamin binds to the cytoplasmic domain of the beta1-integrin. Identification of amino acids responsible for this interaction. J Biol Chem. 1998;273(36):23304-12.

206. D'Addario M, Arora PD, Fan J, Ganss B, Ellen RP, McCulloch CA. Cytoprotection against mechanical forces delivered through beta 1 integrins requires induction of filamin A. J Biol Chem. 2001;276(34):31969-77.
207. Sharma CP, Ezzell RM, Arnaout MA. Direct interaction of filamin (ABP-280) with the beta 2-integrin subunit CD18. J Immunol. 1995;154(7):3461-70.
208. Calderwood DA, Huttenlocher A, Kiosses WB, Rose DM, Woodside DG, Schwartz MA, et al. Increased filamin binding to beta-integrin cytoplasmic domains inhibits cell migration. Nat Cell Biol. 2001;3(12):1060-8.
209. Kim H, Sengupta A, Glogauer M, McCulloch CA. Filamin A regulates cell spreading and survival via beta1 integrins. Exp Cell Res. 2008;314(4):834-46.
210. Meyer SC, Sanan DA, Fox JE. Role of actin-binding protein in insertion of adhesion receptors into the membrane. J Biol Chem. 1998;273(5):3013-20.
211. Ithychanda SS, Das M, Ma YQ, Ding K, Wang X, Gupta S, et al. Migfilin, a molecular switch in regulation of integrin activation. J Biol Chem. 2009;284(7):4713-22.
212. Lad Y, Jiang P, Ruskamo S, Harburger DS, Ylanne J, Campbell ID, et al. Structural basis of the migfilin-filamin interaction and competition with integrin beta tails. J Biol Chem. 2008;283(50):35154-63.
213. Pfaff M, Liu S, Erle DJ, Ginsberg MH. Integrin beta cytoplasmic domains differentially bind to cytoskeletal proteins. J Biol Chem. 1998;273(11):6104-9.
214. Nagano T, Yoneda T, Hatanaka Y, Kubota C, Murakami F, Sato M. Filamin A-interacting protein (FILIP) regulates cortical cell migration out of the ventricular zone. Nat Cell Biol. 2002;4(7):495-501.
215. Cunningham CC, Gorlin JB, Kwiatkowski DJ, Hartwig JH, Janmey PA, Byers HR, et al. Actin-binding protein requirement for cortical stability and efficient locomotion. Science. 1992;255(5042):325-7.
216. Flevaris P, Stojanovic A, Gong H, Chishti A, Welch E, Du X. A molecular switch that controls cell spreading and retraction. J Cell Biol. 2007;179(3):553-65.
217. Simpson KJ, Selfors LM, Bui J, Reynolds A, Leake D, Khvorova A, et al. Identification of genes that regulate epithelial cell migration using an siRNA screening approach. Nat Cell Biol. 2008;10(9):1027-38.
218. Fox JW, Lamperti ED, Eksioglu YZ, Hong SE, Feng Y, Graham DA, et al. Mutations in filamin 1 prevent migration of cerebral cortical neurons in human periventricular heterotopia. Neuron. 1998;21(6):1315-25.
219. Ito R, Matsumiya T, Kon T, Narita N, Kubota K, Sakaki H, et al. Periosteum-derived cells respond to mechanical stretch and activate Wnt and BMP signaling pathways. Biomed Res. 2014;35(1):69-79.
220. O'Connell MP, Fiori JL, Baugher KM, Indig FE, French AD, Camilli TC, et al. Wnt5A activates the calpain-mediated cleavage of filamin A. J Invest Dermatol. 2009;129(7):1782-9.
221. Cox D, Condeelis J, Wessels D, Soll D, Kern H, Knecht DA. Targeted disruption of the ABP-120 gene leads to cells with altered motility. J Cell Biol. 1992;116(4):943-55.
222. Sarkisian MR, Bartley CM, Chi H, Nakamura F, Hashimoto-Torii K, Torii M, et al. MEKK4 signaling regulates filamin expression and neuronal migration. Neuron. 2006;52(5):789-801.
223. Jaffe AB, Hall A. Rho GTPases: biochemistry and biology. Annu Rev Cell Dev Biol. 2005;21:247-69.

224. Leung R, Wang Y, Cuddy K, Sun C, Magalhaes J, Grynpas M, et al. Filamin A regulates monocyte migration through Rho small GTPases during osteoclastogenesis. J Bone Miner Res. 2010;25(5):1077-91.
225. Ohta Y, Hartwig JH, Stossel TP. FilGAP, a Rho- and ROCK-regulated GAP for Rac binds filamin A to control actin remodelling. Nat Cell Biol. 2006;8(8):803-14.
226. Vadlamudi RK, Li F, Adam L, Nguyen D, Ohta Y, Stossel TP, et al. Filamin is essential in actin cytoskeletal assembly mediated by p21-activated kinase 1. Nat Cell Biol. 2002;4(9):681-90.
227. Sasaki A, Masuda Y, Ohta Y, Ikeda K, Watanabe K. Filamin associates with Smads and regulates transforming growth factor-beta signaling. J Biol Chem. 2001;276(21):17871-7.
228. Chen G, Deng C, Li YP. TGF-beta and BMP signaling in osteoblast differentiation and bone formation. Int J Biol Sci. 2012;8(2):272-88.
229. Kim HJ, Rice DP, Kettunen PJ, Thesleff I. FGF-, BMP- and Shh-mediated signalling pathways in the regulation of cranial suture morphogenesis and calvarial bone development. Development. 1998;125(7):1241-51.
230. Derynck R, Zhang Y, Feng XH. Smads: transcriptional activators of TGF-beta responses. Cell. 1998;95(6):737-40.
231. Heldin CH, Miyazono K, ten Dijke P. TGF-beta signalling from cell membrane to nucleus through SMAD proteins. Nature. 1997;390(6659):465-71.
232. Retting KN, Song B, Yoon BS, Lyons KM. BMP canonical Smad signaling through Smad1 and Smad5 is required for endochondral bone formation. Development. 2009;136(7):1093-104.
233. Horiki M, Imamura T, Okamoto M, Hayashi M, Murai J, Myoui A, et al. Smad6/Smurf1 overexpression in cartilage delays chondrocyte hypertrophy and causes dwarfism with osteopenia. J Cell Biol. 2004;165(3):433-45.
234. Hall BK, Miyake T. The membranous skeleton: the role of cell condensations in vertebrate skeletogenesis. Anat Embryol (Berl). 1992;186(2):107-24.
235. Kume T, Deng KY, Winfrey V, Gould DB, Walter MA, Hogan BL. The forkhead/winged helix gene Mf1 is disrupted in the pleiotropic mouse mutation congenital hydrocephalus. Cell. 1998;93(6):985-96.
236. Rice R, Rice DP, Olsen BR, Thesleff I. Progression of calvarial bone development requires Foxc1 regulation of Msx2 and Alx4. Dev Biol. 2003;262(1):75-87.
237. Mirzayans F, Lavy R, Penner-Chea J, Berry FB. Initiation of early osteoblast differentiation events through the direct transcriptional regulation of Msx2 by FOXC1. PLoS One. 2012;7(11):e49095.
238. Rice R, Rice DP, Thesleff I. Foxc1 integrates Fgf and Bmp signalling independently of twist or noggin during calvarial bone development. Dev Dyn. 2005;233(3):847-52.
239. Minami Y, Oishi I, Endo M, Nishita M. Ror-family receptor tyrosine kinases in noncanonical Wnt signaling: their implications in developmental morphogenesis and human diseases. Dev Dyn. 2010;239(1):1-15.
240. Loy CJ, Sim KS, Yong EL. Filamin-A fragment localizes to the nucleus to regulate androgen receptor and coactivator functions. Proc Natl Acad Sci U S A. 2003;100(8):4562-7.
241. Ozanne DM, Brady ME, Cook S, Gaughan L, Neal DE, Robson CN. Androgen receptor nuclear translocation is facilitated by the f-actin cross-linking protein filamin. Mol Endocrinol. 2000;14(10):1618-26.

242. Castoria G, D'Amato L, Ciociola A, Giovannelli P, Giraldi T, Sepe L, et al. Androgen-induced cell migration: role of androgen receptor/filamin A association. PLoS One. 2011;6(2):e17218.
243. Huang CK, Lai KP, Luo J, Tsai MY, Kang HY, Chen Y, et al. Loss of androgen receptor promotes adipogenesis but suppresses osteogenesis in bone marrow stromal cells. Stem Cell Res. 2013;11(2):938-50.
244. Robertson SP. Filamin A: phenotypic diversity. Curr Opin Genet Dev. 2005;15(3):301-7.
245. Robertson SP, Twigg SR, Sutherland-Smith AJ, Biancalana V, Gorlin RJ, Horn D, et al. Localized mutations in the gene encoding the cytoskeletal protein filamin A cause diverse malformations in humans. Nat Genet. 2003;33(4):487-91.
246. Dudding BA, Gorlin RJ, Langer LO. The oto-palato-digital syndrome. A new symptom-complex consisting of deafness, dwarfism, cleft palate, characteristic facies, and a generalized bone dysplasia. Am J Dis Child. 1967;113(2):214-21.
247. Cohen MM, Jr. The new bone biology: pathologic, molecular, and clinical correlates. Am J Med Genet A. 2006;140(23):2646-706.
248. Gorlin RJ, Cohen MM, Hennekam RCM. Syndromes of the head and neck. 4th ed. Oxford England ; New York: Oxford University Press; 2001. xiv, 1283 p. p.
249. Gorlin RJ, Cohen MM, Jr. Frontometaphyseal dysplasia. A new syndrome. Am J Dis Child. 1969;118(3):487-94.
250. Coste F, Maroteaux P, Chouraki L. Osteodysplasty (Melnick and Needles syndrome). Report of a case. Ann Rheum Dis. 1968;27(4):360-6.
251. Gorlin RJ, Langer LO, Jr. Melnick-Needles syndrome: radiographic alterations in the mandible. Radiology. 1978;128(2):351-3.
252. Neou P, Kyrkanides S, Gioureli E, Bartsocas CS. Melnick-Needles syndrome in a mother and her son. Genet Couns. 1996;7(2):123-9.
253. Kaplan JM, Kim SH, North KN, Rennke H, Correia LA, Tong HQ, et al. Mutations in ACTN4, encoding alpha-actinin-4, cause familial focal segmental glomerulosclerosis. Nat Genet. 2000;24(3):251-6.
254. Zenker M, Rauch A, Winterpacht A, Tagariello A, Kraus C, Rupprecht T, et al. A dual phenotype of periventricular nodular heterotopia and frontometaphyseal dysplasia in one patient caused by a single FLNA mutation leading to two functionally different aberrant transcripts. Am J Hum Genet. 2004;74(4):731-7.
255. Fennell N, Foulds N, Johnson DS, Wilson LC, Wyatt M, Robertson SP, et al. Association of mutations in FLNA with craniosynostosis. Eur J Hum Genet. 2015;23(12):1684-8.
256. Foley C, Roberts K, Tchrakian N, Morgan T, Fryer A, Robertson SP, et al. Expansion of the Spectrum of FLNA Mutations Associated with Melnick-Needles Syndrome. Mol Syndromol. 2010;1(3):121-6.
257. Robertson SP, Jenkins ZA, Morgan T, Ades L, Aftimos S, Boute O, et al. Frontometaphyseal dysplasia: mutations in FLNA and phenotypic diversity. Am J Med Genet A. 2006;140(16):1726-36.
258. Kim J, Lee DW, Jang DH. Case Report: Pansynostosis, Chiari I Malformation and Syringomyelia in a Child With Frontometaphyseal Dysplasia 1. Front Pediatr. 2021;9:574402.

259. Feng Y, Chen MH, Moskowitz IP, Mendonza AM, Vidali L, Nakamura F, et al. Filamin A (FLNA) is required for cell-cell contact in vascular development and cardiac morphogenesis. Proc Natl Acad Sci U S A. 2006;103(52):19836-41.
260. Hart AW, Morgan JE, Schneider J, West K, McKie L, Bhattacharya S, et al. Cardiac malformations and midline skeletal defects in mice lacking filamin A. Hum Mol Genet. 2006;15(16):2457-67.
261. Kyndt F, Gueffet JP, Probst V, Jaafar P, Legendre A, Le Bouffant F, et al. Mutations in the gene encoding filamin A as a cause for familial cardiac valvular dystrophy. Circulation. 2007;115(1):40-9.
262. Marti A, Luo Z, Cunningham C, Ohta Y, Hartwig J, Stossel TP, et al. Actin-binding protein-280 binds the stress-activated protein kinase (SAPK) activator SEK-1 and is required for tumor necrosis factor-alpha activation of SAPK in melanoma cells. J Biol Chem. 1997;272(5):2620-8.
263. Kovacevic I, Cram EJ. FLN-1/filamin is required for maintenance of actin and exit of fertilized oocytes from the spermatheca in C. elegans. Dev Biol. 2010;347(2):247-57.
264. Kakita A, Hayashi S, Moro F, Guerrini R, Ozawa T, Ono K, et al. Bilateral periventricular nodular heterotopia due to filamin 1 gene mutation: widespread glomeruloid microvascular anomaly and dysplastic cytoarchitecture in the cerebral cortex. Acta Neuropathol. 2002;104(6):649-57.
265. Thomas P, Bossan A, Lacour JP, Chanalet S, Ortonne JP, Chatel M. Ehlers-Danlos syndrome with subependymal periventricular heterotopias. Neurology. 1996;46(4):1165-7.
266. Lek M, Karczewski KJ, Minikel EV, Samocha KE, Banks E, Fennell T, et al. Analysis of protein-coding genetic variation in 60,706 humans. Nature. 2016;536(7616):285-91.
267. Kircher M, Witten DM, Jain P, O'Roak BJ, Cooper GM, Shendure J. A general framework for estimating the relative pathogenicity of human genetic variants. Nat Genet. 2014;46(3):310-5.
268. Davydov EV, Goode DL, Sirota M, Cooper GM, Sidow A, Batzoglou S. Identifying a high fraction of the human genome to be under selective constraint using GERP++. PLoS Comput Biol. 2010;6(12):e1001025.
269. Adzhubei IA, Schmidt S, Peshkin L, Ramensky VE, Gerasimova A, Bork P, et al. A method and server for predicting damaging missense mutations. Nat Methods. 2010;7(4):248-9.
270. Untergasser A, Cutcutache I, Koressaar T, Ye J, Faircloth BC, Remm M, et al. Primer3--new capabilities and interfaces. Nucleic Acids Res. 2012;40(15):e115.
271. Speir ML, Zweig AS, Rosenbloom KR, Raney BJ, Paten B, Nejad P, et al. The UCSC Genome Browser database: 2016 update. Nucleic Acids Res. 2016;44(D1):D717-25.
272. Yoshida N, Ogata T, Tanabe K, Li S, Nakazato M, Kohu K, et al. Filamin A-bound PEBP2beta/CBFbeta is retained in the cytoplasm and prevented from functioning as a partner of the Runx1 transcription factor. Mol Cell Biol. 2005;25(3):1003-12.
273. Kevin M. Beussman MYM, Andrea Leonard, Jeffrey Miles, John Hocter, Zizhen Song, Moritz Stolla, Sangyoon J. Han, Ashley Emery, Wendy E. Thomas, Nathan J. Sniadecki. Black Dots: Microcontact-Printed, Reference-Free Traction Force Microscopy. Biophysical Journal 2021.
274. Han SJ, Oak Y, Groisman A, Danuser G. Traction microscopy to identify force modulation in subresolution adhesions. Nat Methods. 2015;12(7):653-6.

275. Sabass B, Gardel ML, Waterman CM, Schwarz US. High resolution traction force microscopy based on experimental and computational advances. Biophys J. 2008;94(1):207-20.
276. Schmittgen TD, Livak KJ. Analyzing real-time PCR data by the comparative C(T) method. Nat Protoc. 2008;3(6):1101-8.
277. Kim H, Nakamura F, Lee W, Shifrin Y, Arora P, McCulloch CA. Filamin A is required for vimentin-mediated cell adhesion and spreading. Am J Physiol Cell Physiol. 2010;298(2):C221-36.
278. Timberlake AT, Choi J, Zaidi S, Lu Q, Nelson-Williams C, Brooks ED, et al. Two locus inheritance of non-syndromic midline craniosynostosis via rare SMAD6 and common BMP2 alleles. Elife. 2016;5.
279. Lee MH, Kwon TG, Park HS, Wozney JM, Ryoo HM. BMP-2-induced Osterix expression is mediated by Dlx5 but is independent of Runx2. Biochem Biophys Res Commun. 2003;309(3):689-94.
280. Liu J, Nam HK, Campbell C, Gasque KC, Millan JL, Hatch NE. Tissue-nonspecific alkaline phosphatase deficiency causes abnormal craniofacial bone development in the Alpl(-/-) mouse model of infantile hypophosphatasia. Bone. 2014;67:81-94.
281. Atkins GJ, Rowe PS, Lim HP, Welldon KJ, Ormsby R, Wijenayaka AR, et al. Sclerostin is a locally acting regulator of late-osteoblast/preosteocyte differentiation and regulates mineralization through a MEPE-ASARM-dependent mechanism. J Bone Miner Res. 2011;26(7):1425-36.
282. Shen C, Yang C, Xu S, Zhao H. Comparison of osteogenic differentiation capacity in mesenchymal stem cells derived from human amniotic membrane (AM), umbilical cord (UC), chorionic membrane (CM), and decidua (DC). Cell Biosci. 2019;9:17.
283. Hidalgo-Bravo A, Pompa-Mera EN, Kofman-Alfaro S, Gonzalez-Bonilla CR, Zenteno JC. A novel filamin A D203Y mutation in a female patient with otopalatodigital type 1 syndrome and extremely skewed X chromosome inactivation. Am J Med Genet A. 2005;136(2):190-3.
284. Lyon MF. Sex chromatin and gene action in the mammalian X-chromosome. Am J Hum Genet. 1962;14:135-48.
285. Lyon MF. Gene action in the X-chromosome of the mouse (Mus musculus L.). Nature. 1961;190:372-3.
286. Monteiro J, Derom C, Vlietinck R, Kohn N, Lesser M, Gregersen PK. Commitment to X inactivation precedes the twinning event in monochorionic MZ twins. Am J Hum Genet. 1998;63(2):339-46.
287. Puck JM, Stewart CC, Nussbaum RL. Maximum-likelihood analysis of human T-cell X chromosome inactivation patterns: normal women versus carriers of X-linked severe combined immunodeficiency. Am J Hum Genet. 1992;50(4):742-8.
288. Liu W, Sun X. Skewed X chromosome inactivation in diploid and triploid female human embryonic stem cells. Hum Reprod. 2009;24(8):1834-43.
289. Kristiansen M, Knudsen GP, Soyland A, Westvik J, Orstavik KH. Phenotypic variation in Melnick-Needles syndrome is not reflected in X inactivation patterns from blood or buccal smear. Am J Med Genet. 2002;108(2):120-7.
290. Hall BK, Miyake T. All for one and one for all: condensations and the initiation of skeletal development. Bioessays. 2000;22(2):138-47.
291. Olsen BR, Reginato AM, Wang W. Bone development. Annu Rev Cell Dev Biol. 2000;16:191-220.

292. De Pollack C, Renier D, Hott M, Marie PJ. Increased bone formation and osteoblastic cell phenotype in premature cranial suture ossification (craniosynostosis). J Bone Miner Res. 1996;11(3):401-7.
293. Fragale A, Tartaglia M, Bernardini S, Di Stasi AM, Di Rocco C, Velardi F, et al. Decreased proliferation and altered differentiation in osteoblasts from genetically and clinically distinct craniosynostotic disorders. Am J Pathol. 1999;154(5):1465-77.
294. Ratisoontorn C, Seto ML, Broughton KM, Cunningham ML. In vitro differentiation profile of osteoblasts derived from patients with Saethre-Chotzen syndrome. Bone. 2005;36(4):627-34.
295. Galvin BD, Hart KC, Meyer AN, Webster MK, Donoghue DJ. Constitutive receptor activation by Crouzon syndrome mutations in fibroblast growth factor receptor (FGFR)2 and FGFR2/Neu chimeras. Proc Natl Acad Sci U S A. 1996;93(15):7894-9.
296. Zhou YX, Xu X, Chen L, Li C, Brodie SG, Deng CX. A Pro250Arg substitution in mouse Fgfr1 causes increased expression of Cbfa1 and premature fusion of calvarial sutures. Hum Mol Genet. 2000;9(13):2001-8.
297. Liu YH, Tang Z, Kundu RK, Wu L, Luo W, Zhu D, et al. Msx2 gene dosage influences the number of proliferative osteogenic cells in growth centers of the developing murine skull: a possible mechanism for MSX2-mediated craniosynostosis in humans. Dev Biol. 1999;205(2):260-74.
298. Liu B, Yu HM, Hsu W. Craniosynostosis caused by Axin2 deficiency is mediated through distinct functions of beta-catenin in proliferation and differentiation. Dev Biol. 2007;301(1):298-308.
299. He F, Soriano P. Dysregulated PDGFRalpha signaling alters coronal suture morphogenesis and leads to craniosynostosis through endochondral ossification. Development. 2017;144(21):4026-36.
300. Kramer K, Yang J, Swanson WB, Hayano S, Toda M, Pan H, et al. Rapamycin rescues BMP mediated midline craniosynostosis phenotype through reduction of mTOR signaling in a mouse model. Genesis. 2018;56(6-7):e23220.
301. Lomri A, Lemonnier J, Hott M, de Parseval N, Lajeunie E, Munnich A, et al. Increased calvaria cell differentiation and bone matrix formation induced by fibroblast growth factor receptor 2 mutations in Apert syndrome. J Clin Invest. 1998;101(6):1310-7.
302. Al-Rekabi Z, Cunningham ML, Sniadecki NJ. Cell Mechanics of Craniosynostosis. ACS Biomater Sci Eng. 2017;3(11):2733-43.
303. Steward AJ, Kelly DJ. Mechanical regulation of mesenchymal stem cell differentiation. J Anat. 2015;227(6):717-31.
304. Geiger B, Bershadsky A, Pankov R, Yamada KM. Transmembrane crosstalk between the extracellular matrix--cytoskeleton crosstalk. Nat Rev Mol Cell Biol. 2001;2(11):793-805.
305. Geiger B, Spatz JP, Bershadsky AD. Environmental sensing through focal adhesions. Nat Rev Mol Cell Biol. 2009;10(1):21-33.
306. Discher DE, Janmey P, Wang YL. Tissue cells feel and respond to the stiffness of their substrate. Science. 2005;310(5751):1139-43.
307. Kim H, McCulloch CA. Filamin A mediates interactions between cytoskeletal proteins that control cell adhesion. FEBS Lett. 2011;585(1):18-22.

308. Al-Rekabi Z, Wheeler MM, Leonard A, Fura AM, Juhlin I, Frazar C, et al. Activation of the IGF1 pathway mediates changes in cellular contractility and motility in single-suture craniosynostosis. J Cell Sci. 2016;129(3):483-91.
309. Ting MC, Wu NL, Roybal PG, Sun J, Liu L, Yen Y, et al. EphA4 as an effector of Twist1 in the guidance of osteogenic precursor cells during calvarial bone growth and in craniosynostosis. Development. 2009;136(5):855-64.
310. Retailleau K, Arhatte M, Demolombe S, Jodar M, Baudrie V, Offermanns S, et al. Smooth muscle filamin A is a major determinant of conduit artery structure and function at the adult stage. Pflugers Arch. 2016;468(7):1151-60.
311. Savinko T, Guenther C, Uotila LM, Llort Asens M, Yao S, Tojkander S, et al. Filamin A Is Required for Optimal T Cell Integrin-Mediated Force Transmission, Flow Adhesion, and T Cell Trafficking. J Immunol. 2018;200(9):3109-16.
312. Misra S, Ghatak S, Moreno-Rodriguez RA, Norris RA, Hascall VC, Markwald RR. Periostin/Filamin-A: A Candidate Central Regulatory Axis for Valve Fibrogenesis and Matrix Compaction. Front Cell Dev Biol. 2021;9:649862.
313. Uchida M, Ishii I, Hirata K, Yamamoto F, Tashiro K, Suzuki T, et al. Degradation of filamin induces contraction of vascular smooth muscle cells in type-I collagen matrix honeycombs. Cell Physiol Biochem. 2011;27(6):669-80.
314. Hagmann S, Moradi B, Frank S, Dreher T, Kammerer PW, Richter W, et al. Different culture media affect growth characteristics, surface marker distribution and chondrogenic differentiation of human bone marrow-derived mesenchymal stromal cells. BMC Musculoskelet Disord. 2013;14:223.
315. Sotiropoulou PA, Perez SA, Salagianni M, Baxevanis CN, Papamichail M. Characterization of the optimal culture conditions for clinical scale production of human mesenchymal stem cells. Stem Cells. 2006;24(2):462-71.
316. Watson SL, Marcal H, Sarris M, Di Girolamo N, Coroneo MT, Wakefield D. The effect of mesenchymal stem cell conditioned media on corneal stromal fibroblast wound healing activities. Br J Ophthalmol. 2010;94(8):1067-73.
317. Basalova N, Sagaradze G, Arbatskiy M, Evtushenko E, Kulebyakin K, Grigorieva O, et al. Secretome of Mesenchymal Stromal Cells Prevents Myofibroblasts Differentiation by Transferring Fibrosis-Associated microRNAs within Extracellular Vesicles. Cells. 2020;9(5).
318. Wu X, Gu Y. Signaling Mechanisms Underlying Genetic Pathophysiology of Craniosynostosis. Int J Biol Sci. 2019;15(2):298-311.
319. Mefford HC, Shafer N, Antonacci F, Tsai JM, Park SS, Hing AV, et al. Copy number variation analysis in single-suture craniosynostosis: multiple rare variants including RUNX2 duplication in two cousins with metopic craniosynostosis. Am J Med Genet A. 2010;152A(9):2203-10.
320. Varvagiannis K, Stefanidou A, Gyftodimou Y, Lord H, Williams L, Sarri C, et al. Pure de novo partial trisomy 6p in a girl with craniosynostosis. Am J Med Genet A. 2013;161A(2):343-51.
321. Sodek J, Zhu B, Huynh MH, Brown TJ, Ringuette M. Novel functions of the matricellular proteins osteopontin and osteonectin/SPARC. Connect Tissue Res. 2002;43(2-3):308-19.
322. Bradshaw AD, Sage EH. SPARC, a matricellular protein that functions in cellular differentiation and tissue response to injury. J Clin Invest. 2001;107(9):1049-54.

323. Sahar DE, Longaker MT, Quarto N. Sox9 neural crest determinant gene controls patterning and closure of the posterior frontal cranial suture. Dev Biol. 2005;280(2):344-61.
324. Kreiborg S, Marsh JL, Cohen MM, Jr., Liversage M, Pedersen H, Skovby F, et al. Comparative three-dimensional analysis of CT-scans of the calvaria and cranial base in Apert and Crouzon syndromes. J Craniomaxillofac Surg. 1993;21(5):181-8.
325. Wang Y, Xiao R, Yang F, Karim BO, Iacovelli AJ, Cai J, et al. Abnormalities in cartilage and bone development in the Apert syndrome FGFR2(+/S252W) mouse. Development. 2005;132(15):3537-48.
326. Yin L, Du X, Li C, Xu X, Chen Z, Su N, et al. A Pro253Arg mutation in fibroblast growth factor receptor 2 (Fgfr2) causes skeleton malformation mimicking human Apert syndrome by affecting both chondrogenesis and osteogenesis. Bone. 2008;42(4):631-43.
327. Cohen MM, Jr., Kreiborg S. New indirect method for estimating the birth prevalence of the Apert syndrome. Int J Oral Maxillofac Surg. 1992;21(2):107-9.
328. Cohen MM, Jr., Kreiborg S. Visceral anomalies in the Apert syndrome. Am J Med Genet. 1993;45(6):758-60.
329. Marie PJ, Coffin JD, Hurley MM. FGF and FGFR signaling in chondrodysplasias and craniosynostosis. J Cell Biochem. 2005;96(5):888-96.
330. Behr B, Longaker MT, Quarto N. Differential activation of canonical Wnt signaling determines cranial sutures fate: a novel mechanism for sagittal suture craniosynostosis. Dev Biol. 2010;344(2):922-40.
331. Akiyama H, Chaboissier MC, Martin JF, Schedl A, de Crombrugghe B. The transcription factor Sox9 has essential roles in successive steps of the chondrocyte differentiation pathway and is required for expression of Sox5 and Sox6. Genes Dev. 2002;16(21):2813-28.
332. Akiyama H, Kim JE, Nakashima K, Balmes G, Iwai N, Deng JM, et al. Osteo-chondroprogenitor cells are derived from Sox9 expressing precursors. Proc Natl Acad Sci U S A. 2005;102(41):14665-70.
333. Behr B, Longaker MT, Quarto N. Absence of endochondral ossification and craniosynostosis in posterior frontal cranial sutures of Axin2(-/-) mice. PLoS One. 2013;8(8):e70240.
334. Athwal VS, Pritchett J, Martin K, Llewellyn J, Scott J, Harvey E, et al. SOX9 regulated matrix proteins are increased in patients serum and correlate with severity of liver fibrosis. Sci Rep. 2018;8(1):17905.
335. Albanese I, Daskalopoulou SS, Yu B, You Z, Genest J, Alsheikh-Ali A, et al. The Urotensin II System and Carotid Atherosclerosis: A Role in Vascular Calcification. Front Pharmacol. 2016;7:149.
336. Aigner T, Neureiter D, Campean V, Soder S, Amann K. Expression of cartilage-specific markers in calcified and non-calcified atherosclerotic lesions. Atherosclerosis. 2008;196(1):37-41.
337. Farrokhi E, Samani KG, Chaleshtori MH. Oxidized low-density lipoprotein and upregulated expression of osteonectin and bone sialoprotein in vascular smooth muscle cells. Lab Med. 2014;45(4):297-301.
338. Rotllant J, Liu D, Yan YL, Postlethwait JH, Westerfield M, Du SJ. Sparc (Osteonectin) functions in morphogenesis of the pharyngeal skeleton and inner ear. Matrix Biol. 2008;27(6):561-72.

339. Maruyama T, Mirando AJ, Deng CX, Hsu W. The balance of WNT and FGF signaling influences mesenchymal stem cell fate during skeletal development. Sci Signal. 2010;3(123):ra40.
340. Behr B, Longaker MT, Quarto N. Craniosynostosis of coronal suture in twist1 mice occurs through endochondral ossification recapitulating the physiological closure of posterior frontal suture. Front Physiol. 2011;2:37.
341. Siismets EM, Hatch NE. Cranial Neural Crest Cells and Their Role in the Pathogenesis of Craniofacial Anomalies and Coronal Craniosynostosis. J Dev Biol. 2020;8(3).
342. Peskett E, Kumar S, Baird W, Jaiswal J, Li M, Patel P, et al. Analysis of the Fgfr2(C342Y) mouse model shows condensation defects due to misregulation of Sox9 expression in prechondrocytic mesenchyme. Biol Open. 2017;6(2):223-31.
343. Lee KKL, Peskett E, Quinn CM, Aiello R, Adeeva L, Moulding DA, et al. Overexpression of Fgfr2c causes craniofacial bone hypoplasia and ameliorates craniosynostosis in the Crouzon mouse. Dis Model Mech. 2018;11(11).
344. Friedl G, Schmidt H, Rehak I, Kostner G, Schauenstein K, Windhager R. Undifferentiated human mesenchymal stem cells (hMSCs) are highly sensitive to mechanical strain: transcriptionally controlled early osteo-chondrogenic response in vitro. Osteoarthritis Cartilage. 2007;15(11):1293-300.
345. Takahashi I, Nuckolls GH, Takahashi K, Tanaka O, Semba I, Dashner R, et al. Compressive force promotes sox9, type II collagen and aggrecan and inhibits IL-1beta expression resulting in chondrogenesis in mouse embryonic limb bud mesenchymal cells. J Cell Sci. 1998;111 (Pt 14):2067-76.
346. Herring SW. Mechanical influences on suture development and patency. Front Oral Biol. 2008;12:41-56.
347. Opperman LA, Adab K, Gakunga PT. Transforming growth factor-beta 2 and TGF-beta 3 regulate fetal rat cranial suture morphogenesis by regulating rates of cell proliferation and apoptosis. Dev Dyn. 2000;219(2):237-47.
348. Opperman LA, Fernandez CR, So S, Rawlins JT. Erk1/2 signaling is required for Tgf-beta 2-induced suture closure. Dev Dyn. 2006;235(5):1292-9.
349. Opperman LA, Nolen AA, Ogle RC. TGF-beta 1, TGF-beta 2, and TGF-beta 3 exhibit distinct patterns of expression during cranial suture formation and obliteration in vivo and in vitro. J Bone Miner Res. 1997;12(3):301-10.
350. Komatsu Y, Yu PB, Kamiya N, Pan H, Fukuda T, Scott GJ, et al. Augmentation of Smad-dependent BMP signaling in neural crest cells causes craniosynostosis in mice. J Bone Miner Res. 2013;28(6):1422-33.
351. Kollmer M, Buhrman JS, Zhang Y, Gemeinhart RA. Markers Are Shared Between Adipogenic and Osteogenic Differentiated Mesenchymal Stem Cells. J Dev Biol Tissue Eng. 2013;5(2):18-25.
352. Malaval L, Modrowski D, Gupta AK, Aubin JE. Cellular expression of bone-related proteins during in vitro osteogenesis in rat bone marrow stromal cell cultures. J Cell Physiol. 1994;158(3):555-72.
353. Herrmann H, Aebi U. Intermediate filaments: molecular structure, assembly mechanism, and integration into functionally distinct intracellular Scaffolds. Annu Rev Biochem. 2004;73:749-89.

354. Ivaska J, Pallari HM, Nevo J, Eriksson JE. Novel functions of vimentin in cell adhesion, migration, and signaling. Exp Cell Res. 2007;313(10):2050-62.
355. Steinert PM, Liem RK. Intermediate filament dynamics. Cell. 1990;60(4):521-3.
356. Jackson WM, Jaasma MJ, Tang RY, Keaveny TM. Mechanical loading by fluid shear is sufficient to alter the cytoskeletal composition of osteoblastic cells. Am J Physiol Cell Physiol. 2008;295(4):C1007-15.
357. Lian N, Lin T, Liu W, Wang W, Li L, Sun S, et al. Transforming growth factor beta suppresses osteoblast differentiation via the vimentin activating transcription factor 4 (ATF4) axis. J Biol Chem. 2012;287(43):35975-84.
358. Lian N, Wang W, Li L, Elefteriou F, Yang X. Vimentin inhibits ATF4-mediated osteocalcin transcription and osteoblast differentiation. J Biol Chem. 2009;284(44):30518-25.
359. Nguyen HG, Metavarayuth K, Wang Q. Upregulation of osteogenesis of mesenchymal stem cells with virus-based thin films. Nanotheranostics. 2018;2(1):42-58.
360. Guillot PV, Abass O, Bassett JH, Shefelbine SJ, Bou-Gharios G, Chan J, et al. Intrauterine transplantation of human fetal mesenchymal stem cells from first-trimester blood repairs bone and reduces fractures in osteogenesis imperfecta mice. Blood. 2008;111(3):1717-25.
361. Dong Q, Zhu X, Dai C, Zhang X, Gao X, Wei J, et al. Osteopontin promotes epithelial-mesenchymal transition of hepatocellular carcinoma through regulating vimentin. Oncotarget. 2016;7(11):12997-3012.
362. Djouad F, Delorme B, Maurice M, Bony C, Apparailly F, Louis-Plence P, et al. Microenvironmental changes during differentiation of mesenchymal stem cells towards chondrocytes. Arthritis Res Ther. 2007;9(2):R33.
363. Huang W, Yang S, Shao J, Li YP. Signaling and transcriptional regulation in osteoblast commitment and differentiation. Front Biosci. 2007;12:3068-92.
364. Shi D, Jiang K, Fu Y, Fang R, Liu XI, Chen J. Overexpression of SPARC correlates with poor prognosis in patients with cervical carcinoma and regulates cancer cell epithelial-mesenchymal transition. Oncol Lett. 2016;11(5):3251-8.
365. Mori-Akiyama Y, Akiyama H, Rowitch DH, de Crombrugghe B. Sox9 is required for determination of the chondrogenic cell lineage in the cranial neural crest. Proc Natl Acad Sci U S A. 2003;100(16):9360-5.
366. Yoshida M, Hata K, Takashima R, Ono K, Nakamura E, Takahata Y, et al. The transcription factor Foxc1 is necessary for Ihh-Gli2-regulated endochondral ossification. Nat Commun. 2015;6:6653.
367. Sheen VL, Dixon PH, Fox JW, Hong SE, Kinton L, Sisodiya SM, et al. Mutations in the X-linked filamin 1 gene cause periventricular nodular heterotopia in males as well as in females. Hum Mol Genet. 2001;10(17):1775-83.
368. Wang Y, Lebowitz D, Sun C, Thang H, Grynpas MD, Glogauer M. Identifying the relative contributions of Rac1 and Rac2 to osteoclastogenesis. J Bone Miner Res. 2008;23(2):260-70.
369. Retailleau K, Arhatte M, Demolombe S, Peyronnet R, Baudrie V, Jodar M, et al. Arterial Myogenic Activation through Smooth Muscle Filamin A. Cell Rep. 2016;14(9):2050-8.
370. Jurak Begonja A, Hoffmeister KM, Hartwig JH, Falet H. FlnA-null megakaryocytes prematurely release large and fragile platelets that circulate poorly. Blood. 2011;118(8):2285-95.

371. Uotila LM, Guenther C, Savinko T, Lehti TA, Fagerholm SC. Filamin A Regulates Neutrophil Adhesion, Production of Reactive Oxygen Species, and Neutrophil Extracellular Trap Release. J Immunol. 2017;199(10):3644-53.
372. Greiten JK, Kliewe F, Schnarre A, Artelt N, Schroder S, Rogge H, et al. The role of filamins in mechanically stressed podocytes. FASEB J. 2021;35(5):e21560.
373. Houlihan SL, Lanctot AA, Guo Y, Feng Y. Upregulation of neurovascular communication through filamin abrogation promotes ectopic periventricular neurogenesis. Elife. 2016;5.
374. Komori T, Yagi H, Nomura S, Yamaguchi A, Sasaki K, Deguchi K, et al. Targeted disruption of Cbfa1 results in a complete lack of bone formation owing to maturational arrest of osteoblasts. Cell. 1997;89(5):755-64.
375. Inada M, Yasui T, Nomura S, Miyake S, Deguchi K, Himeno M, et al. Maturational disturbance of chondrocytes in Cbfa1-deficient mice. Dev Dyn. 1999;214(4):279-90.
376. Kawane T, Qin X, Jiang Q, Miyazaki T, Komori H, Yoshida CA, et al. Runx2 is required for the proliferation of osteoblast progenitors and induces proliferation by regulating Fgfr2 and Fgfr3. Sci Rep. 2018;8(1):13551.
377. Jikko A, Harris SE, Chen D, Mendrick DL, Damsky CH. Collagen integrin receptors regulate early osteoblast differentiation induced by BMP-2. J Bone Miner Res. 1999;14(7):1075-83.
378. Xiao G, Wang D, Benson MD, Karsenty G, Franceschi RT. Role of the alpha2-integrin in osteoblast-specific gene expression and activation of the Osf2 transcription factor. J Biol Chem. 1998;273(49):32988-94.
379. Grant SF, Reid DM, Blake G, Herd R, Fogelman I, Ralston SH. Reduced bone density and osteoporosis associated with a polymorphic Sp1 binding site in the collagen type I alpha 1 gene. Nat Genet. 1996;14(2):203-5.
380. Clarke CM, Fok VT, Gustafson JA, Smyth MD, Timms AE, Frazar CD, et al. Single suture craniosynostosis: Identification of rare variants in genes associated with syndromic forms. Am J Med Genet A. 2018;176(2):290-300.